PAULO VINICIUS FERRAZ CORRÊA

Benthic fauna of the Rio Grande Rise, SW Atlantic: ecology and implications for conservation

São Paulo
2022

PAULO VINICIUS FERRAZ CORRÊA

Benthic fauna of the Rio Grande Rise, SW Atlantic: ecology and implications for conservation

A thesis submitted to the Instituto Oceanográfico of the Universidade de São Paulo in partial fulfilment for the degree of Doctor of Science, Oceanography, with emphasis in Biological Oceanography.

Advisor: Prof. Dr. Paulo Yukio Gomes Sumida

São Paulo

2022

CORRÊA, Paulo Vinicius Ferraz. **Benthic fauna of the Rio Grande Rise, SW Atlantic: ecology and implications for conservation.** A thesis submitted to the Instituto Oceanográfico of the Universidade de São Paulo in partial fulfilment for the degree of Doctor of Science, Oceanography, with emphasis in Biological Oceanography.

Evaluated in: ___/___/_____

Corrected Version

Examination committee

Prof. Dr. Paulo Yukio Gomes Sumida Institution: IO/USP

President Signature: _____

Prof. Dr. _____ Institution: _____

Concept: _____ Signature: _____

Prof. Dr. _____ Institution: _____

Concept: _____ Signature: _____

Prof. Dr. _____ Institution: _____

Concept: _____ Signature: _____

ACKNOWLEDGMENTS

I wish to thank my supervisor, Paulo Yukio Gomes Sumida, for the opportunity to work as his student, his advice, and all the doors he opened for me during my PhD.

The Instituto Oceanográfico da Universidade de São Paulo for all infrastructure and resources that made my research possible and the Graduate Program in Oceanography, including Ana, Daniel, and Leticia who helped me many times.

The Fundação de Amparo à Pesquisa do Estado de São Paulo (FAPESP) for granting my doctoral scholarship (grant number 2017/11884-8) and its financial support for my PhD. This study was financed in part by the Coordenação de Aperfeiçoamento de Pessoal de Nível Superior – Brasil (CAPES) – Finance Code 001.

The FAPESP and the Natural Environment Research Council (NERC, UK) for their funding of the Marine E-Tech Project, which my PhD would not be possible without, and everyone involve ed in the project, especially the professors Fred, Luigi, Cristian, Vivian, Camila, Ilson, and Paulo.

The Captain and crew members of the *N/Oc. Alpha Crucis* and *RSS Discovery* for their professionalism and dedication during data acquisition.

Natascha, Daniel, Pedro, Camila, Maysa, Tomas, Chico, Henrique, Ayrton, Arthur, and Banha, who actively helped me before, during and after the cruises.

Maila and Francesc for all discussions and help, especially during my first years.

André, Angel, Arthur, Cristiana, Flávio, Hajdu, Kitahara, Mau, Olemir, Renata, and Stampar, who helped me in the identification of many specimens from my PhD.

People from the lab, Thur, Nay, Henrique, San, Laricão, Paulinha, Pau, Bruno, Zé, Camila, Mau, Linda, Gabriel, Marina, Ney, Mariana, Gelado, Ester, Esponja, Vaca, and Miguel, for their companionship and encouragement throughout my PhD.

To my grandparents, Vick, Airton, Adriana, Guilherme, Gabriel, Márcia, Milton, Mariana, Murillo, Gian, Roseli, João, Leandro, Michele, Uelica, Gustavo, Cris, Tinho, Manu, Nenê, Lourdes, Mario, Claudiana, Adriana, Kazuko, Keidy, Tamires, Kaze, Banza, Carol, Camilão, Edu, Thais, Camila, Glaucon, Bia, and Felipe, for your support and all the happy moments I shared with you.

Especial thanks to my mother, father, and Felipe, who believed in me. Without you, I would never have reached where I am today.

And Lissa, who endured me throughout my PhD. Thank you for always being at my side, I am forever grateful. …and I love you more ;)

RESUMO

CORRÊA, Paulo Vinicius Ferraz. **Fauna bêntica da Elevação do Rio Grande, Atlântico Sudoeste: ecologia e implicações para conservação** [Tese]. São Paulo: Instituto Oceanográfico, Universidade de São Paulo; 2022.

A Elevação do Rio Grande (ERG) é uma região de interesse comercial e científico devido ao seu potencial para extração de terras raras. O uso e a procura desses elementos se expandiu ao longo dos anos, especialmente com a utilização de energias renováveis (tais como usina eólicas, painéis solares e baterias). Neste cenário, a ERG ganhou a atenção de pesquisadores, do governo brasileiro e outras nações devido ao seu grande potencial para a exploração de crostas ferromanganesíferas, que são importantes fontes de terras raras. Ao contrário da mineração terrestre, não existem precedentes para a exploração mineral em águas profundas. Esta tese visa caracterizar a fauna na ERG e examinar potenciais fatores na estrutura de comunidades e distribuição de espécies na região. Uma revisão na literatura e nas bases de dados OBIS e GBIF mostrou que há pouca informação sobre a fauna e ecologia da ERG. Para ajudar a preencher estas lacunas, foram obtidas e analisadas nesta tese amostras biológicas coletadas em dragas de rochas, vídeos do assoalho marinho e dados batimétricos no Projeto MARINE E-TECH, a partir de dois cruzeiros com os navios *N/Oc. Alpha Crucis* e *RSS Discovery* em 2018. Foi observada uma fauna diversa nas amostras, com maior abundância de esponjas, corais, anelídeos, cracas e anfípodes formadores de tubo. Cerca de 30% dos espécimes encontrados estavam associados a organismos maiores. Os vídeos revelaram habitat bastante heterogêneos e que mudavam rapidamente na RGR. Os habitat formados por depósitos de ferromanganês estavam dominados por comunidades distintas, que raramente foram observadas em outros locais. Também foram encontradas variações na estrutura da comunidade em escala regional, com comunidades distintas em cada lado do rifte e no sudoeste da área de estudo. Foram utilizados modelos de aprendizagem de máquina e regressão para predizer a distribuição da *Sarostegia oculata*, uma esponja de vidro arborescente, que apresentou alta abundância em áreas com crostas de ferromanganês. Os modelos tiveram excelente ou boa performance e um elevado poder de discriminação entre locais de presença e ausência. Os principais fatores para modelar a distribuição foram profundidade, Índice de Posicionamento batimétrico (BPI) em fina escala, e aspecto no sentido norte-sul.

Os modelos predisseram uma elevada probabilidade de *S. oculata* ao longo das bordas do rifte e com um baixo grau de incerteza. A compreensão do potencial impacto no ecossistema é fundamental para a perspectiva de mineração em mar profundo se tornar uma fonte viável de terras raras. Os resultados aqui apresentados serão de interesse para todos os atores relacionados às atividades de mineração e facilitarão a tomada de decisões baseada em evidências científicas em relação a essas atividades.

Palavras-chave: Diversidade. Invertebrados. Estrutura de comunidades. Modelo de distribuição de espécies. Crostas de ferromanganês. Mineração de mar profundo.

ABSTRACT

CORRÊA, Paulo Vinicius Ferraz. **Benthic fauna of the Rio Grande Rise, SW Atlantic: ecology and implications for conservation** [Ph.D. thesis]. São Paulo: Instituto Oceanográfico, Universidade de São Paulo; 2022.

The Rio Grande Rise (RGR) is a region of commercial and scientific interest due to its potential for mining rare-earth elements (REEs). The application and demand for REEs have expanded over the years, especially with the use of renewable energy (such as wind farms, solar panels, and batteries). In this scenario, the RGR has gained attention from researchers, the Brazilian government, and other states due to its large potential for the exploitation of ferromanganese (Fe-Mn) crusts, which are a source of REEs. Unlike terrestrial mining, there are effectively no precedents for mineral exploitation in the deep sea. This thesis aims to characterize the RGR fauna and examine potential drivers for community structure and species distribution. A review of the literature and the OBIS and GBIF databases showed there is little information about the fauna and ecology in RGR. To help fill in these gaps, biological samples from rock dredges, seabed videos, and bathymetric data from RGR were collected in the MARINE E-TECH Project from two cruises with the vessels *N/Oc. Alpha Crucis* and *RSS Discovery* in 2018 and analyzed in this thesis. A diverse fauna was observed, with a higher abundance of sponges, corals, annelids, barnacles, and tube-dwelling amphipods, and 30% of the specimens found associated with larger organisms. Seabed videos revealed highly heterogeneous and rapidly changing habitats in RGR. The habitats formed by Fe-Mn deposits were dominated by distinct communities, which were rarely observed elsewhere. We found variations in the community structure at regional scales, with distinct communities on each side of the rift and at the southwest of the study area. Machine learning and regression models were used to predict the distribution of *Sarostegia oculata*, a branched hexactinellid that forms sponge gardens in Fe-Mn crusts. The models had excellent or good performance statistics and a high discrimination power between presence and absence sites. The main drivers for the distribution were depth, fine scale Bathymetric Position Index, and northness. Models predicted a high likelihood of *S. oculata* along with the rift borders with a low degree of uncertainty. Understanding the potential ecosystem impact is critical to any prospect of deep-sea mineral deposits becoming a potentially viable source of REEs. The

results presented here will be of interest to all the stakeholders in the proposed mining activities and will facilitate more informed decision-making regarding these activities.

Keywords: Diversity. Invertebrates. Community structure. Species distribution model. Ferromanganese crusts. Deep-sea mining.

FIGURE INDEX

TABLE INDEX

SUMMARY

1 General Introduction

1.1 Background

The deep sea, commonly defined as regions below 200 m in depth (Gage & Tyler, 1991), represents 63% of the planet's surface area (Thurber et al., 2014). It is one of the largest and most diverse ecosystems on Earth (Ramirez-Llodra et al., 2010), with a great diversity of habitats, species (Grassle & Maciolek, 1992; Mora et al., 2011), and potential living and non-living resources (Herzig & Hannington, 1995). Much of its diversity is explained, in part, by the heterogeneity of this environment, such as seamounts, ocean ridges, trenches, abyssal plains, hydrothermal vents, and many other formations. However, the ability to study the deep sea by researchers remains limited due to the high cost of suitable vessels and restricted available infrastructure (Howell et al., 2021). Therefore, there are still many unknown regions and several gaps about the biodiversity and ecology of this environment (McClain & Hardy, 2010; Perez et al., 2012).

Recently, the knowledge of the deep-sea environment has progressively been required due to increasing human pressure, such as oil and gas extraction, chemical pollutants, fishing (Glover & Smith, 2003), and, more recently, mining of seafloor massive sulfides, polymetallic nodules and ferromanganese (Fe-Mn) crusts (Hein & Koschinsky, 2014; Manceau et al., 2014). These formations are rich in minerals, which are used to manufacture smart technologies and green energy such as batteries, wind turbines, and solar panels. Thus, there is a growing demand in the market for the exploration and consumption of these minerals (Thompson et al., 2018). Deep-sea mining is an industry with high potential, which is expected to become operational in all the world's oceans within the next few decades and will inevitably induce pressures in these unexplored environments (Hein & Koschinsky, 2014; Manceau et al., 2014). These include the removal of specimens attached to Fe-Mn crusts and increased sediment loads caused by mining tailings that may clog the filtering system of many organism (Hughes et al., 2015).

In this scenario, the Rio Grande Rise (RGR) has gained special attention from researchers and the Brazilian government due to the large amount of Fe-Mn crusts. The RGR corresponds to a complex positive feature located between the Argentine and Brazilian abyssal basins (28°S–35°S; 28°W–39°W), approximately 1200 km off

the Brazilian coast and 2000 km off the Mid-Atlantic Ridge (Montserrat et al., 2019). It is the largest submarine elevation off southeastern Brazil (~480,000 km²), rising from depths of 5000 m to peaks less than 600 m (Fig. 1.1) (Mohriak, 2020). RGR is usually divided into two sub-regions: (1) the Western Rio Grande Rise (WRGR) is characterized by a large ellipsoidal bulge that rises to a mean depth of about 2000 m (also referred to as Alpha subregion) and (2) the Eastern Rio Grande Rise (ERGR) with north-south elongated geomorphology, delimited by E-W fractures in both north and south ends. There is a characteristic NW-SE rift structure formed on top of the bathymetric high (sometimes also referred to as 'graben' or Cruzeiro do Sul Lineament in the literature), creating a deep submarine channel.

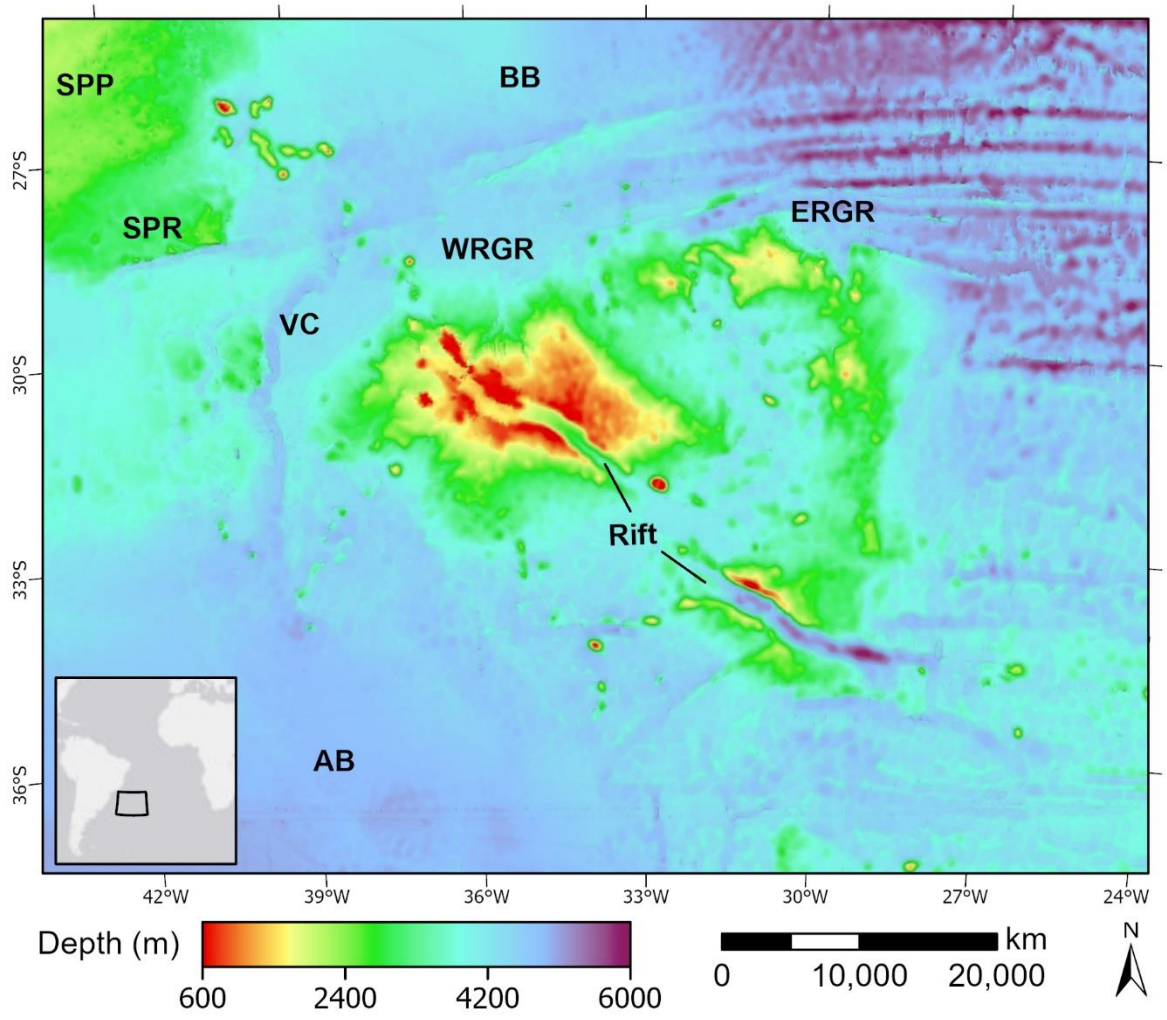

Figure 1.1. The location and bathymetry of the Rio Grande Rise (RGR) in the SW Atlantic off SE Brazil. The RGR is divided into two main subregions, the larger and elliptical Western Rio Grande Rise (WRGR) and the Eastern Rio Grande Rise (ERGR). A large 800 to 3000 m deep rift valley cuts through the RGR from NW-SE. The Vema Channel (VC) connects the southernmost Argentinian Basin (AB) to the Brazilian Basin (BB) to the North and separates RGR from the São Paulo Ridge (SPR) and São Paulo Plateau (SPP) to the northwest.

The RGR supposedly has its origin associated with an intense basalt outpouring in the Mid-Atlantic Ridge between 89–78 Ma ago, which also gave rise to the Walvis Ridge (Montserrat et al., 2019; O'Connor & Duncan, 1990). However, this hypothesis has been contested recently (Mohriak, 2020; Mohriak et al., 2010; Ussami et al., 2013), in which the RGR could be an isolated remnant of continental crust left outboard of the Brazilian continental margin during the westward drifting process. Cobalt-rich ferromanganese (Fe-Mn) crusts cover large areas of the RGR and their genesis are still open to debate (Benites et al., 2020; Sousa et al., 2021).

The Brazilian Government, through the Interministerial Commission for Marine Resources (CIRM), created the Program for prospecting and Exploration of Mineral Resources of the International Seabed Area in the South and Equatorial Atlantic Ocean (PROAREA) in 2009 (CIRM, 2009). In this program, research activities related to marine geology and biology in international waters gained priority in the country, leading to the creation of "*Crostas Cobaltíferas da Elevação do Rio Grande*" Project (PROERG). PROERG aims to identify areas of occurrence of cobalt-rich ferromanganese crusts (also called cobalt crusts) in the region (CIRM, 2016). In 2015, the International Seabed Authority (ISA) and the state-owned *Companhia de Pesquisa de Recursos Minerais* (CPRM) of Brazil have signed a 15-year contract for Fe-Mn crusts exploration in the RGR (Montserrat et al., 2019). Its potential for exploitation of mineral resources is being evaluated (J. A. D. Cavalcanti et al., 2015), with the identification of large areas with cobalt-rich ferromanganese crusts (CRCs) located between 700 and 1500 m on the RGR plateau. Among the elements detected, phosphate, trace elements of Co, Ni, Pb, Zn, Ba and V, and Mn and Ti oxides are worth mentioning.

ISA requires that any human activity to be carried out on the seabed must first establish and maintain sustainable regimes that ensure the protection of the marine environment from harmful effects that may arise from these activities (E. Baker & Beaudoin, 2013; ISA, 2013). It also requires an environmental baseline study to obtain sufficient information on environmental conditions before mining tests can be carried out, and an environmental impact assessment of mining activities, even in small areas (Hein et al., 2010). Such studies should include data on seafloor communities and their variability across different habitats, both within and around areas containing Fe-Mn crusts or polymetallic nodules. Unfortunately, there are few and fragmented biological data on RGR (Montserrat et al., 2019; Perez et al., 2012).

CIRM has another program to gather geophysical and bathymetric data, called the Brazilian Continental Shelf Survey Project (LEPLAC). As a result of the LEPLAC, on 17 May 2004, Brazil submitted to the Commission on the Limits of the Continental Shelf (CLCS) a claim for an extension of the outer continental shelf (OCS) beyond the 200 nautical miles. On 4 April 2007, the CLCS adopted recommendations regarding the Brazilian submission. As a consequence, the Brazilian delegation delivered three partial revised submissions to the Commission over the following years (da Silva, 2021). The latest one was submitted on 7 December 2018, related to the oriental and meridional margins. However, this claim is not limited to revising pending aspects from the 2007 CLCS recommendations and goes further to include the RGR as part of Brazil's continental margin (LEPLAC, 2018). If approved, it adds an economically promising geological feature under the country's jurisdiction and sovereignty rights (Benites et al., 2020). During this process, and until a final decision is reached, the RGR is inaccessible to countries other than Brazil. Nonetheless, data on deep-sea community structure provide important clues about the vulnerability of these habitats and are crucial for the establishment of Marine Protected Areas (MPAs) (ISA, 2008; Wedding et al., 2013). For example, the Clarion-Clipperton Zone, in the Pacific Ocean, is a highly targeted region for deep-sea mining that has been studied for several years, where Areas of Particular Environmental Interest (APEIs) have been established to minimize human impacts (ISA, 2011; M. Lodge et al., 2014; Wedding et al., 2015). In the context of deep-sea mining, MPAs have the objectives of (a) preserving unique marine habitats, (b) preserving marine biodiversity and the structure and functioning of ecosystems, and (c) facilitating the management and sustainability of mining activities.

Due to its current interest, the RGR exploration represents a great opportunity to study the biodiversity of this region, still little known to science (Perez et al., 2012). There are few and fragmented biological data on RGR (Montserrat et al., 2019), except for (a) some records of fish produced by Russian exploratory fisheries between 1974 and 1989 (Clark et al., 2007; Perez et al., 2012), (b) a few benthopelagic studies as a result from the *Iata-Piuna* expedition with the manned submersible *Shinkai 6500* (Cardoso et al., 2018; Hajdu et al., 2017; Mastella, 2017; Perez et al., 2018), (c) works related to samples collected by CPRM (Lima et al., 2019). Data on fauna and community structure are valuable information about the vulnerability of deep-sea habitats. Therefore, understanding the RGR biodiversity and ecological patterns will become essential in the coming years.

1.2 The Marine E-Tech Project

The Marine E-Tech (Marine ferromanganese deposits: a major resource of E-tech elements) project is an international collaboration between NERC (UK) and FAPESP (Brazil) (https://projects.noc.ac.uk/marine-e-tech/). It is a multi-disciplinary research program that combined geology, geophysics, geochemistry, biology, and microbiology to understand the local controls on ferromanganese oxide deposits at a seamount and micro-basin scale. The project focused on the Tropic Seamount (north-east Atlantic) and Rio Grande Rise (south-west Atlantic) to address the value chain from extraction to metal production, while gathering information that will inform and guide future exploration and regulation of what may become a major industry in the future.

The project main key research questions include (a) what are the local-scale processes that control the variation in thickness and E-tech element composition of Fe-Mn deposits?, (b) what is the magnitude of the topography effect and can it be predicted?, (c) what is the impact of the local dominant water-mass on E-tech element budgets?, (d) what is the role of microorganisms in deep-sea Fe-Mn deposit formation and E-tech element concentration?, and (e) what is the potential impact of mineral extraction on deep-sea ecosystems?

Unlike terrestrial mining, there are effectively no precedents for mineral resource exploitation and extraction in the deep sea. Hence understanding the potential ecosystem impact is critical to any prospect of deep-sea mineral deposits becoming a potentially viable source of E-tech elements. These are rare-earth elements (REEs) used in the development of green energy technologies. While the project focuses on the cycling of E-tech elements and the formation of mineral deposits within the deep sea, it also had the opportunity to investigate what are believed to be the most likely environmental impacts (Oebius et al., 2001) resulting from seafloor mineral exploitation. While the project did not explore all possible impacts of deep-sea mining, two areas have been identified as especially critical by the ISA. These broadly fall into two spatially concentric zones of impact: (a) a proximal zone where there is potential for acute conflict between the location of sessile biology and the highest grade Fe-Mn deposits, and (b) a peripheral zone which is likely to suffer chronic impact from detrital particulate plumes resulting from mining activity.

The samples analyzed here were collected within the scope of the Marine E-Tech project, and this thesis is mainly focused to investigate the fauna and its distribution patterns at RGR, and help to understand the potential impact of mineral extraction in this area.

1.3 Thesis Structure

This thesis resulted from research undertaken at the Instituto Oceanográfico da Universidade de São Paulo, with financial support of the Fundação de Amparo à Pesquisa do Estado e São Paulo (FAPESP), grant number 2017/11884-8. This thesis aims to characterize the fauna in RGR and examine potential drivers for community structure and species distribution in the region, thus helping to understand the potential impacts of deep-sea mining in RGR and facilitating decision making of stakeholders regarding mining activities. This thesis is organized in chapters.

Chapter 2 contains my contributions to the review paper "*Deep-sea mining on the Rio Grande Rise (Southwestern Atlantic): A review on environmental baseline, ecosystem services and potential impacts"*, published in 2019 in *Deep-Sea Research Part I*. In this chapter, I made a literature review of the benthic biodiversity in RGR; described the method used for data mining of environment variables in global and open databases available for RGR; and showed the results of data mining related to the biodiversity of RGR, including biological data from OBIS and GBIF databases and global habitat suitability models. The following three chapters are structured in a manuscript-style.

Chapter 3 show my results working with the collected specimens from rock dredges and *RUV HyBIS*, where I characterized the fauna and analyzed environment drivers that could explain the variation in fauna composition among dredges.

In Chapter 4 I used the seabed videos acquired with the *RUV HyBIS* to characterize the fauna (now with a different method compared to Chapter 3) and the habitats found in the study area. Based on the videos and environment variables derived from multibeam echosounder surveys, the key objectives of this chapter are: (a) annotate, classify, and identify organisms seen in the videos, (b) identify habitats based on geomorphology, slope, and substrate textures, (c) find and describe distinct communities from the annotations, and (d) find which variables were the most important to explain the variability in the community structure. This chapter was

published in *Deep-Sea Research Part I* and is available at https://doi.org/10.1016/j.dsr.2022.103811.

Finally, in Chapter 5 I selected *Sarostegia oculata* to build species distribution models that could predict its occurrence in the study area. *S. oculata* was the dominant organism in areas rich in Fe-Mn crusts (Hajdu et al., 2017) and support unique communities in RGR (Chapter 4). Such models use environmental data to calculate the presence likelihood of a species in areas still not surveyed. Previous findings suggest that *S. oculata* abundance is near the rift borders, an area rich in Fe-Mn crusts and target to deep-sea mining (Montserrat et al., 2019). In this case, mining activities would cause a severe impact in the communities sustained by *S. oculata.* In this chapter, I want to investigate if these models can confirm that the sponge distribution is related to the rift border and which environment variables drives its distribution.

Code for analysis associated with the current thesis is available at the following GitHub repositories:

- Chapter 2 - https://github.com/correapvf/RGR-bio-review
- Chapter 3 - https://github.com/correapvf/RGR-dredges-fauna
- Chapter 4 - https://github.com/correapvf/RGR-analysis
- Chapter 5 - https://github.com/correapvf/SDM-RGR-2022 and https://github.com/correapvf/caretSDM

2 Deep-sea mining on the Rio Grande Rise (Southwestern Atlantic): A review

The paper "*Deep-sea mining on the Rio Grande Rise (Southwestern Atlantic): A review on environmental baseline, ecosystem services and potential impacts"* was a collaborative work led by Montserrat and written by multiple researchers from the *Instituto Oceanográfico da Universidade de São Paulo* (IOUSP) that were participating in the Marine E-Tech project. The objective of the paper was to build a review about our state of knowledge in Rio Grande Rise (RGR), involving several oceanographic fields. The paper consists of four main parts: (a) a literature review on different aspects (geology and oceanography, pelagic geochemistry and primary production, benthic biodiversity, formation and function of cobalt crusts as benthic habitat) of the RGR; (b) a data mining exercise, in which modeled and extrapolated environmental data from public, global and quality-controlled databases are presented in the shape of time-averaged maps; (c) a valuation of the RGR ecosystem, by determining the ecosystem services that derive from it; and (d) a discussion of the environmental impacts on the RGR as a consequence of proposed CRC mining activities.

The paper was published in 2019 in *Deep-Sea Research Part I*. This chapter compiles all contributions I have made to the paper, especially for parts (a) and (b). Section **2.1 Benthic biodiversity** is a literature review of the benthic biodiversity in RGR, and corresponds to section 3.5 of Montserrat et al. (2019). Section **2.2 Environmental baseline** describes the method used for data mining of environment variables in global and open databases, which were discussed by collaborators throughout section 4 of Montserrat et al. (2019). This section is written in the supplementary material of the paper, and the maps produced are gathered in Appendix A. Finally, section **2.3 Benthic biogeography and habitat suitability** describes and show the results of datamining that is closely related to the biodiversity of RGR. This section corresponds to section 4.3 Benthic biogeography and habitat suitability of Montserrat et al. (2019). It includes (a) biological data from OBIS and GBIF databases, (b) the number of seamounts and knolls known for the region, and (c) three global habitat suitability models of Vulnerable Marine Ecosystems (VMEs) indicator taxa, which were discussed in the paper elsewhere.

2.1 Benthic biodiversity

The RGR represents habitat heterogeneity on both a large, ocean basin-scale and on a smaller spatial scale (J. A. D. Cavalcanti et al., 2015; Gamboa & Rabinowitz, 1984). Rising about 3500 m from the surrounding ocean floor, the western RGR bulge (Alpha subregion) represents a giant seamount-like structure, while small-scale or local topographic heterogeneity is represented by the slopes, summits, ridges, and canyons of the RGR (Mohriak et al., 2010). Structural heterogeneity of the seafloor is linked to gradients in environmental conditions due to differences in depth, hydrodynamics, sediment, and substrate composition, and is potentially responsible for strong variations in abundance, biomass, and diversity of benthic communities (Costello & Chaudhary, 2017; ISA, 2007).

Due to habitat diversity and its isolation from other oceanic bottom features, the RGR may offer high degrees of endemism and unique assemblages in terms of abundance or frequency of species, as traditionally reported for several seamounts (Lundsten et al., 2009; Richer de Forges et al., 2000; Wilson & Kaufmann, 1987). However, recent studies and reviews have suggested seamounts are generally not ecologically isolated and indicated problems with estimates of endemism (Clark et al., 2012; Rowden et al., 2010; Schlacher et al., 2010). Thus, a large remaining question is whether and how much difference there is between RGR benthic communities and those on the neighbouring features and abyssal plains.

The location of the RGR in oligotrophic waters with relatively low phytoplankton biomass in surface waters, suggests that both primary and secondary productivity originates locally (Perez et al., 2012). Despite low primary productivity over the RGR, processes like Taylor-column concentration of nutrients (Genin & Boehlert, 1985; ISA, 2007), upwelling of deep Antarctic Bottom Water (AABW), and bentho-pelagic coupling in the shallower parts may enhance biological production (Le et al., 2017). This regionally increased primary production would then lead to increased organic matter deposition and thus fuel the RGR benthic foodweb. The apex of the Alpha subregion is indeed modelled to receive a higher POC flux (Morato et al., 2016) compared to surrounding abyssal basins. It is also characterised by relatively low-oxygen water layers, indicating the presence of an oxygen-minimum zone (OMZ) around 1200-1500 m depth (Florindo et al., 2015).

In a joint Brazilian-Japanese expedition, the manned submersible *Shinkai 6500* made two dives on the Alpha western bulge of the RGR in 2013, as part of the Japanese “QUELLE” project and the Brazilian “Iata-Piuna” expedition. Both the dives lasted for about 4 hours and a half and took place in similar depths. The first transect briefly explored the bottom of the graben in the NW part, ascending the graben wall to the summit and surveyed crusts and carbonate rocks pavement while following the summit. The second transect was situated ca. 200 km towards the SE from the first transect, and surveyed only the summit (Perez et al., 2018). Although the two locations comprised notably distinct seascapes, there was a clear overlap in habitat types.

The habitat type along the graben bottom was a uniform soft-sediment substrate, with regular ripple marks, while that along the graben wall consisted of hard substrate formed by outcrops, alternately covered with CRCs and sediment pockets (Hajdu et al., 2017; Perez et al., 2018). The abrupt relief of the outcrops provided habitat for obvious hard-substrate organisms, such as Hexactinellid sponges and other associated fauna, which occurred in abundance (Hajdu et al., 2017). The crusts along the summit surveyed during the first dive consisted mainly of a gentle relief of alternating soft-sediment pockets and hard substrate, covered by plate-like CRCs (Perez et al., 2018). The hard substrate was covered by both Hexactinellid sponges and scleractinian (stony) corals, both in moderate abundances. The carbonate rock pavement observed along the summit during the first dive also presented hard substrate habitat for Hexactinellid sponges and smaller suspension feeders (Hajdu et al., 2017; Perez et al., 2018). The fact that the carbonate pavement was subject to strong currents, caused a virtual absence of soft sediment.

The second dive along the summit, in a sector towards the SE of the first dive, described a plain benthic terrain of which the first half was covered with soft sediment with both regular and irregular ripple marks (Perez et al., 2018). Benthic organisms were rarely observed on this soft sediment. The second half of the second dive consisted of interspersed soft sediment pools and plate-like CRCs, on which stony corals and Hexactinellid sponges were sparsely present.

Both the records mean and variability were higher during the first dive, in which the highest variation in seascape and habitat type were observed as well. In total, an assumed 30 fish species (“morphotypes”) belonging to 17 families were found, along with recordings of 7 decapods, including some shrimp-like species (Cardoso et al.,

2018; Perez et al., 2018). Although the graben wall was excluded from quantitative analysis, records of large, mobile benthic and bentho-pelagic organisms (fish and crustaceans) showed a significant higher abundance in the first dive. Between habitat types, the highest overall abundance was observed in the “carbonate rock pavement” habitat type along the summits of both locations. This higher abundance was ascribed to the dominant presence of two fish species (*Chaunax* sp. and *Malacocephalus okamurai*), so that the carbonate rock pavement habitat type was at the same time also the least diverse (Perez et al., 2018).

2.2 Environmental baseline

To construct a bathymetric map of the region, we used the bathymetric data from the General Bathymetric Chart of the Oceans (GEBCO) (Becker et al., 2009). The region of interest or “buffer area” was defined calculating the contour line of 4000 m around the RGR and creating a buffer of 30 km around it. Slope was calculated from GEBCO depth using the GRASS-GIS software (Hofierka et al., 2009). Sediment type, sediment thickness and seamount locations were gathered from Dutkiewicz et al. (2015), Whittaker et al. (2013) and Yesson et al. (2011), respectively. Global Open Ocean and Deep Seabed (GOODS) (Wedding et al., 2013) biogeographic classification and Ecologically or Biologically Significant Areas (EBSA) (Bax et al., 2016) datasets were downloaded from MarineRegions.org database (Claus et al., 2017). Optimal cobalt crust locations were derived from GEBCO data.

Environmental layers of temperature (Locarnini et al., 2013), salinity (Zweng et al., 2013), dissolved oxygen (Garcia, Boyer, et al., 2013), phosphate, nitrate and silicate concentrations (Garcia, Locarnini, et al., 2013) were obtained from World Ocean Atlas 2013 (WOA13) (Boyer et al., 2013), using objectively analyzed climatologies of averaged decades. Total inorganic CO_2, pH, total alkalinity and aragonite saturation were gathered from Global Ocean Data Analysis Project (GLODAP), version 2 (Key et al., 2015; Lauvset et al., 2016). For horizontal and vertical currents, we used Simple Ocean Data Assimilation (SODA) 3.3.1 model (Carton et al., 2018), based on a monthly mean over a 10-year period (2007-2016). Each environment layer was arranged in gridded z-layers of different depths that were re-sampled to match GEBCO resolution without interpolation. Subsequently, these layers

were draped over the seafloor, in correspondence with the depth range, following similar methods described by Davies and Guinotte (2011), to produce a continuous raster with seabed data. When a z-layer had no data in a cell that intercepted its depth range, we assumed the above z-layer as a good proxy for it, keeping the limits defined by the Table 4 of Key et al. (2010).

The monthly mean primary productivity was based on the Vertically Generalized Production Model (VGPM) of Behrenfeld and Falkowski (1997), calculated from the monthly MODIS chlorophyll-a concentration, Sea-surface temperature (4μ) and Photosynthetically Active Radiation (PAR) (NASA Goddard Space Flight Center, 2014) from 2007 to 2017. Then, we estimated export POC flux of the seafloor by using equations of Lutz et al. (2007) (see also Sweetman et al., 2017). The euphotic zone was calculated using the Case I model of Morel and Berthon (1989).The reference of each variable that were obtained from open and global databases is found in Table 2.1.

We selected biologically relevant data layers, based on Harris and Whiteway (2009), Brown et al. (2011) and Sweetman et al. (2017) from Table 2.1. These include depth, slope, temperature, dissolved oxygen, nutrients (phosphate, nitrate and silicate), primary production, POC flux and carbonate system-related variables (pH, Alkalinity, Aragonite and Calcite saturation states Ω). Next, we calculated a pair-wise Pearson's correlation between layers to avoid strong linear correlation between variables. We removed layers with strong correlation ($-0.5 > r > 0.5$) and chose to keep those with strong and obvious control on biodiversity (Harris & Whiteway, 2009). Four variables were used in the model: POC flux, slope, temperature and dissolved oxygen. Seascapes classification were performed in RGR (Figure S5) using ESRI ArcGIS ISOCluster Unsupervised Classification tool, similar to the methods outlined by Harris et al. (2008) and Smith (2017). Each data layer was scaled to a range from 0 to 100, as recommended by the tool's Help Page. We used 40 as minimum class size (number of data layers times 10) and 1 as sample interval, to ensure that all cells are used in the cluster calculations. The tool was run interactively using 3 to 15 number of classes and the optimal number was chosen by the "distance ratio" value (= average of the mean distance of each class member to the corresponding class mean). In this study, 7 classes were chosen as the optimal number, as the points reaches a local asymptote for that given number of classes.

Table 2.1. Summary of maps available in the paper of Montserrat et al. (2019), with their respective sources and figures where they appear, both in the original paper and in this thesis (inside parentheses). Note that "S" stands for figures in Appendix A.

Figure	Variable	Source
6A (S1A)	Depth (m)	GEBCO 2014 (Becker et al., 2009)
6B (S1B)	Slope (degrees)	Derived from GEBCO depth
6C (S1C)	Sediment Thickness (m)	Whittaker et al. (2013)
6D (S1D)	Sediment Type	Dutkiewicz et al. (2015)
6E (S1E)	Seafloor Velocity (m/s) [1,5]	SODA 3.3.1 (Carton et al., 2018)
6F (S1F)	Seafloor Vertical Velocity (m/s) [1,5]	SODA 3.3.1 (Carton et al., 2018)
7A (S2A)	Seafloor Temperature (°C) [2,5]	WOA13 (Locarnini et al., 2013)
7B (S2B)	Seafloor Salinity (psu) [2,5]	WOA13 (Zweng et al., 2013)
7C (S2C)	Seafloor Dissolved Oxygen (ml/l) [2,5]	WOA13 (Garcia, Boyer, et al., 2013)
7D (S2D)	Seafloor Silicate (µmol/l) [2,5]	WOA13 (Garcia, Locarnini, et al., 2013)
7E (S2E)	Seafloor Nitrate (µmol/l) [2,5]	WOA13 (Garcia, Locarnini, et al., 2013)
7F (S2F)	Seafloor Phosphate (µmol/l) [2,5]	WOA13 (Garcia, Locarnini, et al., 2013)
8A (S3A)	Seafloor pH [3,5]	GLODAPv2 (Lauvset et al., 2016)
8B (S3B)	Seafloor Alkalinity (µmol/kgSW) [3,5]	GLODAPv2 (Lauvset et al., 2016)
8C (S3C)	Seafloor Ω Aragonite Saturation [3,5]	GLODAPv2 (Lauvset et al., 2016)
8D (S3D)	Seafloor Ω Calcite Saturation [3,5]	GLODAPv2 (Lauvset et al., 2016)
8E (S3E)	VGPM Net Primary Production (mgC m^{-2} day^{-1}) [4]	Modeled from MODIS data as described by Behrenfeld & Falkowski (1997)
8F (S3F)	Seafloor POC flux (mgC m^{-2} day^{-1}) [4]	Modeled from MODIS data as described by Lutz el al (2007)
9A (2.1A)	Benthic fauna occurrences	OBIS and GBIF
9B (2.1B)	Seamounts and Knolls locations	Yesson et al. (2011)
9C (2.1C)	Framework-forming corals habitat suitability consensus	Davies and Guinotte (2011)
9D (2.1D)	Octocoral habitat suitability consensus	Yesson et al. (2012)
9E (2.1E)	Black corals habitat suitability	Yesson et al. (2015)
10B (S4B)	Shipping lanes	Halpern et al. (2015)
10C (S4C)	Ocean-based pollution	Halpern et al. (2015)
10D (S4D)	Submarine cables locations	TeleGeography (2017)
10E (S4E)	ESBA locations	Bax et al. (2016)
10F (S4F)	GOODS Biogeographic Provinces	Watling et al. (2013)

[1] 50 z-layers, each was calculated from monthly mean from 2007 to 2016.
[2] 102 z-layers, mapped climatology from 1955 to 2012
[3] 33 z-layers, mapped climatology from 1972 to 2013
[4] based on monthly data from 2007 to 2016
[5] each z-layer was draped over the seafloor, as described by Davies and Guinotte (2011)

2.3 Benthic biogeography and habitat suitability

The GBIF (http://doi.org/10.15468/dl.indh75) and OBIS databases (accessed 15 June 2017) returned a total of 60477 and 21640 occurrences, respectively, where the former also returned 10166 occurrences of fossils, most of Foraminifera and several pertaining to Plantae. A table with 11867 records was generated, where the great majority (76.3%) were Foraminifera. Depth ranged from the surface to 4818 m deep, of which 870 occurrences (7.3%) did not have information on depth. We removed 4744 occurrences without level of identification, 110 occurrences of terrestrial plants and insects, and 35 occurrences provided by the "Vulnerable Marine Ecosystems in the South Pacific Ocean region" dataset (NIWA, 2016). These occurrences were removed because (a) the dataset metadata clearly states that the records are from the South Pacific Ocean, and (b) most occurrences are benthic invertebrates, but their associated depths, based on coordinates, are incompatible with the depth of the RGR. The occurrences were grouped by species, date, depth, longitude and latitude, and tables from both databases were cross-referenced to remove duplicates.

After processing, only 22 Animalia records were classified as "Benthic" (18 species) (Table 2.2), ranging from 185 to 4818 m in depth, spread over 21 locations within the RGR buffer (11 points in western RGR Alpha bulge; Fig. 2.1a). While Morato et al. (2016) show at least a few records of Vulnerable Marine Ecosystems (VME) indicator taxa in the RGR, our search yielded no such records in the RGR, due to removal of records from the South Pacific Ocean dataset (NIWA, 2016).

Apart from being pelagic biodiversity hotspots (Morato et al., 2010), deep seamounts and smaller knolls are important benthic habitats for deep-sea corals and VME indicator species, like octocorals, crinoids and sponges (J. S. Davies et al., 2015; Tittensor et al., 2009). A total of 47 seamounts and 122 knolls were recorded within the RGR buffer area (Fig. 2.1b), occupying a total base area of ca. 44000 (7% of RGR buffer), and 99400 km^2 (15% of RGR buffer), respectively.

Table 2.2. Records of Animalia, classified hierarchically to realm (Benthic, Pelagic), phylum and class. N_{spec} = number of species observed; $N_{records}$ = total number of records; N_{inds} = number of individuals recorded.

Habitat	Phylum	Class	N_{spec}	$N_{records}$	N_{inds}
Pelagic	Annelida	“Polychaeta”	9	16	27
	Arthropoda	Hexanauplia	3	3	44
	Arthropoda	Malacostraca	34	145	1383
	Chaetognatha	Sagittoidea	1	1	2
	Chordata	Actinopterygii	98	299	446
	Chordata	Elasmobranchii	9	30	42
	Chordata	Mammalia	5	60	63
	Chordata	Reptilia	1	4	4
	Chordata	Thaliacea	1	1	1
	Cnidaria	Hydrozoa	18	27	102
	Mollusca	Cephalopoda	1	1	1
	Mollusca	Gastropoda	2	2	5
		Total	182	589	2120
Benthic	Arthropoda	Malacostraca	3	4	4
	Arthropoda	Ostracoda	1	1	2
	Chordata	Actinopterygii	3	3	6
	Chordata	Elasmobranchii	1	1	1
	Mollusca	Bivalvia	2	2	2
	Mollusca	Cephalopoda	1	3	11
	Mollusca	Gastropoda	6	7	17
	Nematoda	Adenophorea	1	1	1
		Total	18	22	44

As records from RGR are scarce, we also used three habitat suitability models available from the literature to define areas more likely to presence of corals. The consensus of species occurrence of hard (framework-forming) cold-water corals (A. J. Davies & Guinotte, 2011) ranges between 0 and 5 species, with the maximum number of species to be expected along the shallowest summits (Fig. 2.1c). Similarly, the number of octocoral (Alcyonaria) species (Yesson et al., 2012) is expected to be highest along the shallowest summits, and decreasing with depth due to low current speeds, inconsistent food supply, and the reduced aragonite saturation state (A. J. Davies & Guinotte, 2011). However, a maximum is found along the deeper slopes (2000-2500 m) of both the Alpha bulge and the northern bulge of the Delta arc, with a large area of maximum consensus (7 species) along the northern deep slopes of the Alpha bulge (Fig. 2.1d). Habitat suitability of black corals (Yesson et al., 2015) is uniformly highest along the shallowest summits, decreasing more or less linearly with depth until ca. 2500 m (Fig. 2.1e).

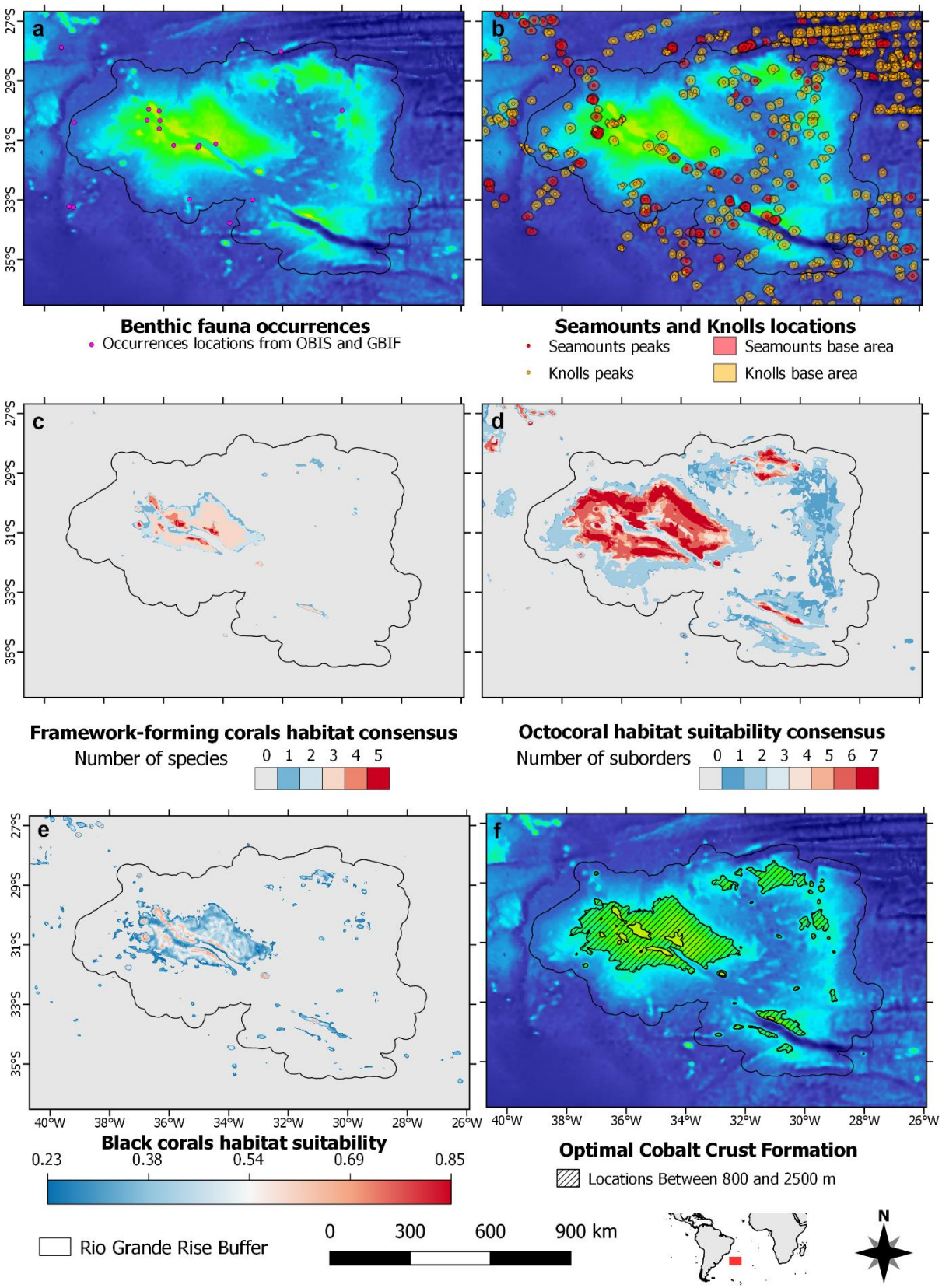

Figure 2.1. Maps showing biogeographic data for the RGR buffer area and surroundings. **(a)** Benthic fauna occurrences (GBIF and OBIS databases). **(b)** Locations of seamounts (red) and knolls (yellow) with their respective estimated base area (Yesson et al., 2011). **(c)** Habitat consensus for framework-forming (stony) corals (A. J. Davies & Guinotte, 2011). **(d)** Habitat suitability for octocorals (Yesson et al., 2012). **(e)** Habitat suitability for black corals (Yesson et al., 2015). **(f)** Zonation for cobalt-rich crust (CRC) optimal formation conditions (hashed area) (Hein, 2004) over the RGR.

3 Fauna characterization of the collected specimens in the Marine E-Tech project at Rio Grande Rise (SW Atlantic)

Abstract

The Rio Grande Rise (RGR) is an area rich in ferromanganese crusts, considered a great resource for the mining of rare earth minerals. Scarce information about the fauna and ecology is available for RGR, which is crucial to inform decisions to stakeholders. Biological baseline studies and an assessment of the possible environmental impacts of mining should be made to avoid loss of biodiversity and ecosystem services and lead to better management of mining activities. In this scenario, the MARINE E-TECH Project led to two cruises in 2018 with the *N/Oc. Alpha Crucis* and *RSS Discovery*, which collected biological samples from rock dredges and the *RUV HyBIS*. Collected specimens were removed from rocks, photographed, and classified in the lowest taxonomic group possible using the help of experts. We counted 1344 specimens classified in 155 morphotypes, and the classes Demospongiae, Anthozoa, Scyphozoa, “Polychaeta”, Thecostraca, and Malacostraca were among the most abundant. We also examined the surface of large organisms and found 350 specimens, classified in 54 morphotypes, were associated with them. The variables side of the plateau and depth were statically significant to explain the variability in fauna composition. Accumulation curves suggest the number of dredges analyzed here was not enough to capture most of the diversity in the area. Future surveys should target a higher sampling effort and a broader range of habitats.

Keywords: Biodiversity. Invertebrates. Rock dredges. Fe-Mn crusts. Deep sea.

3.1 Introduction

Human activities have become progressively frequent in recent decades in the deep sea, such as oil and gas extraction, fishing, and exploration of polymetallic nodules and ferromanganese crusts (Glover & Smith, 2003). Deep-sea mining is an industry with high commercial potential, which is expected to become operational in all the world's oceans within the next few decades and will inevitably induce several pressures (e.g., destruction of fauna, increase in suspended material in the water) in

these unexplored environments (Hein & Koschinsky, 2014; Manceau et al., 2014). The most obvious impact of deep-sea mining will be the direct removal of ferromanganese crusts (Dunn et al., 2018). The extraction and transport to the surface will also release high loads of sediment plumes and toxic chemicals into adjacent areas, as well as cause other disturbances to marine life, like light and noise.

The Rio Grande Rise (RGR) is a heterogeneous feature and consists of seamounts, guyots, and escarpments. Along with its conjugate Walvis Ridge and the Mid-Atlantic Ridge, forms the most prominent bathymetric features in the South Atlantic Ocean basin (Mohriak et al., 2010; O'Connor & Duncan, 1990). The RGR extends between latitudes 28° and 34ºS and longitudes 28° and 40ºW, delimited to the north and south by two oceanic fracture zones and in the west by the Vema Channel. It also has a major rift-like structure aligned in the NW-SE direction, more than 2000 m in depth. RGR is also a ferromanganese (Fe-Mn) crust-rich area and for this reason the Brazilian government has shown a particular interest in RGR in the last few years (da Silva, 2021; Montserrat et al., 2019).

The fauna on Rio Grande Rise is still mostly unknown to science, with only a few records and studies made in recent years (Cardoso et al., 2018; Hajdu et al., 2017; Lima et al., 2019; Montserrat et al., 2019; Perez et al., 2012, 2018), and mining will likely lead to loss of biodiversity, modifications in these communities and ecosystem functions, and possibly the loss of species not described to science yet. Thus, it is important, and mandatory by the International Seabed Authority (ISA) regulations, to create environmental baseline studies, including biological communities, and monitoring during exploration and exploitation to ensure that no serious harm is caused to these ecosystems (Levin et al., 2016). Here, we characterize a diverse fauna sampled with dredges and by the Robotic Underwater Vehicle (*RUV*) *HyBIS* (Hydraulic Benthic Interactive Sampler) and analyze a set of environmental variables, namely plateau side, distance from rift, mean depth, mean slope, and mean direction, that may explain the variation in community structure. We found that many species are associated with other organisms, using them as habitat, and there are distinct fauna compositions on both sides of the rift. Our results suggest dredges observed in this study were not enough to sample most of the diversity in the area.

3.2 Material and methods

Samples were collected on two oceanographic cruises throughout 2018, within the scope of the project “Marine ferromanganese deposits: a major resource of E-tech elements” (MARINE E-TECH), funded by FAPESP and Research Council UK (RCUK). The first cruise (named RGR1) took place from January 29 to February 20 in the *N/Oc. Alpha Crucis* (Jovane et al., 2019), where 15 sites were dredged (Fig. 3.1a) in the central area of WRGR, close to the NW-SE rift. The second cruise (named DY094) was carried out from October 26 to November 8 2018 on the *RSS Discovery*, where 16 rock dredges (Fig. 3.1b) and 13 dives with the *RUV HyBIS* (Fig. 3.1c) were performed. *RUV HyBIS* was equipped with a mechanical arm for collecting rocks and benthic organisms, as determined by scientists during the dive. The map in Figure 3.2 shows the sites that were sampled on each cruise.

Figure 3.1. Sampling devices used in the *N/Oc. Alpha Crucis* (RGR1) (a) and *RSS Discovery* (DY94) (b and c) cruises. (**a)** Squared rock dredge with a meshed bottom. **(b)** Rectangular rock dredge with a collection bag of interlaced metal rings. Source: Rees et al. (2009). **(c)** *RUV HyBIS* being deployed in the water.

Sampled rocks were inspected for encrusted and attached organisms. These were carefully removed and photographed while still alive, when possible, and fixed in 96% ethanol. Part of the tissues of larger specimens (> 5 cm) was removed and frozen for molecular biology analyses. For the most abundant species, a few individuals were selected and fixed in 4% formalin for morphological analysis, then preserved in 70% ethanol. In the laboratory, the collected specimens were separated into morphotypes and identified to the lowest taxonomic group possible. Part of the material was identified by taxonomic experts of each group and some individuals were also identified with the help of molecular analysis, using the COI marker and BOLD system (Ratnasingham & Hebert, 2007). DNA was extracted using the QIAGEN Blood & Tissue kit following the manufacturer’s protocol and COI was amplified using primers

LCO and HCO (Folmer et al., 1994), with GoTaq Green Master Mix (Promega) kit following the manufacturer's instructions. PCRs cycles consisted of 95°C for 2 mins, 35 cycles of 95°C for 40 s, 43-52°C for 60 s, 72°C for 1 min 30 s, and a final step of 72°C for 7 mins. PCR products were purified with QIAGEN Purification kit and sequenced at either Myleus (Brazil) or Macrogen (South Korea). Photos of the subjects were taken using a Leica M205C stereomicroscope with an attached camera. Pieces of corals, sponges, and large organisms were carefully examined for the presence of associated fauna.

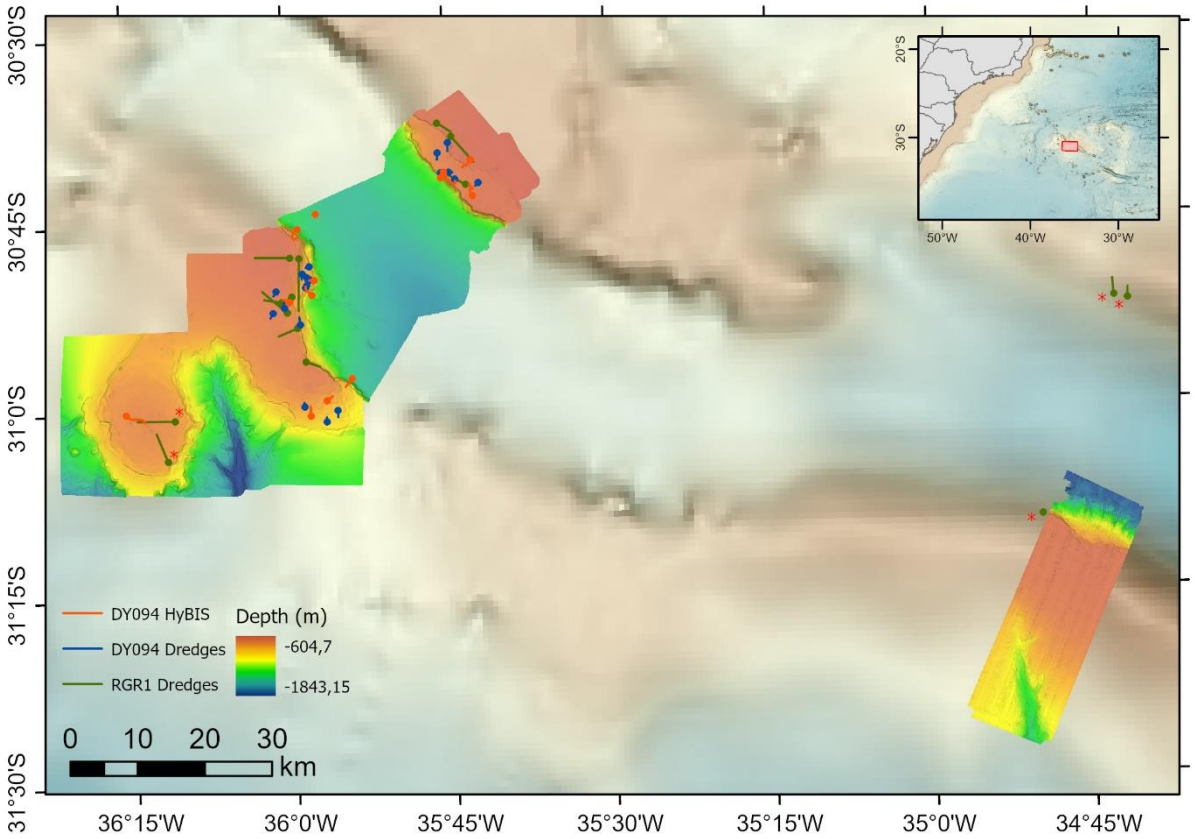

Figure 3.2. Rio Grande Rise. Dredged sites with RGR1 (green) and DY094 (blue) cruises, and dives with the *RUV HyBIS* (orange). The circle at one end of the line indicates where the dredge/dive started. Red asterisks indicate dredges removed from the statical analysis.

Statistical analyses were computed in R 4.1.3 (R Core Team, 2020) and the *vegan* package (Oksanen et al., 2019). Specimens sampled with *HyBIS* were removed from further analysis because they are biased toward how researchers select samples to be obtained and a priori PERMANOVA test indicated a distinct community found in these samples. Dredging distances and dredge models were different in our study, hence we executed multiple regression and ANOVA analysis to test for bias in the number of specimens (abundance) and morphotype richness (S). We also only

considered dredges on the northwest side of the study area and near the rift in the analysis (excluded dredges D02, D03, D04, D11, and D12 collected in the RGR1 cruise, indicated by a red asterisks in Fig. 3.2), because they are geographically isolated from the remaining sites.

Multibeam echosounder (MBES) data obtained in both cruises were used to create a bathymetric model of the area, gridded at 25 m resolution. Using the multibeam bathymetry, depth, slope, and aspect were calculated using the Spatial Analyst Tools within ArcGIS Pro 2.9.1. These variables were extracted for each dredge transect, and we used the mean depth and slope to inform statistical analyses. Mean direction was derived from aspect and computed as in Long and Baco (2014) with the mean direction equations from Fisher (1995). The percentage of collected rocks covered with Fe-Mn crusts was calculated for each dredge as well. We included the distance from the transect midpoint to the rift border as another variable in the analysis. This was achieved by using the Benthic Terrain Model 3.0 tool (Walbridge et al., 2018) to create a broad-scale (20/200 radius) Bathymetric Position Index, and generate a contour at value 0. This will result in two contours outlining the NE and SW rift borders, which were used in the Near tool to calculate the distance from the rift. We also classified each site in North and South plateaus, whether they were made near the NE and SW plateaus, respectively. Collinearity between variables was checked using Pearson's correlation coefficient and the Variance Inflation Factors (VIFs) using the *usdm* package (Naimi et al., 2014).

Generalized Linear Models (GLM) were used to test the effects of plateau side, distance from rift, mean depth, mean slope, and mean direction on abundance and morphotype richness. Models were fitted with quasi-Poisson errors and log as a link function. Abundance data was transformed using Hellinger distance. Effects of variables were evaluated with homogeneity of dispersions tests (*betadisper*), followed by PERMANOVA (M. J. Anderson, 2001; McArdle & Anderson, 2001) using the *adonis2* function with terms added sequentially and 999 permutations. A non-metric Multidimensional Scaling (nMDS) ordination technique was used to obtain a 2-dimension representation of morphotype composition similarities among all dredges. We plotted accumulation curves from morphotypes collected in the north and south plateaus, using the number of dredges as a measure of sampling effort.

3.3 Results and discussion

3.3.1 Fauna characterization

We counted 1165 specimens collected in the dredges and 179 collected with the *RUV HyBIS* (Table 3.1), which were classified in 155 morphotypes, included in ten phyla (Fig. 3.3). The abundance found in each site ranged from a few (< 10) to 115 specimens. The dredge RGR1-D03 and dive HY40 had the largest morphotype richness (29), while others had only one morphotype collected. The classes Demospongiae, Anthozoa, Scyphozoa, “Polychaeta”, Thecostraca, and Malacostraca were among the most abundant (> 100). Polychaetes were the most morphotype-rich taxon (32), followed by Anthozoa, Demospongiae, Malacostraca, and Ophiuroidea. The remaining classes had a low number of specimens (< 40).

Table 3.1. Dredges (coded D--) and *RUV HyBIS* (coded HY--) dives made in the RGR1 (*N/Oc. Alpha Crucis*) and DY94 (*RSS Discovery*) cruises on Rio Grande Rise. Table include dredge/dive characteristics, the number of specimens collected, and morphotype richness (S).

Cruise	Site	Latitude	Longitude	Length (m)	Depth (m)	Fe-Mn Crust coverage (%)	No. specimens	S
RGR1	D02	31°09.4'S	34°49.8'W	168	1051	30	25	8
RGR1	D03	30°51.7'S	34°41.6'W	1546	893	0	64	29
RGR1	D04	30°51.2'S	34°42.9'W	2385	914	0	27	15
RGR1	D05	30°49.9'S	35°58.9'W	7706	771	90	27	19
RGR1	D06	30°53.7'S	35°60.0'W	3050	695	95	23	11
RGR1	D07	30°51.1'S	36°01.3'W	2644	681	65	91	19
RGR1	D08	30°50.8'S	35°59.7'W	506	714	100	20	9
RGR1	D09	30°47.6'S	36°01.3'W	5225	642	99	73	14
RGR1	D10	30°51.2'S	36°01.1'W	4857	684	20	42	8
RGR1	D11	31°00.5'S	36°12.5'W	5591	727	75	12	8
RGR1	D12	31°02.7'S	36°12.0'W	4529	760	30	30	7
RGR1	D13	30°56.3'S	35°57.7'W	2231	724	100	5	5
RGR1	D15	30°37.5'S	35°45.0'W	2492	648	100	13	6
RGR1	D16	30°39.3'S	35°43.3'W	5016	632	50	7	5
RGR1	D17	30°41.5'S	35°44.3'W	4426	692	60	90	25
DY94	D01	30°41.3'S	35°45.2'W	846	709	30	9	7
DY94	D03	30°39.8'S	35°45.7'W	1019	712	0	3	1
DY94	D04	30°39.0'S	35°44.7'W	1294	699	0	22	13
DY94	D05	30°49.8'S	35°58.1'W	360	819	92	39	11
DY94	D06	30°49.4'S	35°58.1'W	386	793	70	115	33
DY94	D07	30°49.2'S	35°58.5'W	817	768	0	29	16
DY94	D09	30°49.5'S	35°58.0'W	713	815	94	82	22
DY94	D10	30°48.5'S	35°58.0'W	527	829	0	2	1

Table 3.1. Continued.

Cruise	Site	Latitude	Longitude	Length (m)	Depth (m)	Fe-Mn Crust coverage (%)	No. specimens	S
DY94	D11	30°49.9'S	35°58.2'W	578	820	70	46	11
DY94	D12	30°51.5'S	36°00.3'W	813	695	100	46	27
DY94	D13	30°52.8'S	35°58.8'W	1155	794	0	55	26
DY94	D15	31°00.7'S	35°56.6'W	665	909	100	9	7
DY94	D16	31°00.3'S	35°55.5'W	979	921	68	89	10
DY94	D17	30°50.5'S	36°01.1'W	817	670	84	24	15
DY94	D19	30°41.8'S	35°44.3'W	817	691	25	7	5
DY94	D20	30°42.1'S	35°42.1'W	705	665	22	39	12
DY94	HY31	30°41.5'S	35°45.3'W	434	897	0	1	1
DY94	HY32	30°40.5'S	35°43.0'W	1914	662	0	4	3
DY94	HY33	30°50.4'S	35°58.1'W	1784	1027	100	3	3
DY94	HY34	30°51.1'S	35°59.7'W	2178	706	0	14	9
DY94	HY35	30°44.3'S	35°57.2'W	533	1454	20	2	2
DY94	HY36	30°49.5'S	35°57.6'W	854	925	100	6	5
DY94	HY37	30°57.9'S	35°54.5'W	1945	1096	0	7	6
DY94	HY38	30°59.0'S	35°56.2'W	1197	786	0	10	5
DY94	HY39	31°00.3'S	36°14.4'W	3394	750	70	23	14
DY94	HY40	31°00.0'S	35°58.0'W	1576	829	100	53	29
DY94	HY41	30°45.9'S	35°59.3'W	2562	841	0	7	5
DY94	HY42	30°41.7'S	35°44.7'W	3957	698	60	31	15
DY94	HY43	30°42.5'S	35°42.6'W	2799	673	0	18	11

The phylum Porifera was the fourth most abundant and third most diverse (in terms of morphotype richness). We collected fragments of *Sarostegia oculata* (Fig. 3.4a), a glass sponge that mimics the framework of actual corals, in the dredges and an undamaged *Aphrocallistes* cf. *beatrix* (Fig. 3.4b) using the *HyBIS* arm. Both hexactinellids had abundant epibiotic zoanthids on their surface. However, most sponges were demosponges, attached to the surface of rocks. Some species were also found inside holes in rocks (Fig. 3.4c), inside and on the surface (Fig. 3.4d) of dead corals, and the surface of Fe-Mn crusts (Figs. 3.4e, f). Individuals of the phylum Cnidaria were sampled in all dredges, except for D02, D08, and D10 of DY94. We collected fragments of the deep-water, reef-forming stony coral *Enallopsammia rostrata* (Fig. 3.4g), several solitary corals attached to rocks, including the genera *Crispatotrochus*, *Stenocyathus, and Caryophyllia* (Fig. 3.4h), black corals (likely *Aphanostichopathes paucispina* and *Bathypathes* sp.), sea anemones, bamboo corals, a new species of the ceriantharian *Botrucnidifer* sp. (Fig. 3.4i) (S.N. Stampar, personal communication, 2019), and hydrozoans. A large anemone (~8 cm width) was also collected with the help of the *HyBIS* arm (Fig. 3.4j). Polyps of the order Coronatae

(identified as Scyphozoa in Fig. 3.3) were abundant as well (143 specimens), attached to both rocks and crusts.

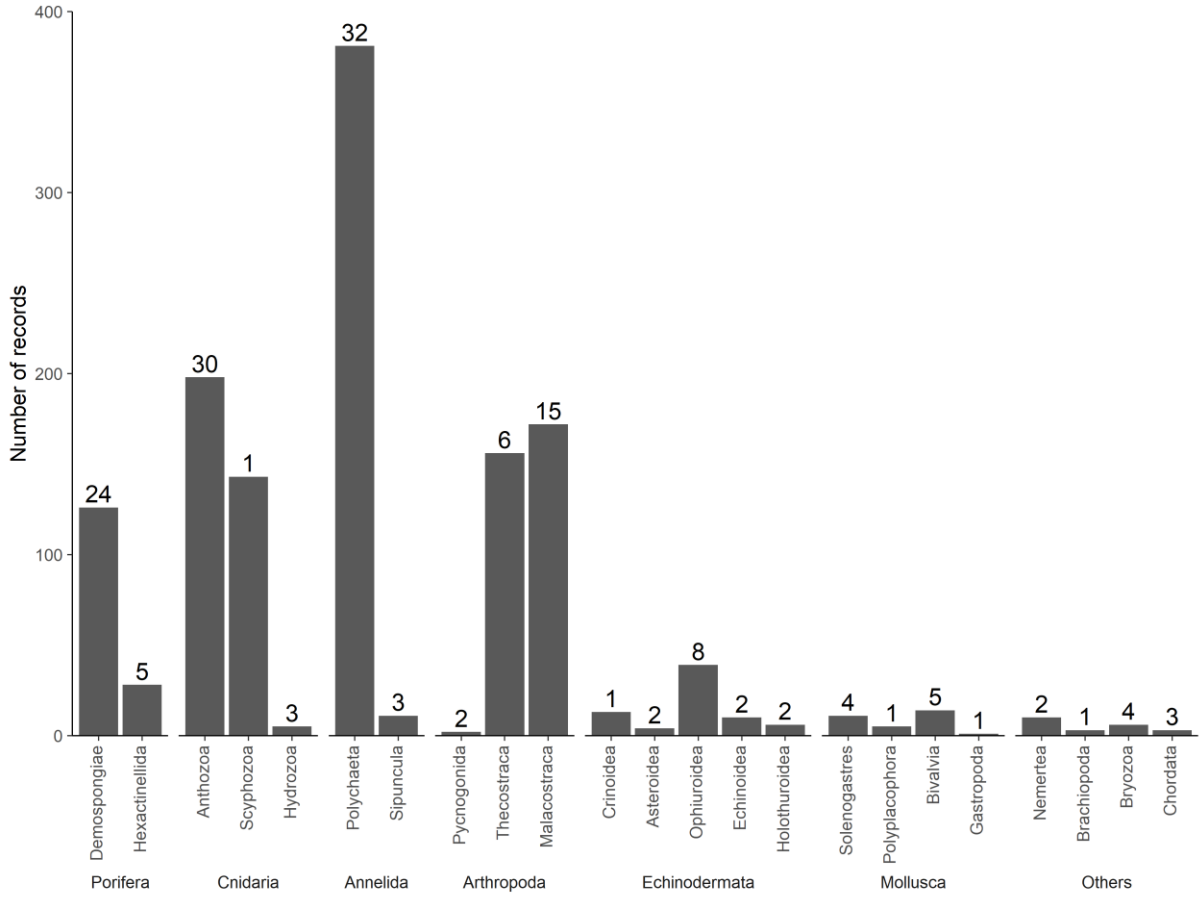

Figure 3.3. Number of records by phyla and classes of all sampled organisms with dredges and the *RUV HyBIS*. Numbers above bars indicate the number of morphotypes.

Polychaetes (phylum Annelida) was the most abundant and most diverse taxon found in the samples. In addition, five morphotypes had a larger number of individuals (> 30) compared to others, and three of these morphotypes were always associated with sponges and corals (see text below). We also found tube-forming annelids of the family Serpulidae (Fig. 3.5a) and Sabellidae, along with several specimens inside small cavities (Fig. 3.5b) on rocks and crusts in several dredges. A few specimens of Sipuncula were sampled as well. Thecostraca and Malacostraca of the phylum Arthropoda (“crustaceans”) had a high abundance too, mostly due to two morphotypes. One is a barnacle (65 individuals, Cirripedia, Thecostraca), from which 81% were collected in a single rock sampled in dredge RGR1-D09. The other is a tube-dwelling amphipod (143 individuals, Amphipoda, Malacostraca) found on the surface of rocks on multiple sites, of the genus *Corophium* (Fig. 3.5c). Other morphotypes of the order

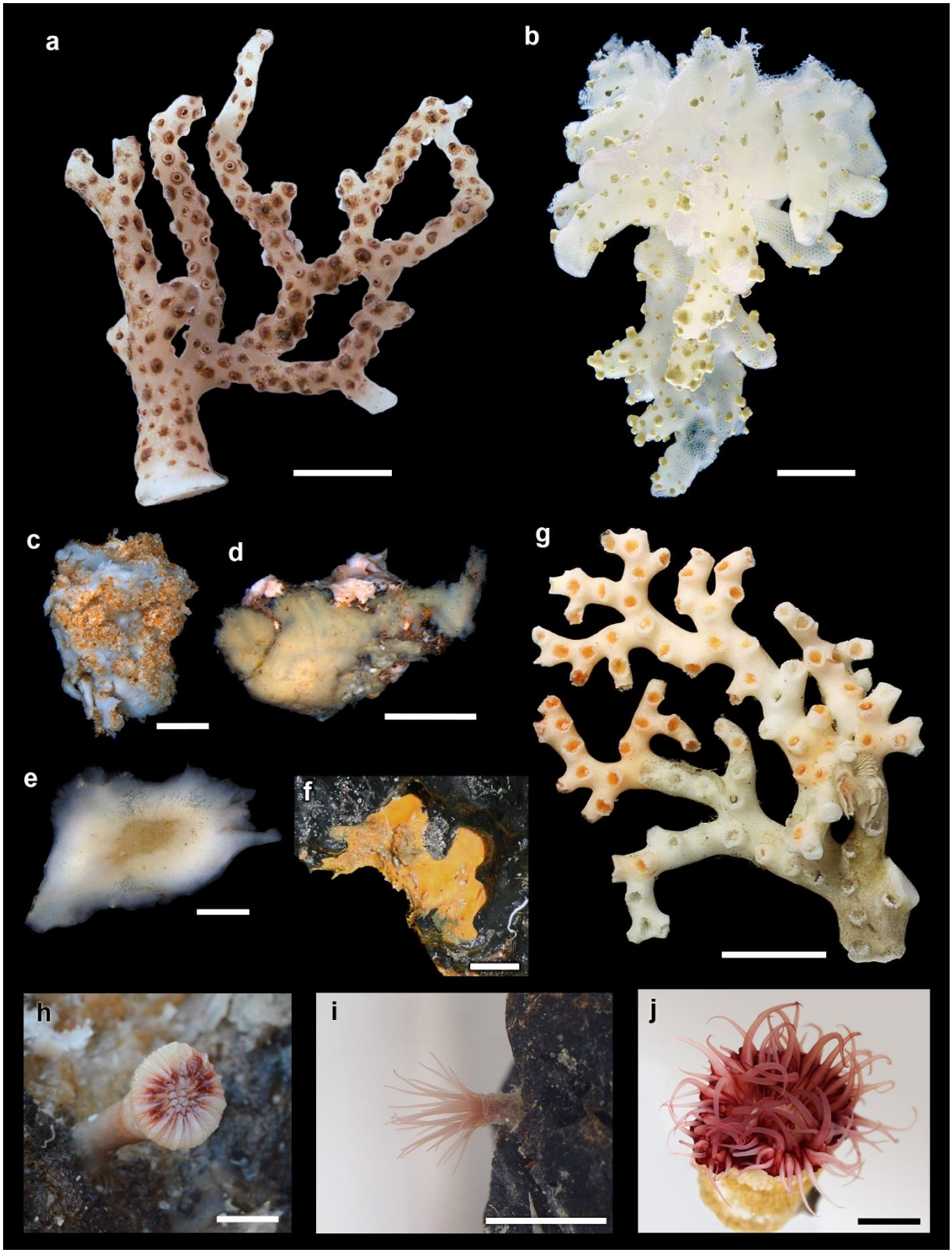

Figure 3.4. Specimens collected with dredges (a, c–i) and *HyBIS* (b, j). **(a)** *Sarostegia oculata* and **(b)** *Aphrocallistes cf. Beatrix*. Families **(c)** Alectonidae, found inside a rock, **(d)** Hemiasterellidae, **(e)** Ancorinidae, possibly *Steletta* sp., and **(f)** Hymedesmiidae. **(g)** *Enallopsammia rostrata*. **(h)** *Caryophyllia diomedeae.* **(i)** Ceriantharia, *Botrucnidifer* sp. **(j)** *Paraphelliactis* sp., possibly *Paraphelliactis michaelsarsi*. (a and b) Hexactinellida, (c–f) Demospongiae, and (g–j) Anthozoa. Scales in a, b and g: 20 mm, c and d: 5 mm, e: 2 mm, f, h and i: 10 mm, and j: 30 mm.

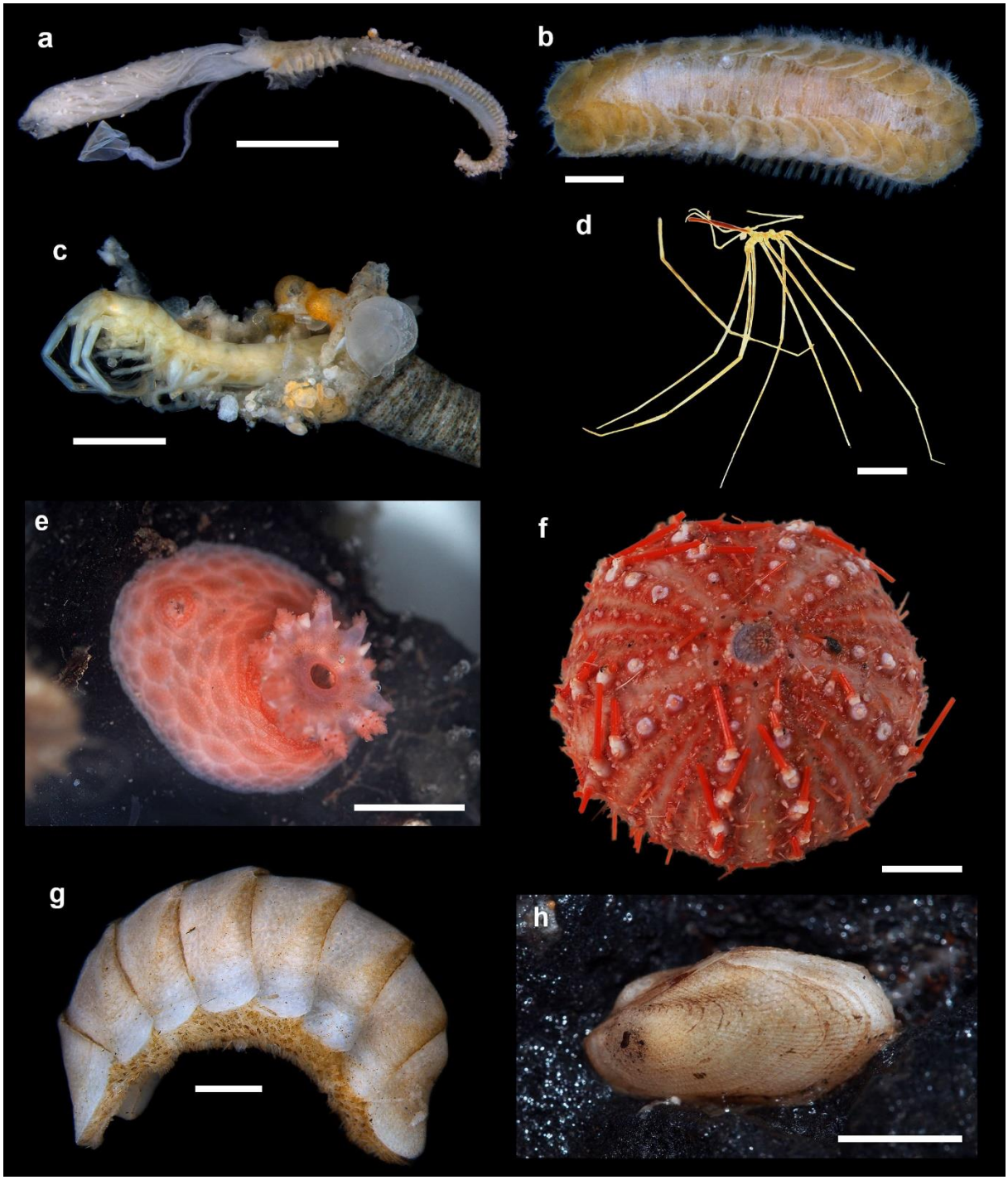

Figure 3.5. Specimens collected with dredges (a–d, f–h) and *HyBIS* (e). Families **(a)** Serpulidae and **(b)** Pholoidae, "Polychaeta". **(c)** *Corophium* sp., Amphipoda. **(d)** *Colossendeis macerrima*, Pycnogonida. **(e)** Family Psolidae, Holothuroidea. **(f)** *Gracilechinus* sp., possibly *Gracilechinus lucidus*, Echinoidea. **(g)** Polyplacophora, possibly *Leptochiton* sp. **(h)** Family Arcidae, Bivalvia. Scales in a and h: 3 mm, b and c: 1 mm, d and f: 20 mm, e: 10 mm, and g: 500 µm.

Amphipoda, Isopoda, and Tanaidacea were collected in lower abundance. Within Arthropoda, we also sampled a few pycnogonids in dredgings (Fig. 3.5d). The phyla Echinodermata and Mollusca had lower abundance compared to others, but were diverse nevertheless, including brittle stars, starfishes, holothurians (Fig. 3.5e), sea

urchins (Fig. 3.5f), solenogasters, chitons (Fig. 3.5g), and bivalves (Fig. 3.5h). We also sampled a few morphotypes from Nemertea, one articulate brachiopod, colonial bryozoans, ascidians, and a benthic fish, *Chaunax suttkusi*.

From the total, 350 specimens (30%) and 54 morphotypes (35%) were associated with other organisms, usually using them as a substrate (not including the epibiotic zoanthids on hexactinellids mentioned above). The main epizooic phylum was Annelida, with 196 individuals and 23 morphotypes (Table 3.2), which were found on sponges (Fig. 3.6a), octocorals (Fig. 3.6b), black corals (Fig. 3.6c), *Enallopsammia rostrata*, and inside tube of other annelids (Fig. 3.5b). But the most abundant relationship was between *Sarostegia oculata* and an annelid inside the lumen of its branches (Fig. 3.6d), possibly *Hermadion fauveli* cf. Gravier (1918). A total of 93 individuals were found in fragments of *S. oculata* in 6 distinct sites. *E. rostrata* was the host with most morphotypes associated (30, 154 individuals) found within its septa (Figs. 3.6e, f, i) and on its surface (Figs. 3.6g, h). Arthropoda represents 47% of the fauna associated with *E. rostrata*, mainly cirripedians (Figs. 3.6e–f) and a few tube-dwelling amphipods, Annelida represents 33%, mostly polychaetes (Figs. 3.6h, i), and we also found a few sponges, sea anemones, solenogasters, and nemerteans. *S. oculata* was the second host with the most morphotypes (16, 131 individuals), including anemones, annelids, crinoids, ophiuroids, and solenogasters. Table 3.2 shows other associations between organisms as well.

Table 3.2. Associated specimens grouped by phylum, showing the number of specimens, number of morphotypes (S), and list of the main hosts where they were found.

Phylum	No. sps.	S	Hosts
Porifera	14	7	*Enallopsammia.rostrata*
Cnidaria	9	6	*Sarostegia.oculata*, *Enallopsammia.rostrata*, Isididae
Annelida	196	23	Demospongiae (multiple), *Aphrocallistes* cf. *beatrix*, *Sarostegia.oculata*, *Bathypathes* sp., *Enallopsammia.rostrata*, Isididae, Zoantharia, Serpulidae (empty tubes)
Arthropoda	96	7	Demospongiae, *Enallopsammia.rostrata*, Isididae, Pycnogonida
Echinodermata	15	3	Demospongiae, *Aphrocallistes* cf. *beatrix*, *Sarostegia.oculata*
Mollusca	11	5	Demospongiae, Actiniaria, *Enallopsammia.rostrata*, *Sarostegia.oculata*
Others	9	3	*Sarostegia.oculata*, *Enallopsammia.rostrata*

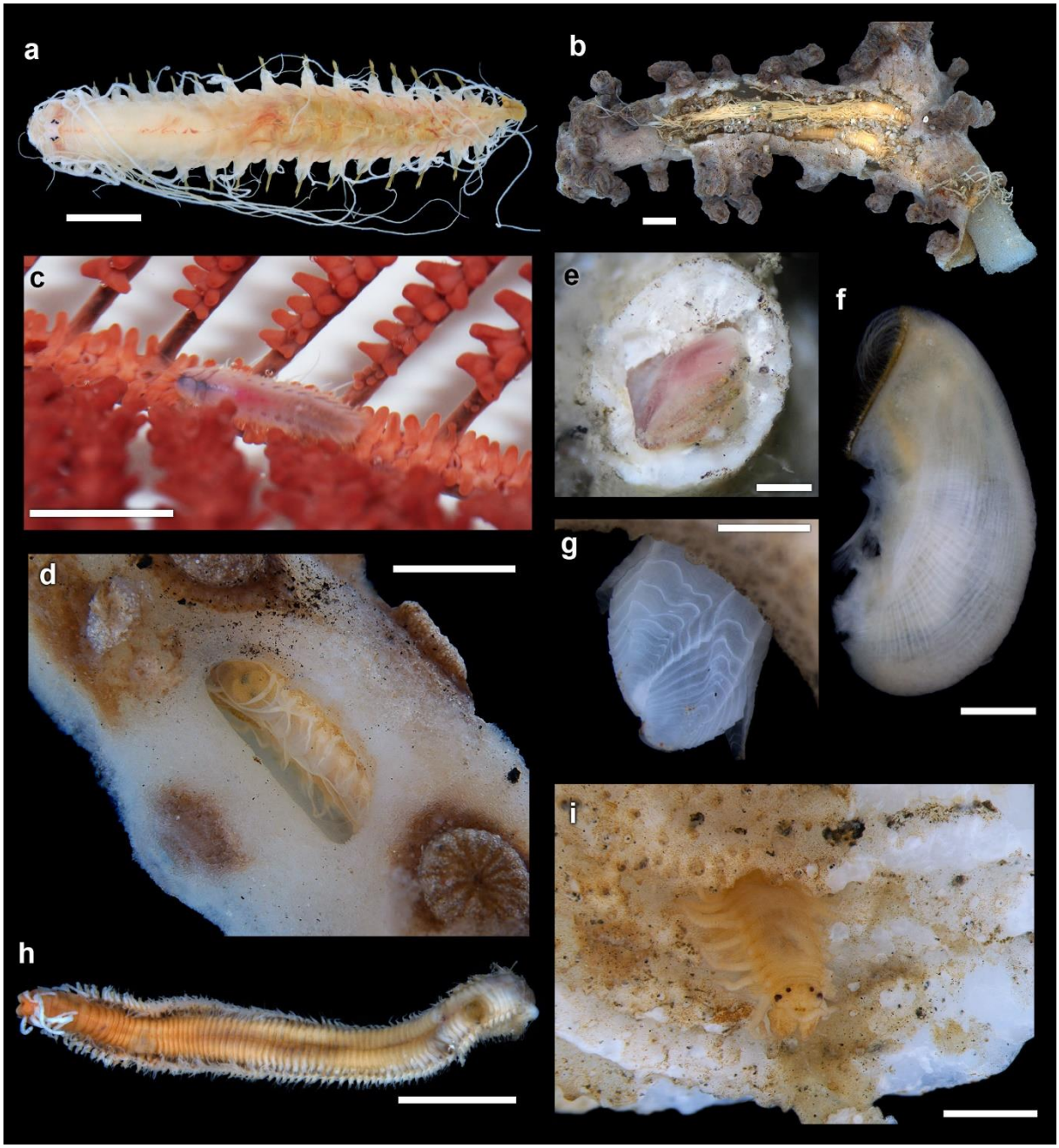

Figure 3.6. Specimens associated with *Aphrocallistes* cf. *beatrix* (a), between a zoanthid growing in a hexactinellid branch (b), black coral *Bathypathes* sp. (c), inside *Sarostegia oculata* (d), and *Enallopsammia rostrata* (e–i). Families **(a)** Hesionidae, **(b)** Terebellidae, **(c)** Polynoidae, **(d)** Polynoidae, possibly *Hermadion fauveli*, and **(e)** Family Lithoglyptidae, Acrothoracica, inside the coral. **(f)** Same as (e), after being removed from the coral. **(g)** Thoracica. Families **(h)** Eunicidae and **(i)** Syllidae. Scales in a–c, h: 5 mm, d: 2 mm, e–g: 1 mm, and i: 500 µm.

Corals and sponges are important ecosystem engineers, as they provide substrate and an environment for various other organisms (Ashford et al., 2019). These animals have great ecological importance and are considered indicators of vulnerable habitats that should be prioritized for the selection of protected areas (Levin et al., 2016). Our results confirm the presence of such species in samples collected at RGR

and illustrate a diverse fauna that is associated with corals and sponges. This suggests that species like *E. rostrata* and *S. oculata* provide important ecosystem functions in the area, which should be considered when defining management plans and conservation areas within RGR in the future.

3.3.2 Statical analysis

Dredges lengths ranged greatly from 168 m to 7.5 km (average 2092 m, Table 3.1). Regressions showed no significant correlation ($p > 0.79$) for transect distance with abundance and richness, ANOVA showed no significant difference in abundance and richness between dredge types ($p > 0.67$), and PERMANOVA indicated that neither transect distance and dredge type significantly explained community structure ($p > 0.1$). The GLMs showed no evidence of distinct abundance ($p > 0.24$) and morphotype richness ($p > 0.23$) in the dredges between north and south plateaus and trends with Fe-Mn crusts coverage, rift distance, depth, slope, and mean direction. Dredges sampled a mean 23.7 individuals/dredge in the north plateau and 45.4 individuals/dredge in the south, but the variation in abundance observed in the dredges was too high for this difference to be statically significant. The accumulation curves (Fig. 3.7) did not reach an asymptote, suggesting that many species were not sampled and overall diversity is underestimated, thus a higher sampling effort is required in future studies. It also suggests a higher morphotype richness in the south plateau, which was not significant either.

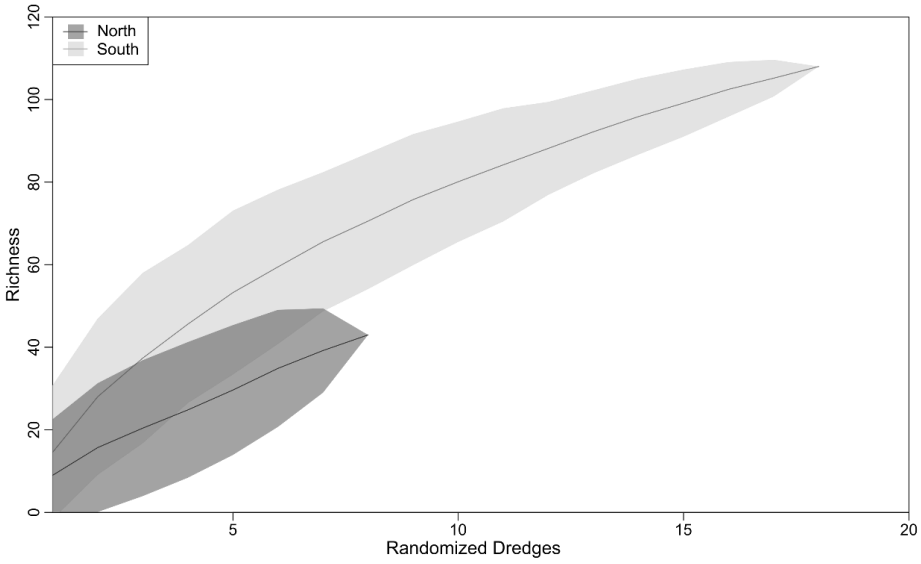

Figure 3.7. Morphotype accumulation curve for the dredges in the north and south plateaus (except dredges RGR1-D02, D03, D04, D11, and D12).

The test for homogeneity of dispersions was significant (F = 10.781, *p* = 0.003), and PERMANOVA showed evidence for distinct faunal composition between north and south plateaus (R^2 = 0.094, *p* = 0.001) and within distinct depth (R^2 = 0.057, *p* = 0.034). The nMDS ordination plot (Fig. 3.8a) illustrates that dredges were grouped in distinct plateaus, and the south plateau is more dispersed around the centroid. PERMANOVA can confound location and dispersion effects, leading to a false detection of location effect when there is evidence of dispersion effect. Hence, results of the PERMANOVA should be interpreted carefully, but the nMDS suggests a location effect as well as a dispersion effect. The north plateau had a larger relative abundance of sponges and cnidarians, while the south had a larger relative abundance of annelids, arthropods, and echinoderms (Fig. 3.8b).

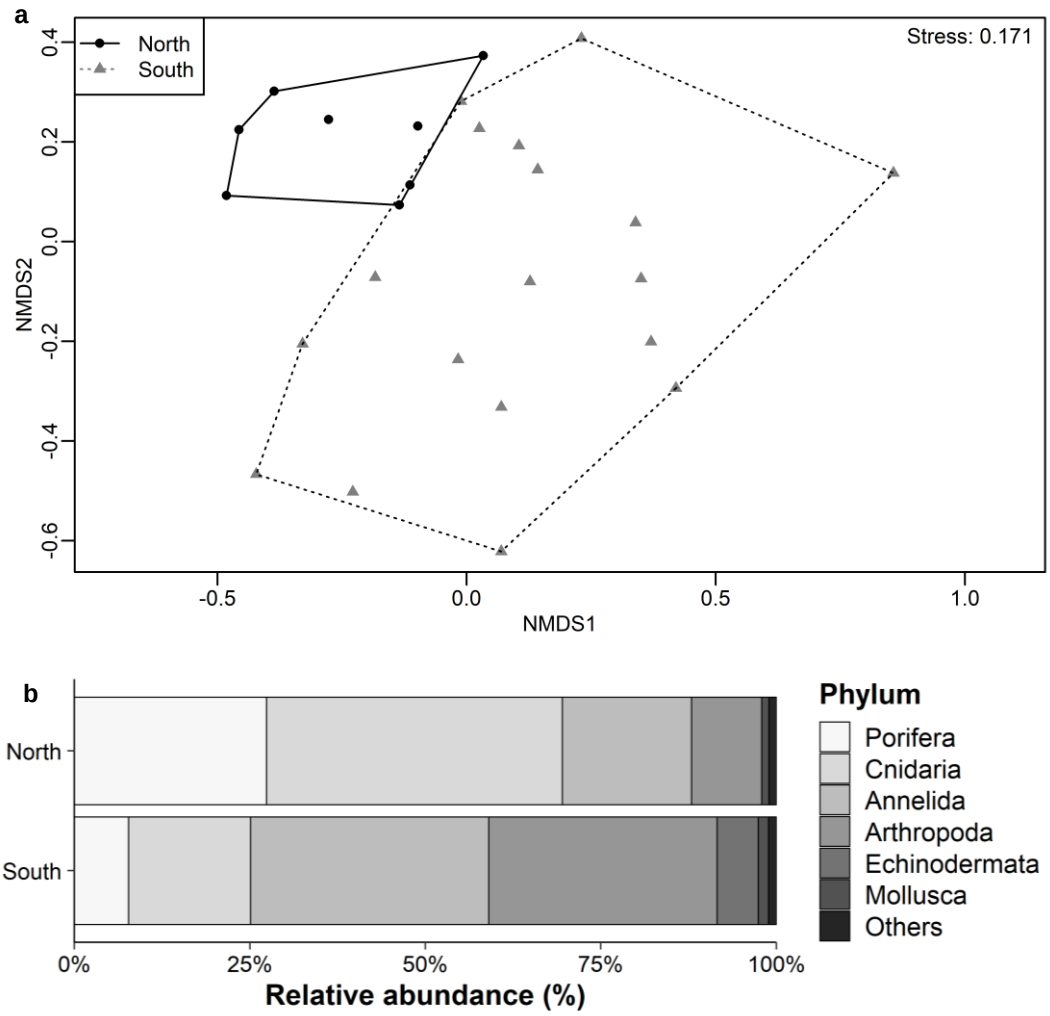

Figure 3.8. (a) Ordination plot (nMDS) of the dredges on Rio Grande Rise (except RGR1-D02, D03, D04, D11, and D12). Symbol and color indicate from which plateau (north or south) the dredge was sampled. **(b)** Relative abundances of each phylum sampled in the north and south plateau.

Data collected by dredges are semi-quantitative, which makes it difficult to compare from one dredge to another. The transects distances are different and dredging efficiency varies greatly with substrate type and relief. In addition, rock dredges are made to forcefully remove rocks from outcrops, which cause damage to organisms, as seen in larger specimens such as sponges, and possibly loss of animals during dredging. Thus, the biodiversity reported here is likely to be just a fraction of the benthic fauna that exists in the area. An alternative method to compare the dredges is to use rarefaction curves (O'Hara & Tittensor, 2010). However, this method requires a large number of individuals to be collected in multiple sites, and in this study the abundance of specimens was heterogeneous, with several dredges collecting only a few individuals. In both cruises, dredges were performed near the rift border, which is the region most likely to find Fe-Mn crusts and the main scope of the project. However, future surveys should aim for a more sparse and evenly distributed sampling strategy in order to capture the fauna in a broader range of habitats and better test how environment variables are related to fauna composition.

4 Benthic megafauna habitats, community structure and environmental drivers at Rio Grande Rise (SW Atlantic)

Abstract

The Rio Grande Rise (RGR) is a large and geomorphologically complex feature located in the Southwest Atlantic, with great commercial and scientific interest due to its potential for mining rare earth elements that are critical for low-carbon technologies. Brazilian interest in this area led to the submission of a petition to the UN Commission on the Limits of the Continental Shelf in 2018 to include RGR on the limits of its continental shelf beyond 200 nautical miles. However, mining activities are potentially harmful to deep-sea ecosystems and will likely cause some extent of biodiversity loss. Thus, baseline and continuous environmental studies in the RGR are important to address potential conflicts between mineral extraction and the conservation of deep-sea biodiversity. The RGR is characterized by a series of summit plateaus of ~600 m deep divided NE-SW by a rift valley, up to 2000 m deep. In 2018, the plateaus and rift of a small area in RGR (30º35'S–31°03'S, 35º36'W–36°16'W) were explored through 13 dives of the Robotic Underwater Vehicle (*RUV*) *HyBIS*. Videos were analyzed for the description of structuring factors (topography and habitat types) and to record benthic megafauna occurrences. Video transects revealed highly heterogeneous and rapidly changing habitats. Eleven habitats, five in the rift and six in the plateaus are proposed based on geomorphology, slope, and substrate textures. We recorded 17,008 megabenthic organisms classified in 83 morphotypes and six different phyla, from which Porifera (42.7%) and Cnidaria (41.5%) were the most representative. Samples were characterized by a high dominance and the dissimilarities result chiefly from differences in abundance scores. PERMANOVA tests indicated that Habitat and Region variables were the most important to explain structure within the community data, followed by depth and slope. The rift floor exhibited a low abundance of megabenthic epifauna, except in a sinkhole in the northern part of the rift. The lower and upper rift walls were characterized by different communities delimited by the transition between the Antarctic Intermediate Water and the Upper Circumpolar Deep Water. The habitats formed by Fe-Mn deposits were dominated by distinct communities, which were rarely observed elsewhere. Additionally, we found variations in community structure at regional scales (20–30 km), with distinct communities on

each side of the rift and at the southwest of the study area. Our results contribute toward understanding the diversity, biogeography, and environmental drivers of the RGR. Fauna distribution is patchy, linked to habitats with potential mining resources, and dominated by Vulnerable Marine Ecosystems (VMEs) indicator taxa. Extensive community analysis should occur at a given site prior to consideration for the exploitation of natural resources.

Keywords: Biodiversity. Invertebrates. Geomorphology. Fe-Mn crusts. Deep-sea mining.

4.1 Introduction

The deep sea is the largest environment on the planet, the ocean floor representing 63% of its entire area (Thurber et al., 2014) with a large potential for living and non-living resources (Herzig & Hannington, 1995). It exhibits one of the highest biodiversities on the planet (Mora et al., 2011; Ramirez-Llodra et al., 2010), much of it related to the heterogeneity of habitats, such as seamounts, continental margins, abyssal plains, ocean trenches, and particularly "extreme" physical-chemical environments such as hydrothermal vents and cold seeps. However, there are various challenges to study the deep sea, including those related to the high costs and complex logistics involved in expeditions. Therefore, there are large extensions of deep seafloor that are still little known to science, including important gaps in its biodiversity and ecology (McClain & Hardy, 2010; Perez et al., 2012).

Interest in deep-sea benthic environments has increased mainly owing to the search for commodities such as oil and gas, seafood, and high-tech minerals (Glover & Smith, 2003). The latter include rare-earth elements which are used in various applications, such as the manufacture of batteries, wind turbines, and solar panels (Hein & Koschinsky, 2014). Thus, there is a growing demand in the market for the consumption of these elements (Thompson et al., 2018). Deep-sea mining is a potential multibillion-dollar industry, expected to become operational in all the world's oceans within the next few decades, and it will invariably induce pressures in these uncharted environments (Hein & Koschinsky, 2014; Manceau et al., 2014).

In this scenario, the Rio Grande Rise (RGR) has gained special attention of researchers and governments around the world due to its mining potential for

ferromanganese crusts (Fe-Mn). RGR is an extensive seamount region located between Brazil and Argentine basins (J. A. D. Cavalcanti et al., 2015) with origin commonly associated with an intense basalt spill in the Tristan da Cunha mantle plume (South Mid-Atlantic Ridge) about 75 million years ago. This event also gave rise to Walvis Ridge on the eastern side of the South Atlantic (Montserrat et al., 2019; O'Connor & Duncan, 1990). However, this hypothesis has been re-examined recently (Alberoni et al., 2020; Constantino et al., 2017; Graça et al., 2019). Most of the knowledge about RGR geology was collected during the *Deep-Sea Drilling Project* (DSDP) in the mid-1980s (P. F. Baker, 1983) and just in the last ten years, more expeditions were made in this area. The genesis of Fe-Mn crust deposits is still being discussed (Benites et al., 2020, 2021; Mohriak et al., 2010; Ussami et al., 2013).

The Brazilian government has a particular interest in this region. In 2015, the International Seabed Authority (ISA) and the state-owned Geological Survey of Brazil (CPRM) signed a 15-year contract for the exploration of 3,000 km² in RGR (ISA, 2014; Montserrat et al., 2019). In 2018, the Brazilian government submitted its petition to the UN Commission on the Limits of the Continental Shelf (CLCS) to incorporate the RGR to the limits of its continental shelf beyond 200 nautical miles (LEPLAC, 2018). CLCS recommendations are thought to occur within the next few years and, if approved, RGR would be incorporated into Brazil's Economic Exclusive Zone.

Mining activities are potentially harmful to deep-sea ecosystems and will very likely cause some extent of biodiversity loss (Miller et al., 2018; Montserrat et al., 2019; Van Dover et al., 2017). Impacts include the direct removal of Fe-Mn crusts, increased sediment loads caused by mining tailings, release of wastewater at the sea surface (Hughes et al., 2015), and disturbance by noise. Given the lack of knowledge and species distribution data in the area these activities may result in the removal of potentially undescribed species and the full impact will be unknown. Hence, baseline and continuous environmental studies on the sites and their surrounding areas before and during mining activities are important (Dunn et al., 2018). Data on fauna and community structure are essential so that mining activities remain sustainable and guarantee the protection of the deep-sea environment (E. Baker & Beaudoin, 2013). Valuable information about the vulnerability of habitats in the deep sea will provide supporting evidence in the creation of marine protected areas (Wedding et al., 2013) that will safeguard biodiversity and ecosystem function near mining sites (Guilhon et al., 2021).

At present, there are only fragmented biological data on RGR (Perez et al., 2012) that include fish records produced by Russian exploratory fishing from 1974 to 1988–1989 (Clark et al., 2007; Perez et al., 2012) and data from OBIS and GBIF databases (Montserrat et al., 2019). Recently, accounts on sponge gardens, dominated by the hexactinellid *Sarostegia oculata* (Hajdu et al., 2017), and benthopelagic fauna, limited to fishes and crustaceans (Perez et al., 2018) came to our knowledge. Demersal and longline fishing are also known to occur in the region (Morato et al., 2016), including the pelagic blue shark (*Prionace glauca*) and swordfish (*Xiphias gladius*) (Mourato et al., 2011) and the demersal alfonsino (*Berix splendens*) (Perez et al., 2012), representing additional human uses that may be compromised by deep-sea mining. Therefore, studying the biodiversity and understanding the ecological patterns of RGR communities are imperative during the following years to mitigate human impacts and better preserve this unique ecosystem.

4.2 Material and methods

4.2.1 Study area

The Rio Grande Rise is a complex positive feature located between the Argentine and Brazilian abyssal basins (28°S–35°S; 28°W–39°W), approximately 1200 km off the Brazilian coast and 2000 km off the Mid-Atlantic Ridge (Montserrat et al., 2019). It corresponds to the largest submarine elevation in southeastern Brazil (~480,000 km²), rising from depths of 5000 m to peaks less than 600 m (Mohriak, 2020). RGR is usually divided into two sub-regions (Fig. 4.1a): (1) the Western Rio Grande Rise (WRGR) is characterized by a large ellipsoidal bulge that rises to a mean depth of about 2000 m and (2) the Eastern Rio Grande Rise (ERGR) with a north-south elongated geomorphology, delimited by E-W fractures in both north and south ends. There is a characteristic NW-SE rift structure formed on top of the bathymetric high (sometimes also referred to as ‘graben’ in the literature), creating a deep submarine channel, also called Cruzeiro do Sul rift.

The rift extends along the center of WRGR to the southern of the ERGR (Fig. 4.1a). It provides an extremely steep slope up to the rim of the RGR plateaus, where Fe-Mn crusts are more common (Montserrat et al., 2019). Due to the large size of RGR, sampling was focused in a small area in the middle of WRGR, between latitudes

30º35’S–31°03’S and longitudes 35º36’W–36°16’W (Fig. 4.1b). The rift bottom in the study area is up to 1,500 m deep and 22 to 33 km wide. On both sides of the rift there are plateaus, ranging from 600 to 700 m depth, that extends beyond the study area.

Three water masses are found in the study region: the South Atlantic Central Water (SACW), the Antarctic Intermediate Water (AAIW), and the Upper Circumpolar Deep Water (UCDW) (da Silveira et al., 2020; Jovane et al., 2019; Peterson & Whitworth, 1989; Stramma & England, 1999). The shallowest portion of the studied area (ca. 100–600 m depth) is bathed by the SACW, which originates in the South Atlantic Subtropical Gyre, characterized by a local oxygen minimum (~4.7 mL/L O_2). Below the SACW, the AAIW is present, being characterized by a minimum salinity and maximum oxygen (~5.1 mL/L O_2) at around 800–900 m. AAIW, originating from the Subantarctic Front, is considered nutrient-rich and it ranges from 600 to 1100 m depth. The UCDW originates between the Subantarctic and the Polar Fronts and it is identified by a second local oxygen minimum (~4.2 mL/L O_2) together with a silicate maximum, ranging approximately from 1100 m to 1600 m depth.

4.2.2 Data collection

Data was collected during the DY094 expedition of the *RRS Discovery* (National Oceanography Centre, Southampton, UK) as part of the FAPESP/RCUK funded project Marine E-Tech, from October 26 to November 8, 2018. The expedition included 13 dives of the Robotic Underwater Vehicle, *RUV HyBIS* (Murton et al., 2012), used to collect physical samples and video footage of the seafloor (Fig. 4.1b-g). *HyBIS* was equipped with a Sony Full HD camera that recorded over 36 hours and 26 km of the seabed (Table 4.1) and a robotic arm used to collect 10 voucher specimens from the most abundant representatives found during the survey. *HyBIS* was connected to the ship USBL system to record its position (latitude, longitude, and depth). Multibeam echosounder and backscatter data were acquired using a ship-mounted Kongsberg EM122. Multibeam processing was done using Caris HIPS and SIPS v9.1.8 and the data were gridded at 15 m. Backscatter processing was done with FM Geocoder Toolbox v7.8.3 and the data were gridded at 5 m.

A set of additional seafloor variables was derived from the bathymetric data using the Benthic Terrain Model 3.0 tool (Walbridge et al., 2018) in ArcGIS 10.8. These variables were slope, aspect (measured in terms of northness and eastness),

roughness (11 neighborhood size), curvature, fine-scale (3/30 radius) Bathymetric Position Index (BPI), and broad-scale (20/200 radius) BPI. Neighborhood size and radius were chosen to minimize correlation between variables.

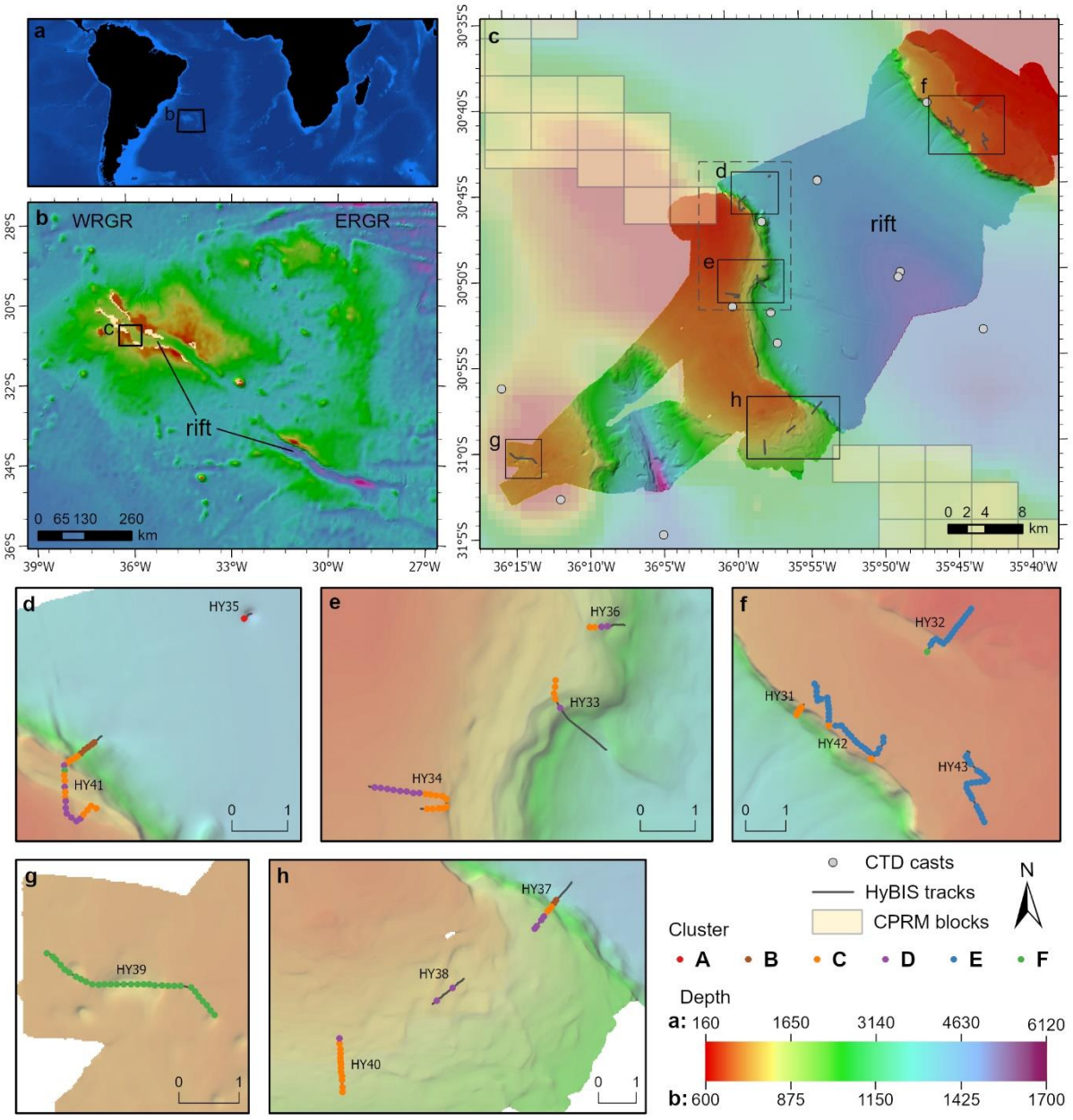

Figure 4.1. (a) General South Atlantic view and area where the Rio Grande Rise is located. **(b)** Rio Grande Rise, South Atlantic. WRGR - Western Rio Grande Rise and ERGR - Eastern Rio Grande Rise. **(c)** Study area and bathymetry data acquired during the DY094 expedition in the *RSS Discovery*, and CTD casts made during the *N/Oc. Alpha Crucis* expedition, 2018. Black rectangles represent the extent area of the panel with its corresponding letter. Yellow rectangles represent exploration contract between ISA and CPRM. **(d-h)** *HyBIS* dives (HY-- codes) from the DY094 expedition. Greyed lines are the RUV tracks and each dot is a 120 m long segment extracted from the track. Dot colors represent clusters in which the segment was assigned (see results). Scales are in kilometers. **(d, e).** Center region. **(f)** Northeast region. **(g)** Southwest region. **(h)** South region.

HyBIS videos were analyzed in two steps. Firstly, we annotated seafloor characteristics according to geomorphology, slope, and substrate textures following the classification system proposed by Greene et al. (1999, 2007), similar to the classification made by (Perez et al., 2018) on adjacent areas in RGR. Habitats, observed along with the RUV dive, were defined based on a unique combination of these features. Habitats were classified in three spatial scales: (1) 'Subsystem' (tens of kilometers to a kilometer), (2) 'Class' (a kilometer to tens of meters), and (3) 'Subclass' (one to tens of meters). We only considered a transition from one habitat to another when their features changed abruptly (~10 s) and remained changed for at least 30 seconds. Secondly, we annotated and counted the benthic fauna directly from the videos in a macro-enabled Microsoft Excel file, which supports reading timestamp from the video player and opening a video in at any specific annotation. Records were classified in the lowest possible taxonomic group and identified to morphotypes based on morphological features observed in the images, except for cases where identification to the species level was possible. Highly motile fish and crustaceans were noted but not included here, as distinct drivers may affect this fauna and will be subject of future studies. Observations and morphotypes classification were double checked to ensure consistency in the video annotations. Voucher specimens were collected to improve identification of morphotypes. We assigned a unique code for each morphotype/species, composed of four letters and one number. The number of records from the videos was used as abundance and the count of morphotypes as species richness.

In addition, data from a previous expedition to RGR on board the *N/Oc. Alpha Crucis* in February 2018, also as part of the Marine E-Tech Project, were used. During this cruise, 13 CTD casts (stations 468 – 497, see Jovane et al., 2019 for details) were made in the study area to record water column properties, namely Temperature (°C), Salinity (PSU), and Oxygen (mg/L). Each cast was averaged in 10 m depth bins and calculated by draping the RUV depth in each bin and interpolating using the IDW function of the gstat package (Gräler et al., 2016) in R.

4.2.3 Data analysis

All statistical analyses were performed in R, version 4.0.3 (R Core Team, 2020), and package *vegan* for community and multivariate analysis (Oksanen et al., 2019).

Permutation tests were made using 9,999 permutations and a restricted permutation of type series within each dive to account for dependence of the data. Graphs were made using the *ggplot2* package (Wickham, 2016).

HyBIS tracks were divided in segments (samples) to conduct quantitative analysis. These segments followed the previously defined habitat delimitation to assure that no segment would cover two distinct habitats. Segments were allowed to vary down to 80% of the segment size to ensure the track was covered by the segments as much as possible. Segments with lower than 20 faunal observations were removed from further analysis as they bear little information about the community in these areas. Multiple threshold lengths for the segments were tested and we chose the one that accounts for the most abundance overall (Fig. 4.3). Smaller values generate more fragmented segments with lower abundance and more segments are discarded for not having a minimal 20 observations. On the other hand, larger values generate fewer longer segments, but more regions are discarded for not having the minimal length required.

We grouped *HyBIS* dives based on the region within the study area they were made (Fig. 4.1). “Northeast” as dives HY31, HY32, HY42, and HY43 on the northern side of the rift; “Center” as dives HY33, HY34, HY35, HY36, and HY41 on the west side of the rift; “South” with dives HY37, HY38, and HY40 in the south of the rift; and “Southwest” as the single dive HY39 in the southwest extreme of the study area.

We plotted species accumulation curves and richness estimators with samples randomized 1000 times to analyze the overall diversity that was detected in the videos, namely Chao1, First-order jackknife, ACE, and Bootstrap (Magurran, 2004). Community data was log-transformed using R function *log1p* to decrease the influence of abundant species. Then, we calculated Bray-Curtis dissimilarities (also referred to as percentage difference) to compare changes in communities along with samples. We used Unweighted Pair Grouping Method with Arithmetic Mean (UPGMA) clustering to identify segments with similar community structures within the study area. Fusion levels and silhouette plots were used to identify the optimal number of clusters, following the methods described by Borcard et al. (2018). The obtained community clusters were validated by using non-metric Multidimensional Scaling (nMDS) ordination technique, which makes a 2-dimension representation of morphotype composition similarities among all samples.

The identified clusters were then characterized based on their most abundant taxa and Indicator Value indices (IndVal) (Dufrêne & Legendre, 1997). The IndVal method is aimed to compare the association between species patterns and combinations of groups of sites and identify species that can be used to discriminate a group of samples from all other samples in the analysis. The Multilevel pattern analysis was carried out with the *indicspecies* package (Cáceres & Legendre, 2009) using IndVal as a function with a correction for clusters with different sizes. Furthermore, clusters were characterized based on the regions and habitats they were more predominant and by using univariate diversity measures, mean abundance, richness (S), Shannon index ($H'_{\log e}$), and Pielou's evenness (J) (Pielou, 1966). We used a chi-square test to check a significant association between the clustering typology to distinct regions and habitats.

Collinearity between environment linear variables (derived from multibeam data plus CTD casts) was checked using Pearson's rank correlation coefficient and variables with a high correlation (> 0.7) were removed from further analysis. Effects of habitat, region, and linear variables in the community data were tested with PERMANOVA (M. J. Anderson, 2001; McArdle & Anderson, 2001) using the *adonis2* function with terms added sequentially. We used the PERMDISP2 (M. J. Anderson, 2006) to verify the homogeneity of dispersions of habitat and region groups, as otherwise, PERMANOVA can result in false detection of a difference of means. We made violin plots of the variables that significantly explained the variance in the community grouped by the clusters and used a non-parametric Kruskal-Wallis test (Kruskal & Wallis, 1952) and its corresponding post-hoc comparisons (with Holm correction) to compare the selected variables between the community clusters (Borcard et al., 2018). We previously used ANOVA, but the test failed its assumptions.

Finally, we carried out a Multivariate Regression Tree analysis (MRT) (De'ath, 2002). The method is an extension of Classification and Regression Tree analysis (CART) to multivariate data. It tries to identify discontinuities in the response data, e.g. community composition, and associate these discontinuities to specific values of the explanatory data, e.g. environmental data. The analysis was carried out using the *mvpart* package (De'ath, 2002; Borcard et al., 2018) with Hellinger transformed abundance data, as other dissimilarities (e.g. Bray-Curtis) are not fully implemented in the method, and environment variables with significant effect in the PERMANOVA test. The optimal size of the tree (i.e., the number of leaves) was decided based on the

Cross-Validation Relative Error (CVRE) closest to one standard error of the smallest CVRE value. Ten folds were used in cross-validation, repeated 100 times.

4.3 Results

4.3.1 Habitat classification

We observed 11 habitats during the *HyBIS* dives differentiated by depth, slope, and substrate type (Fig. 4.2, Table 4.1, and Table 4.2). Five were found in the rift and six on the plateaus. The rift floor was filled with soft sediment and Fe-Mn coated pieces of corals (mostly Isididae) and cobbles on top (RiftDeb, Fig. 4.2a) or by pteropods shells and forams (RiftSed, Fig. 4.2b). The latter was found next to rift walls on dives HY33 and HY37, but not in dive HY41, in which RiftDeb was next to the rift wall. Both habitats had a smaller number of animal sightings when compared to other areas of RGR (Table 4.1). The northwest end of the rift featured a sinkhole, which was observed during the dive HY35. The bottom of the sinkhole was composed of soft sediments, like other areas of the rift, and its wall was composed of layered calcareous chalks (RiftHole, Fig. 4.2c). The rift wall on both sides was steep, varying from 30° to 60°, and was almost vertical at its upper half. Walls were mainly composed of exposed basaltic outcrops near the bottom (RiftRock, Fig. 4.2d) and irregular Fe-Mn crusts or Fe-Mn coated outcrops near the top of the rift (RiftCr, Fig. 4.2e). The transition from one substrate to another was not well defined and it occurred at multiple depths across dives. The plateaus were flat (0° to 10°) with an abrupt chasm from the rift in most places.

The plateaus area was partially composed of soft sediment with conspicuous ripple marks, pteropods shells, and foraminiferal tests (Sed, Fig. 4.2f). However, three habitats were the most common during our survey (Table 4.1). One was composed of large pavements of carbonate rock and seemingly exposed to strong current flux (CalPav, Fig. 4.2g). The second is formed by large plate-like Fe-Mn crusts (CrPav, Fig. 4.2h). The third is composed of these two substrates, with plate-like crusts intermingled by calcarenite pavements and often with sediment pools (CrSed, Fig. 4.2i). During Dive HY32, we observed two more habitats that were almost exclusive of the northeast of the study area. Above the terrace at the northeast area of the dive was formed by irregular volcanic outcrops with Fe-Mn crust cover and a few sediment pools (Cr, Fig.

4.2j), similar to the substrate found in the RiftCr. The area below the terrace on dive HY32 and in a small segment of dive HY39 (which were not included in the analysis due to its small size) was composed of pavements of carbonate rock with fields of Fe-Mn coated cobbles and small boulders (CrCob, Fig. 4.2k). Outcrops with hardground rocks of volcanic and other origin have been recognized, but they were not long enough to be classified as a single habitat. Habitat classification and modifiers can be seen in Table 4.2. Habitats RiftSed, RiftRock, CalPav, Cr, Sed, and CrPav are respectively similar to GB, GW, SCA, SCR, SSD, and SCT in Perez et al. (2018).

Table 4.1. Benthic habitats observed during the *HyBIS* survey in the DY094 cruise in Rio Grande Rise (SW Atlantic). See Table 4.2 for a description of each habitat and Fig. 4.2 for a visual reference of each region. "Moving ahead time" ignores time spent when *HyBIS* was stopped collecting samples or performing system checks. Note that number of segments, time, distance, and number of records were pooled for habitat and region. Number of segments refers only to continuous segments above the threshold of 96 m long (80% of 120 m) and 20 records.

Habitat	Region	Dives	# segments	Moving ahead time	Distance (m)	# records
Rift Coral Debris (RiftDeb)	Center	33, 41	0	00:40:32	443.9	29
	South	37	0	00:52:31	574.1	29
Rift Floor Sediment (RiftSed)	Center	33, 35	0	01:10:05	840.1	43
	South	37	0	00:14:02	127.3	31
Rift Sinkhole (RiftHole)	Center	35	1	00:35:56	167.7	154
Rift Wall (RiftRock)	Center	33, 36, 41	18	03:42:41	2494.5	1171
	South	37	2	00:34:31	437.7	96
Rift Wall Crusts (RiftCr)	Center	34, 36, 41	7	01:04:30	871.8	1414
	Northeast	31	5	00:49:32	584.2	1268
	South	37	3	00:24:51	331.9	351
Sediment (Sed)	Northeast	32, 42, 43	11	02:43:38	1792.1	429
	Southwest	39	5	00:43:49	631.5	408
Calcarenite Pavement (CalPav)	Center	34, 41	18	02:59:10	2184.7	1026
	Northeast	32	1	00:07:30	124.8	60
	South	37, 38	6	02:28:46	1722	350
	Southwest	39	26	03:18:13	2821.5	4589
Crust Pavement (CrPav)	Center	33, 34	10	01:26:52	1206.8	1246
	Northeast	31, 42, 43	14	02:53:53	1921.6	624
Crust Sediment (CrSed)	Northeast	42	28	04:44:20	3361.2	1177
	South	40	13	02:18:01	1690.7	1261
Crust (Cr)	Northeast	32	10	01:24:25	1107	915
Crust Cobble (CrCob)	Northeast	32	5	00:50:59	583.9	306
	Southwest	39	0	00:03:10	50.6	31
Total			**183**	**36:11:57**	**26071.6**	**17008**

Table 4.2. Classification and description of benthic habitats observed in Rio Grande Rise (SW Atlantic). The classification system is in accordance with the scheme proposed by Greene et al. (1999), based on the DTM of the area and in-situ video data. Mean depth (m) and slope (°) are provided in round brackets in subsystem and subclass respectively. Values after semicolons are minimum and maximum, respectively.

Habitat	Subsystem	Class	Subclass	Modifiers
RiftDeb	Rift floor (1311.4; 1197–1396)	Debris Field	Sloping (13.8°) Sand with pebble and corals debris	Contiguous Fe-Mn coated coral (Isididae) debris on top of soft sediment Scattered Fe-Mn coated pebble
RiftSed	Rift floor (1250.0; 1021–1486)	Bedform, Sediment waves	Sloping (13.9°) Mixed sand and ooze	Undulated surface and Ripples (≈ 10 cm in amplitude), thick, semi to well consolidated Scattered thin deposition of pteropods shells and forams Occasional sparsely cobbles and coral debris Regular calcarenite pavement underlying
RiftHole	Rift floor (1449.0; 1419–1489)	Scarp Wall	Steeply Sloping (35.9°) Bedrock - Igneous	Wall of a sinkhole in the floor of the Rift Layered calcareous chalks Scattered deposition of sediment near the top of the hole
RiftRock	Rift wall (941.6; 708–1268)	Scarp Wall	Sloping to Steeply Sloping (21.2°) Bedrock - Igneous	Irregular volcanic outcrops (basalts) Scattered fractures Scattered thin deposition of sediment accumulated in cracks and crevices Occasional boulders or Fe-Mn crusts debris
RiftCr	Rift wall (882.3; 709–1114)	Scarp Wall	Steeply Sloping (38.8°) Bedrock - Fe-Mn crust	Irregular Fe-Mn crust or Fe-Mn coated outcrops Scattered thin deposition of sediment accumulated in cracks and crevices Patchy distribution of *Sarostegia oculata*
Sed	Plateaus (701.5; 668–810)	Bedform, Sediment waves	Flat (2.5°) Mixed sand and ooze	Undulated surface and Ripples (≈ 10 cm in amplitude), thick, semi to well consolidated Scattered thin deposition of pteropods shells and forams Occasional sparse cobbles Regular calcarenite pavement underlying
CalPav	Plateaus (751.9; 679–921)	Flat	Flat to Sloping (7.5°) Pavement - Calcarenite	Regular calcarenite pavement Occasional Fe-Mn coated boulders Dusting sediment cover Patchy distribution of black corals, sea urchins, and other suspension feeders
CrPav	Plateaus (707.4; 664–906)	Flat	Flat (5.3°) Pavement - Fe-Mn crust	Regular Fe-Mn crusts pavement Scattered dusting or thin sediment cover Occasional step-like structures (< 1m in height), with calcarenite on bottom and Fe-Mn crusts on top Most likely target area for exploration Patchy distribution of *Sarostegia oculata*
CrSed	Plateaus (740.3; 687–865)	Flat	Flat to Sloping (2.2°) Mixed Fe-Mn crust Pavement and sand	Mixed Regular Fe-Mn crusts with calcarenite pavement, alternating every 5-10 m Often deposition of thin to thick sediment Scattered ripple marks on the sediment Fauna often fixed on Fe-Mn crusts
Cr	Plateaus (636.3; 627–688)	Exposure - outcrops	Flat to Sloping (3.8°) Bedrock - Fe-Mn crust	Irregular volcanic outcrops with Fe-Mn crust cover Scattered thin deposition of sediment Patchy distribution of sponges and brisingid sea stars
CrCob	Plateaus (702.3; 688–746)	Flat	Flat to Sloping (3.6°) Fe-Mn cobble field	Contiguous Fe-Mn coated cobbles and small boulders (< 60 cm) on top of regular calcarenite pavement and red clays Scattered deposition of thin to thick sediment cover

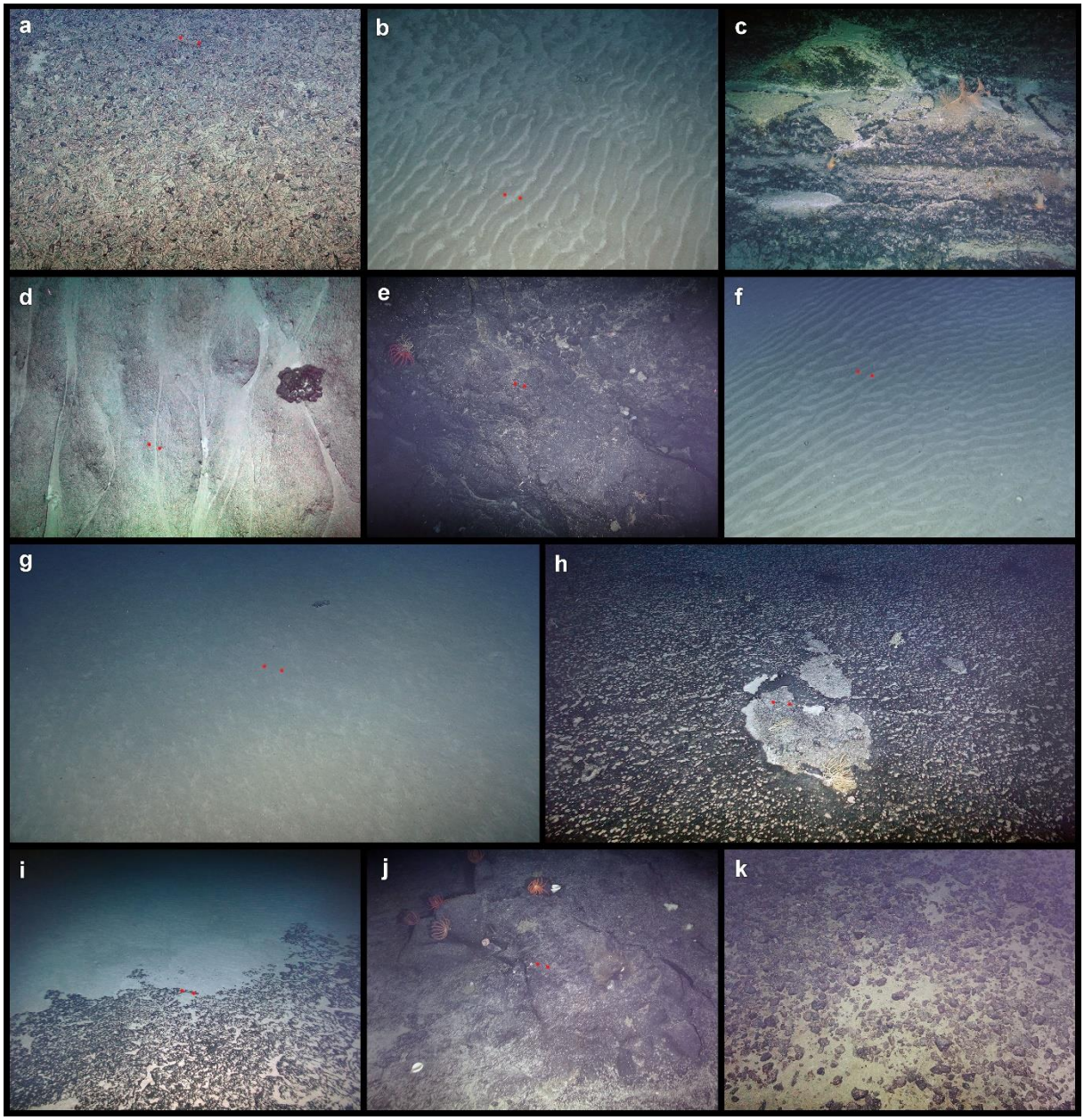

Figure 4.2. Benthic habitats observed in Rio Grande Rise (SW Atlantic). **(a)** Rift Coral Debris (RiftDeb), HY33. **(b)** Rift Floor Sediment (RiftSed), HY33. **(c)** Rift Sinkhole (RiftHole), HY35. **(d)** Rift Wall (RiftRock), HY33. **(e)** Rift Wall Crusts (RiftCr), HY41. **(f)** Sediment (Sed), HY43. **(g)** Calcarenite Pavement (CalPav), HY34. **(h)** Crust Pavement (CrPav), HY33. **(i)** Crust Sediment (CrSed), HY40. **(j)** Crust (Cr), HY32. **(k)** Crust Cobble (CrCob), HY32. Laser dots are 10 cm apart and visibility was manually enhanced, except in panels (c) and (k), where they were not visible.

4.3.2 Faunal community

We found 83 different morphotypes representing six different phyla (Appendix B) and 17,008 records of megabenthic organisms. Porifera contributed 42.7% to the abundance; Cnidaria, 41.5%; Echinodermata, 12.9%; Mollusca, 0.3% and Arthropoda,

0.03%. Nineteen of these taxa were rare, i.e. represented by one or two individuals. The overall community was characterized by a great dominance of five morphotypes: the coral-mimicking hexactinellid sponge *Sarostegia oculata* Topsent, 1904 (Scep1) and its epibiont *Thoracactis topsenti* represented 29.3% of all individuals in this study, followed by the unbranched black coral *Aphanostichopathes* sp. (Anti1, 24.9%), the sea urchin *Gracilechinus* sp. (Echi2, 7.1%), the hexactinellid *Aphrocallistes* cf. *beatrix* Gray, 1858 (Scep2, 7.1%), and the scleractinian *Enallopsammia rostrata* (Pourtalès, 1878) (Scle1, 6.2%). These five taxa represent 74.6% of all abundance captured by the images.

The best length for segments that would maximize the number of faunal observations was 120 m (Fig. 4.3). Regression analysis showed this difference was not significant in comparison with abundance (r = -0.552, p = 0.55) and richness (r = 0.005, p = 0.94). *HyBIS* tracks were divided into 183 segments (Table 4.1) comprising 16,176 observations and 80 morphotypes total. The remaining 832 individuals and 3 morphotypes were from small habitat areas and were discarded from further analysis. The number of specimens observed in each segment varied largely from 20 to 492. Fifty-one segments had more than 100 records, 80 segments had less than 50 records, and 36 (not accounted for the 183 total) segments were discarded from ecological analysis due to the small number of individuals (< 20). Most of these comprised the RiftRock, RiftSed, RiftDeb, and South-CalPav habitats.

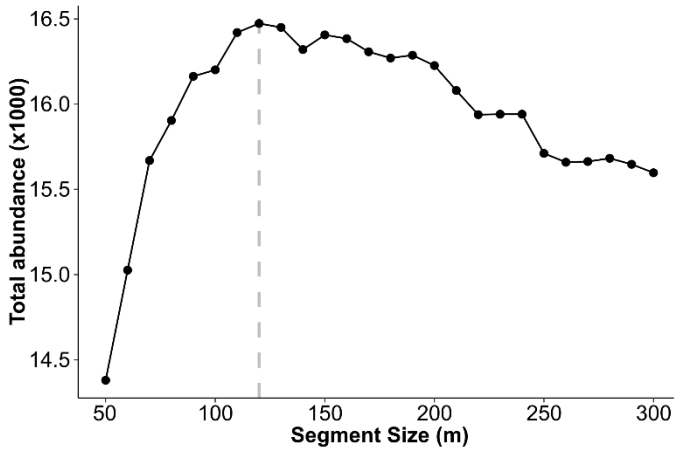

Figure 4.3. Overall abundance accounted within the segments when using multiple threshold lengths to define the segments. The vertical dashed line indicates the value used in this work, 120 m.

Aphrocallistes cf. *beatrix* (Scep2) was the most frequent taxon and it was present in 112 segments, followed by *Gracilechinus* sp. (Echi2) which is present in 100

segments (Fig. 4.4). *Chaunax suttkusi* Caruso, 1989 (Loph1), Astrophorina (Desm1), *Enallopsammia rostrata* (Scle1), Brisingidae (Bris1), and *Helicolenus* sp. (Scor1) were present in more than 80 segments, but they had low abundance (< 300 records) compared to the dominant taxa, with exception of *E. rostrata*. *Sarostegia oculata* (Scep1) and *Aphanostichopathes* sp. (Anti1) were the two most dominant taxa, and they had a frequency of 66 and 64%, respectively. Half of the morphotypes were found in 10 or fewer segments and a quarter was found in one or two segments. Morphotype accumulation curves show that all habitats did not reach the asymptote (Fig. 4.5a, b), especially for habitat 'RifHole' where only a small area was observed. Habitats 'RiftSed' and 'RiftDeb' had much smaller accumulation curves compared to the other habitats. Likewise, richness estimators did not reach the asymptote (Fig. 4.5c), except for Chao1. They estimate a richness from 85.6 to 93.9 for 183 segments.

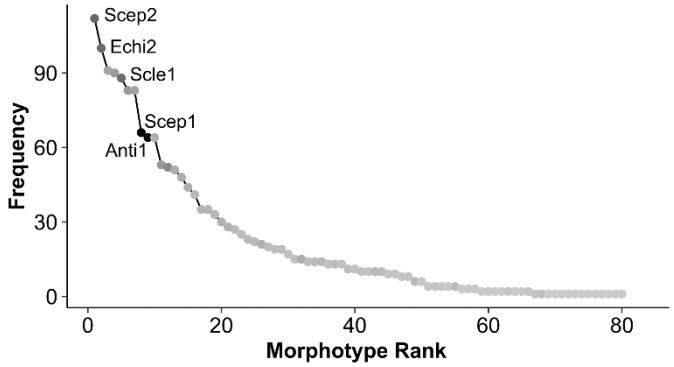

Figure 4.4. Rank frequency diagram of the morphotypes observed by the *HyBIS* in Rio Grande Rise (SW Atlantic). The five most abundant taxa are labeled. Scep1 - *Sarostegia oculata*, Anti1 - *Aphanostichopathes* sp., Echi2 - *Gracilechinus* sp., Scep2 - *Aphrocallistes* cf. *beatrix*, and Scle1 - *Enallopsammia rostrata*. Darker colors indicate morphotypes with higher abundance.

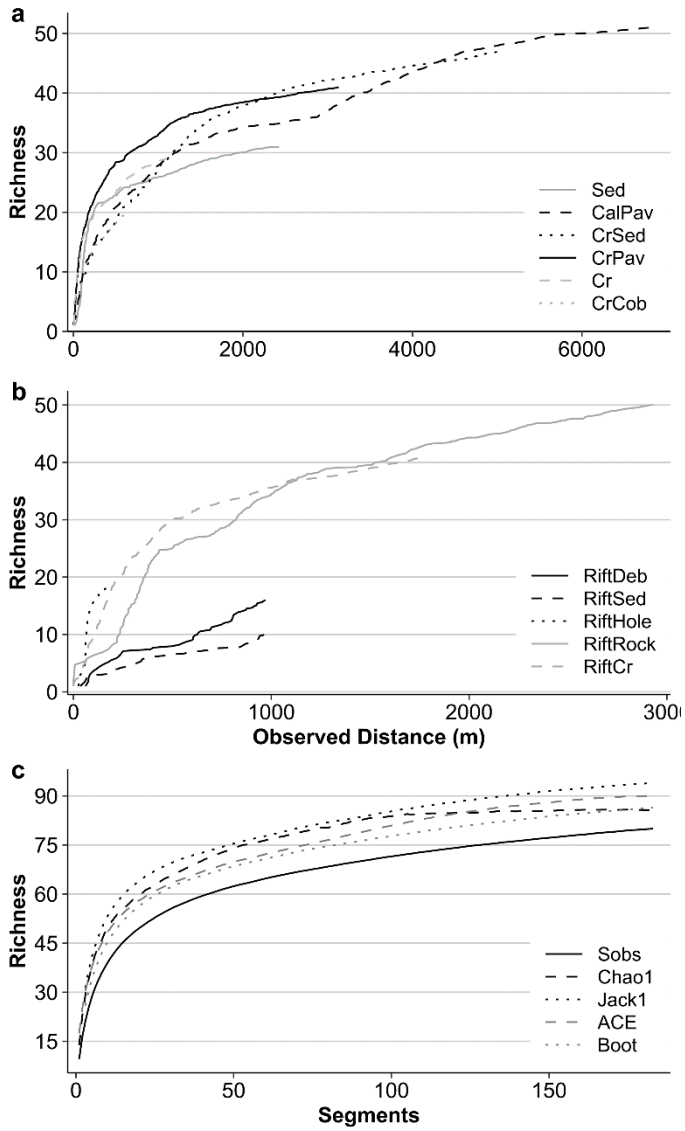

Figure 4.5. Benthic randomized morphotypes accumulation curves in Rio Grande Rise (SW Atlantic). **(a, b)** Richness of each habitat based on the observed distance with the *HyBIS*. **(a)** Habitats in the plateaus. **(b)** Habitats in the rift. Note that X-axis scales are different in (a, b). **(c)** Overall observed accumulation curve (Sobs) and estimates (Chao1, Jakknife1, ACE, and Bootstrap) of morphotypes based on the number of segments.

The UPGMA clustering analysis identified six distinct community clusters (Fig. 4.6 a). There are four main clusters (C, D, E, and F) that contained 175 segments out of 183. The Chi-squared test indicated a significant association of the clustering with different habitats (x^2 = 461.7, p < 0.001) and regions (x^2 = 323.4, p < 0.001). Figure 4.6b shows a clear higher relative abundance of *S. oculata*, *Gracilechinus* sp., *Aphrocallistes* cf. *beatrix*, and *Aphanostichopathes* sp. in clusters C, D, E, and F respectively. Cluster A is composed of a single segment from the RiftHole habitat at the Center region (Figs. 4.1c, 4.7a). Cluster B consists of 7 segments in the west rift wall in both Center and South regions, near the rift floor (Fig. 4.1c, g), exclusively in

the RiftRock habitat (Fig. 4.7b). Cluster C includes segments on both sides of the rift wall, in the plateaus near the rift wall, or the sloping area in the South region (Fig. 4.1c–e, g). This cluster was predominant in habitats with Fe-Mn crust substrate and it has a few segments of RiftRock and CalPav as well (Fig. 4.7c). Cluster D comprises segments at the Center and South regions (Fig. 4.1c–d, g) and it was predominant in the habitat CalPav on the plateaus (Fig. 4.7d). Cluster E was the largest one with 66 segments and it was located exclusively in the Northeast region (Fig. 4.1c–d, g). It mostly occurred in habitats with Fe-Mn crust substrate as well (Fig. 4.7e). Cluster F consists of segments that completely cover the Southwest region and in dives HY32 and HY41 (Fig. 4.1c, e–f). This cluster was predominant in the CalPav habitat (Fig. 4.7f).

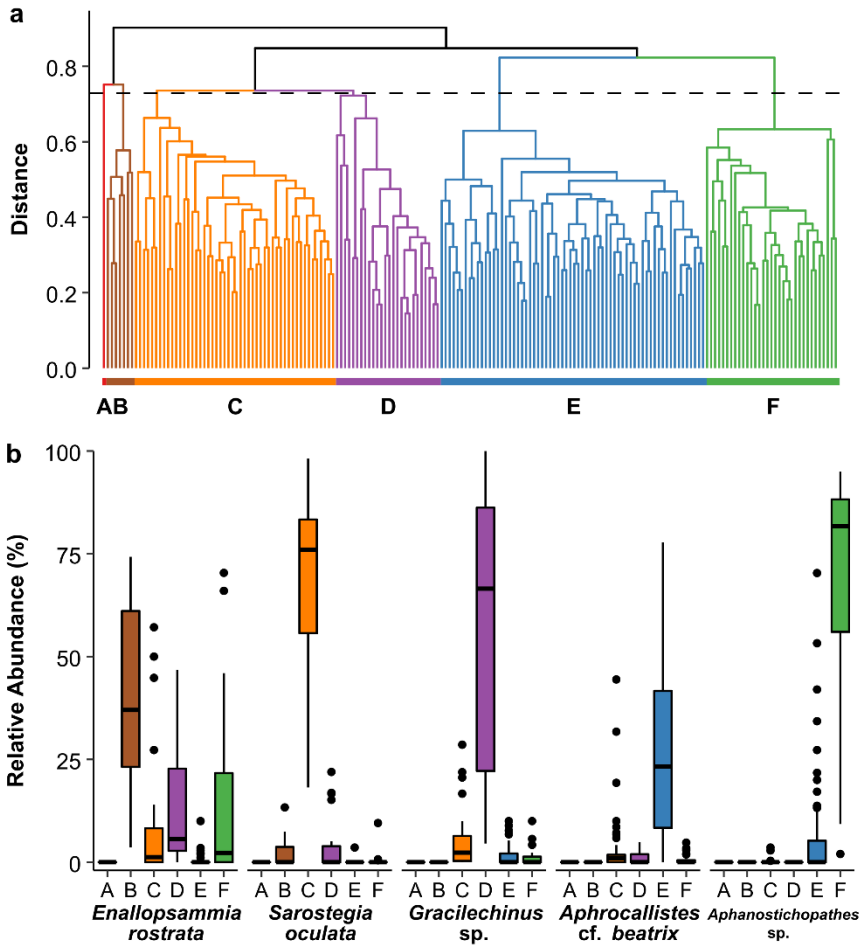

Figure 4.6. (a) Dendrogram of the UPGMA clustering using Bray-Curtis dissimilarities of the log-transformed abundance of the segments. The dashed line indicates the height where the dendrogram was cut to create six clusters, labeled from A to F. **(b)** Boxplot of relative abundances in each cluster of the five most abundant taxa observed by *HyBIS* in Rio Grande Rise (SW Atlantic). The horizontal line through the box is the median and the lower and upper hinges correspond to the first and third quartiles, respectively. Upper and lower whiskers extend to the largest and smallest values, respectively, no further than 1.5 × interquartile range (IQR). Values beyond the end of the whiskers are plotted individually as points.

According to the Indicator Value indices (IndVal) and pattern analysis (Appendix C), Cluster A had the largest number of indicator species (10 species; Fig. 4.7a). Five of these taxa with IndVal indices of 1.00 were found exclusively in this cluster. The most abundant morphotype was *Umbellapathes* sp. with 33 records and a relative abundance within the cluster of 22.3%. *E. rostrata* was the most abundant taxa in Cluster B but, it also had a high relative abundance in clusters C, D, and F (Fig. 4.6b), and the pattern analysis associated *E. rostrata* with these four clusters as well. IndVal indices for morphotypes associated with cluster B were comparatively low (< 0.53) with other clusters (Fig. 4.7b). Clusters C and D had a single species associated with them, *Sarostegia oculata* and *Gracilechinus* sp. respectively, which were the most abundant

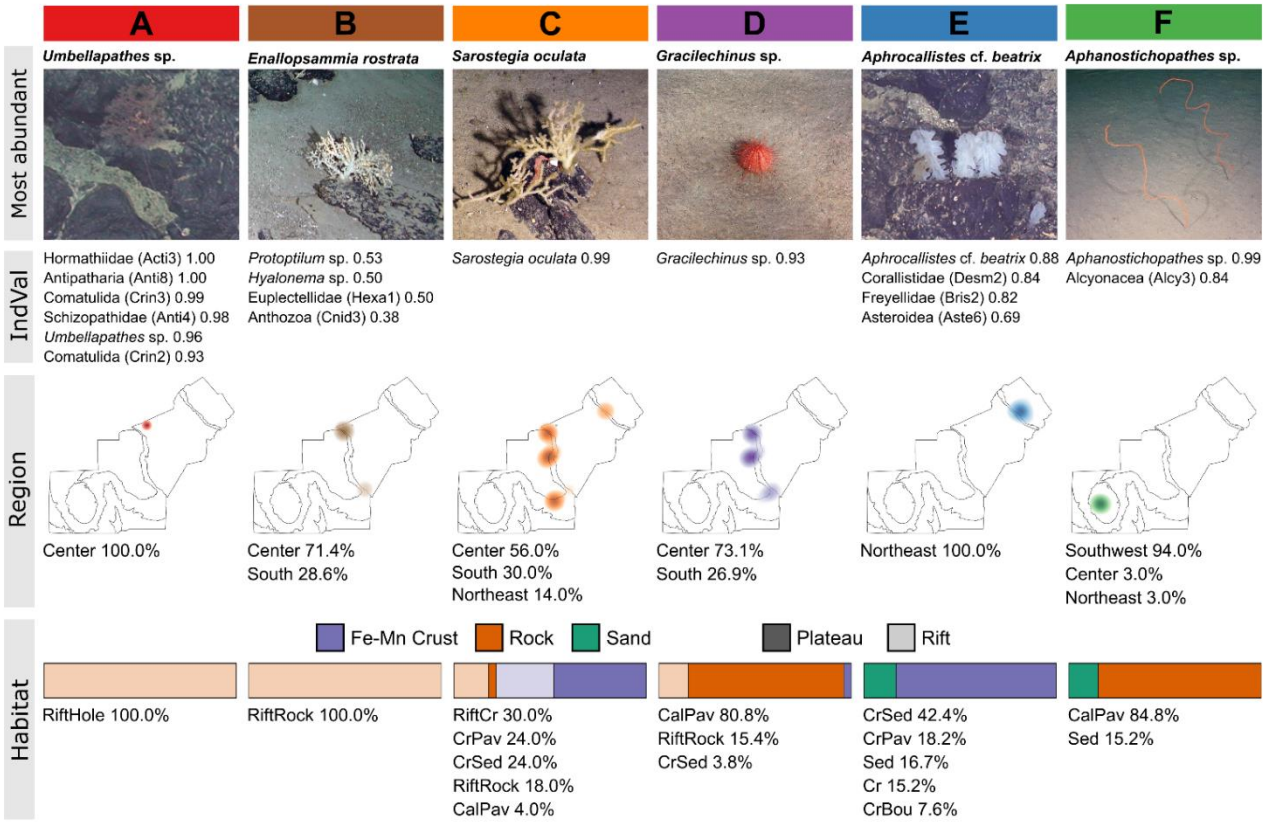

Figure 4.7. Diagram summarizing key features of each cluster (columns), which corresponds to letters a-f in figure citations. **First row** shows photos of the most abundant morphotypes found in each cluster. They are from left to right: *Umbellapathes* sp, *Enallopsammia rostrata*, *Sarostegia oculata*, *Gracilechinus* sp., *Aphrocallistes* cf. *beatrix,* and *Aphanostichopathes* sp. **Second row** shows taxa associated with each cluster with $p < 0.05$ in the multilevel pattern analysis using IndVal as a function with a correction for clusters with different sizes. Values next to the taxa names are their respective IndVal indices. Note that for cluster A we omitted four morphotypes that had three or fewer records (Chry2, 1.00; Crin4, 1.00; Isid5, 1.00; and Desm3, 0.95). **Third row** shows a schematic map of the study area with locations where each cluster was detected and the percentage of segments for each region. **Fourth row** shows horizontal bars with the relative number of segments based on the type of substrate and whether the segment was located in the plateaus or the rift. Below is the percent of segments for each habitat. Fe-Mn crusts substrate includes RiftCr, CrSed, CrPav, Cr, and CrCob habitats; Rock includes RiftHole, RiftRock, and CalPav; and Sediment includes RiftSed and Sed habitats.

Table 4.3. Summary of the characteristics of the identified segment clusters. Values are reported as average ± standard deviation, except for Cluster A, as it has only one segment. The total richness is reported as general information and should not be directly compared between clusters due to the different segment numbers. VME - Vulnerable Marine Ecosystem

Cluster		A	B	C	D	E	F
Number of segments		1	7	50	26	66	33
Abundance		148	42.29 ± 17.0	122.78 ± 93.0	52.54 ± 24.2	47.92 ± 28.7	153.55 ± 109.6
Average Richness (S)		18	8.57 ± 2.9	9.50 ± 2.8	7.19 ± 3.1	10.42 ± 2.8	10.12 ± 2.8
Total Richness		18	23	61	38	44	42
Shannon index (H')		2.32	1.57 ± 0.48	1.04 ± 0.47	1.12 ± 0.65	1.74 ± 0.39	0.91 ± 0.45
Pielou's Evenness (J)		0.8	0.74 ± 0.15	0.47 ± 0.20	0.55 ± 0.24	0.75 ± 0.13	0.40 ± 0.19
VME indicators (% abundance)	**Sponges**	1.4	5.5 ± 4.3	75.9 ± 16.6	11.4 ± 18.3	48.4 ± 23.3	2.9 ± 5.9
	Corals	87.8	86.4 ± 4.3	11.7 ± 14.3	19.4 ± 19.8	32.9 ± 24.0	88.3 ± 14.6

species for these clusters (Fig. 4.7c, d). Cluster E had four associated taxa whereas cluster F had two, all of them with IndVal indices above 0.82, except Aste6. In both clusters, species with the highest abundance were the ones with the highest IndVal indices (Fig. 4.7e, f).

The clusters showed distinct diversity characteristics and a trade-off between abundance and evenness (Table 4.3). Cluster A had the highest richness, Shannon index, and evenness across all clusters. Clusters C and F were characterized by a high abundance and richness, but a low evenness, which was primarily caused by the extreme dominance of *Sarostegia oculata* and *Aphanostichopathes* sp. In contrast, clusters B and E showed high evenness and low abundance and cluster D had an overall low abundance, Shannon index, and evenness. Segments in all clusters, except D, had a high dominance of VMEs indicator taxa. There was also a trade-off between sponges and corals dominance in clusters A, B, C, and F.

4.3.3 Environmental drivers

The variables rugosity and temperature were initially removed from further analysis due to high correlation (> 0.7) with other variables. The PERMANOVA test identified four environmental variables that significantly explain some structure within the community data. The most noticeable were the factor variables Habitat ($R^2 = 0.347$, $p < 0.001$) and Region ($R^2 = 0.215$, $p < 0.001$), which together explained 56% of the variance in the data. Linear variables explained a much lower fraction of the variance, which only depth ($R^2 = 0.036$, $p < 0.001$) and slope ($R^2 = 0.009$, $p = 0.021$) of

significance. The model had 35% of unexplained variance. The PERMDISP2 test showed no evidence of divergent dispersions for habitat (F = 8.114, $p < 0.001$) and region (F = 7.929, $p < 0.001$).

The nMDS ordination analysis supported the identified community clusters (Fig. 4.8 a). The six clusters were separated from each other along the two axes and there was a small overlap in the confidence ellipses, more noticeably between clusters C and D. The nMDS plot showed a partial differentiation of segments based on habitat (Fig. 4.8b). It was possible to discern groups of segments with the same habitat, although some overlapping occurred between them. There was a pattern where segments of the same habitat were split into two clumps and amidst them is the habitat centroid (where the lines from all points converge). Each clump of the same habitat was associated with distinct regions (Fig. 4.8c), as the case for CalPav, CrSed, CrPav, and Sed. The segments obtained in the Northeast, Southwest, and the Center/South showed clear segregation between them in the nMDS plot (Fig. 4.8c), except for segments found in RiftCr habitat on both sides of the rift. Additionally, the segments obtained in the Center and South regions almost completely overlapped each other.

The Krustal-Wallis test indicated a significant difference in depth (x^2 = 121.1, $p < 0.001$) and slope (x^2 = 96.6, $p < 0.001$) in at least one cluster. Cluster A was the deepest one followed by cluster B, with a depth range from 1050 to 1250 m (Fig. 4.8d). Cluster E was the shallowest one, occurring above 700 m. Clusters C, D, and F were located mostly between 700 and 900 m, with no significant difference among them. Clusters A and B occurred in steeper areas than clusters D, E, and F (Fig. 4.8e). Cluster C was composed of segments in a wide slope extent, ranging from 0° to 70°. Cluster E had a significantly lower slope than others, with segments mostly occurring in flat areas.

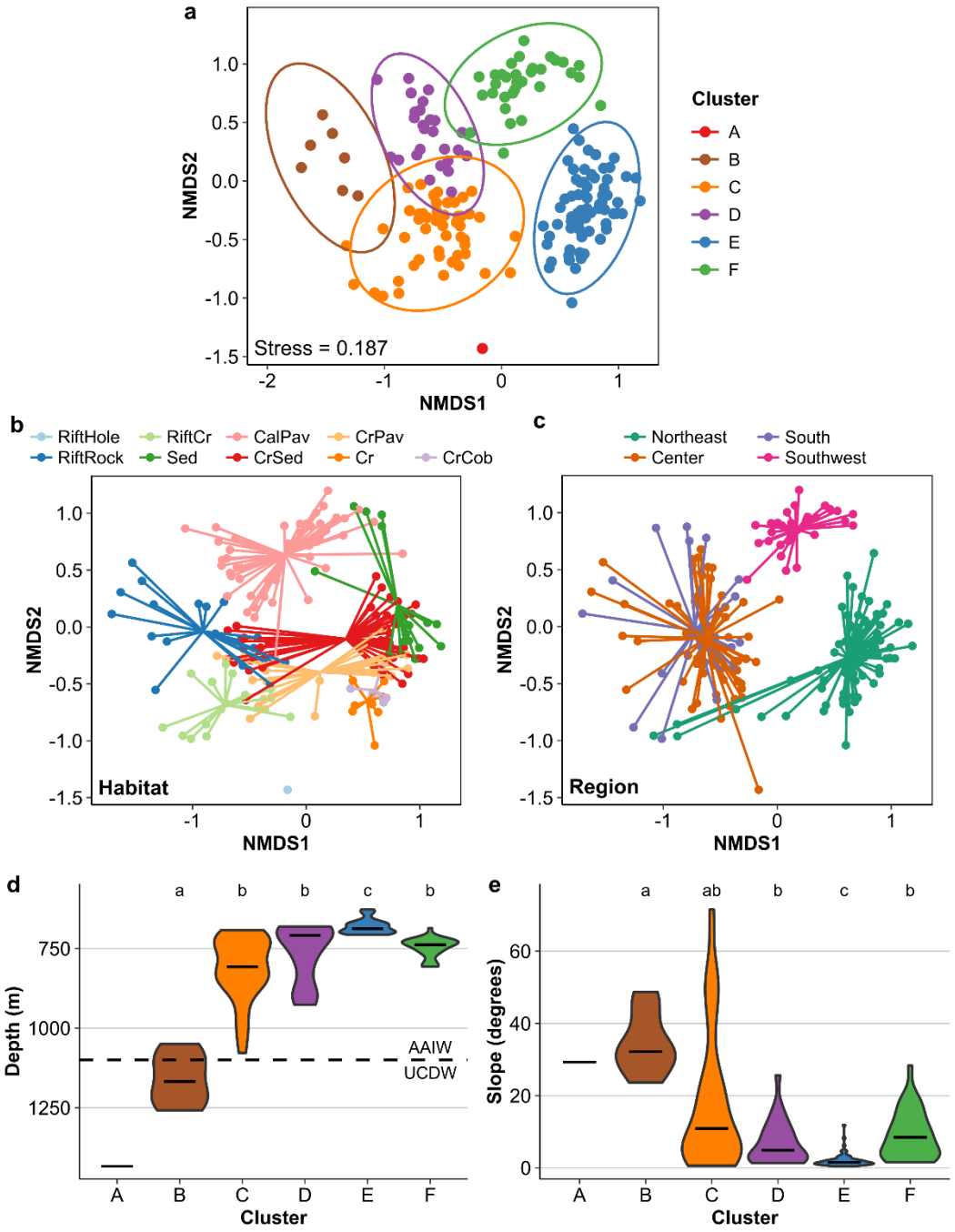

Figure 4.8. (a) non-metric Multidimensional Scaling (nMDS) of the log-transformed abundance data using Bray-Curtis dissimilarities and two axes. Points are segments with 95% confidence ellipses and the colors represent different clusters. **(b-e)** All environmental variables selected by the PERMANOVA test with terms added sequentially. **(b, c)** Same nMDS as (a), but colors represent different habitats (b) and regions (c). Each point is connected to its group centroid. **(d, e)** Violin plots of depth (d) and slope (e). The letters above indicate the post-hoc Kruskal-Wallis comparison. Groups with the same letter are not significantly different. Cluster A was excluded from this analysis because it has only one segment. Dashed lines in (d) correspond to the transition between water masses. AAIW - Antarctic Intermediate Water and UCDW - Upper Circumpolar Deep Water.

The MRT analysis gave a seven-leaf tree with the splits based on region, habitat, depth, and slope (Fig. 4.9). The tree explained 58.6% of the Hellinger transformed morphotypes variance. Community structured varied strongly across the seven groups

and displayed large contrasts in the multivariate mean of the most dominant morphotypes. The first split (Fig. 4.9) divided segments between Center/South and Northeast/Southwest regions. Segments in the Center/South regions were further split based on habitat. The habitat CalPav formed a node with a high abundance of *Gracilechinus* sp., and the other habitats were further split based on depth at 1077 m. The deeper node was dominated by *Enallopsammia rostrata* and the shallower one by *Sarostegia oculata*. A similar split at this depth range is visible in Figure 4.8d, between cluster B and C. Region Southwest was split from Northeast and formed a node dominated by *Aphanostichopathes* sp. The Northeast region was further divided based on slope at 16.13º and steeper segments were also dominated by *S. oculata*. The other segments were in more flat areas (< 16.13º) and were split into two nodes, based on habitat, and both had a high abundance of *Aphrocallistes* cf. *beatrix*. One node was formed by Cr and CrCob habitats, found uniquely at dive HY32, above and below the terrace in the northeast plateau, and showed a high abundance of a sponge classified as Corallistidae. The other node, in contrast, had a high abundance of another black coral, *Stichopathes* sp. (Anti2).

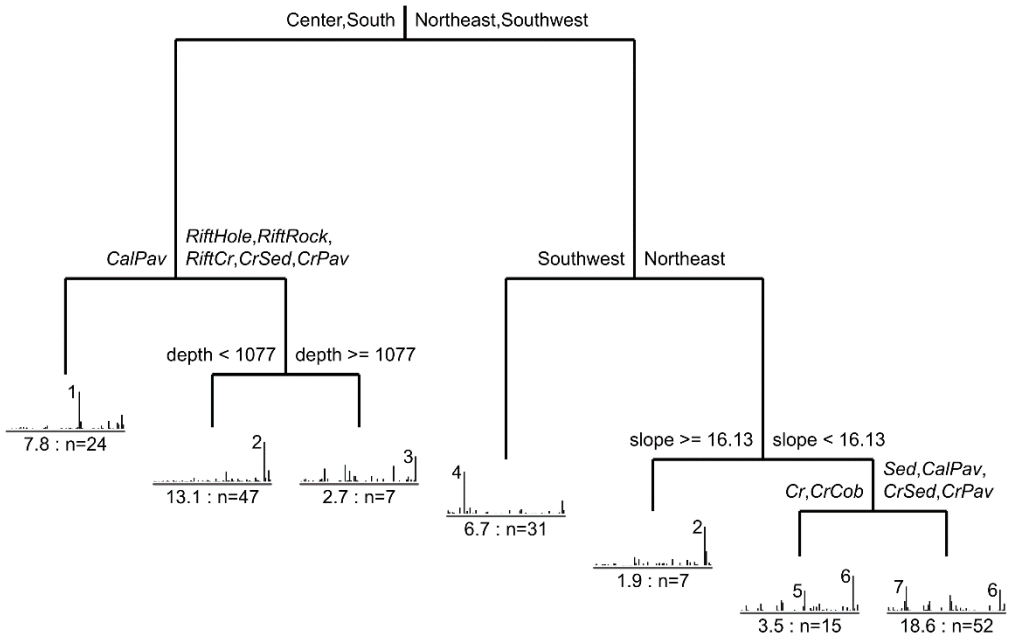

Figure 4.9. Multivariate regression tree for Hellinger transformed abundance data. Relative error: 0.414, CVRE: 0.474, and CVRE standard error: 0.0262. Euclidean distance was used for splitting. Barplots show the multivariate morphotype mean at each node. Under barplots, the first value is the sum of squared errors and n is the number of sites in the leaf. Habitats are in italics; regions, in normal font; depth, in meters; and slope, in degrees. The morphotypes with the largest means are indicated with numbers next to their respective bars. 1 - *Gracilechinus* sp. (Echi2), 2 - *Sarostegia oculata* (Scep1), 3 - *Enallopsammia rostrata* (Scle1), 4 - *Aphanostichopathes* sp. (Anti1), 5 - Corallistidae (Desm2), 6 - *Aphrocallistes* cf. b*eatrix* (Scep2), 7 - *Stichopathes* sp. (Anti2).

4.4 Discussion

Clear differences in megabenthic abundance were observed between the thirteen dives in the study area, which vary considerably in different spatial scales, ranging from nearly deserted bottoms to sponge gardens. The dives and Digital Terrain Model (DTM) exhibited highly heterogeneous habitats in RGR at different spatial scales (from meters to kilometers), changing rapidly from habitat to habitat. The community structure reflects the heterogeneous features of the RGR and it was strongly associated with habitat type and geographical regions of the study area. Similar patterns were observed by Perez et al. (2018) in the benthopelagic megafauna (restricted to fishes and crustaceans) outside of the study area. The fauna of RGR shows a high dominance of a few morphotypes, with *Sarostegia oculata* and *Aphanostichopathes* sp. each being 3.5 times more abundant than any other morphotype found. Hajdu et al. (2017) described a similar dominance of *S. oculata* at the rift wall and plateaus. In addition, species accumulation curves and richness estimators in our study did not reach asymptotes, indicating that longer dives in each habitat might be necessary to representatively quantify and assess megafauna diversity.

The PERMANOVA analysis suggests that seafloor characteristics (habitat type, depth, and slope) and geographic location were potential drivers of community structure, a result similar to comparable studies in Fe-Mn deposits areas in the Pacific Ocean (Delavenne et al., 2019; Morgan et al., 2015; Schlacher et al., 2014). The small area in our study revealed a wide range of habitats and potentially more could be found in RGR as an outcome of its complex topographic features, complex geological history, and associated environmental processes (Alberoni et al., 2020; Montserrat et al., 2019). Consistent with general patterns in the deep-sea (Levin et al., 2001; Rex & Etter, 2010), our observations show that a high beta diversity was reflected by high habitat heterogeneity.

Habitats covered with Fe-Mn crusts (RiftCr, CrPav, Cr, CrSed, and CrCob) had more than one distinct community compared with other hard substrates, grouped in clusters C and E, and were rarely observed in other habitats. Likewise, Morgan et al. (2015) found evidence of changeover in diversity and community structure within cobalt-rich crusts areas and Schlacher et al. (2014) suggested the cover of cobalt-rich deposits may drive the structure of benthic communities. Polymetallic nodules in the

Clarion-Clipperton Zone (CCZ) are also a potential driver for megafaunal community structure (Cuvelier et al., 2020; Durden et al., 2021; Simon-Lledó et al., 2020). Nevertheless, the exact relationship between the fauna and the chemical nature of the crusts and nodules remains to be further investigated. Based on microbial functional predictions performed in the study area, nitrification (i.e., ammonia oxidation and nitrite oxidation) and carbon fixation might be the main processes occurring in the Fe-Mn substrates by microbial communities (Bergo et al., 2021; Kfouri et al., 2021; Millo et al., 2022). The ecological roles microorganisms play in Fe-Mn crusts benthic ecosystems and in fauna colonization remains unknown (Orcutt et al., 2020), but they could be important contributors to the ecological process occurring in Fe-Mn crusts.

Geographic location (here factorized in four regions) explained more than one-fifth of the community structure. Removing Region from the PERMANOVA analysis reduced the model explained variation in 12.3% by other environmental variables. Region is likely a proxy for unmeasured parameters along the study area, including food availability, sedimentation, and bottom currents, or more complicated interactions between environmental variables. These parameters may drive drastic changes in communities (Levin et al., 2001) and account for differences between the Northeast, Center/South, and Southwest regions. Currents around RGR are strong (up to 50 cm/s) but variable due to tidal effects (Harlamov et al., 2015). The horizontal current velocity at the seabed is enhanced along with the shallower areas of the RGR summit plateaus (Montserrat et al., 2019) and the collected crusts show signs of erosion, indicating strong currents (Benites et al., 2020), as well as ripple marks found in soft sediment (this work). Currents are known to drive sponge species distribution on seamounts (Ramiro-Sánchez et al., 2019) and a fine circulation model in RGR could elucidate the effects of currents in the benthic fauna. The complex outlines of the rift wall and terraces possibly generate vortices and resuspensions favoring higher or lower food supply in specific areas. Moreover, the rift floor had a large amount of sediments and scarce hard substrate for sessile fauna. Suspension feeders, especially corals and sponges, are sensitive to high sediment loads (Morgan et al., 2015), which may account for the lower number of benthic fauna in this habitat.

The other two significant environmental drivers were depth and slope, albeit they explained only 4% of the variance. The lower rift wall was characterized by the cluster B communities in the RiftRock habitat, but the upper rift wall was marked by RiftCr and RiftRock habitats which accommodate communities grouped in cluster C.

This shows that depth had a stronger effect on fauna composition than habitat at the rift wall, at roughly 1050 m depth near the transition from UCDW to AAIW. Water masses are known to have a significant influence on the distribution and composition of coral communities in the Southeast Brazilian continental slope (Arantes et al., 2009; G. de H. Cavalcanti et al., 2017; Sumida et al., 2004), due to their distinct properties in the water column (temperature, salinity, oxygen, nutrients). In addition, microbial communities from pelagic zones in RGR are structured by water masses (Ferreira et al., 2021). Studies had shown that hexactinellids have high assimilation-to-respiration efficiency for bacteria (Bart et al., 2020), and they are an important functional group that links the pelagic microbial food web to the benthos (Pile & Young, 2006). Thus, our results suggest that water masses could explain some patterns observed in benthic fauna distribution, especially at distinct depths.

Other linear variables did not explain significant variance in the model, although they are proxies for habitat classification (Walbridge et al., 2018, and references therein) and are known to influence the abundance and distribution of species (e.g. García-Alegre et al., 2014; Morgan et al., 2015; Ramiro-Sánchez et al., 2019; Schlacher et al., 2014; Simon-Lledó et al., 2019). RGR is a complex structure, and the resolution of 15 m may not be sufficiently detailed to reveal small features (e.g. scarps, boulders) that are located within one grid cell and abrupt changes in slope that are found in the rift wall. Similarly, the sampling area in our study was limited and a broader geographic range could help to identify other environmental variables that drive the abundance and fauna composition in RGR.

The seamount megabenthic fauna tends to be dominated by suspension feeders, especially in deep-sea ecosystems (Rogers, 2018). Currents are accelerated by kilometer-scale topographic features, such as the rims or crests of seamount summits or ridges (Genin et al., 1989; Rogers, 2018), which increase food availability in these regions. The same patterns were observed in RGR, with the dominance of suspension feeders (*Sarostegia oculata*, *Aphanostichopathes* sp., *Enallopsammia rostrata,* and *Aphrocallistes* cf. *beatrix*) and evidence of strong currents (as discussed above). Topology and habitat are also known to drive deep-sea communities in seamounts (J. S. Davies et al., 2015; Guinotte & Davies, 2014; Victorero et al., 2018). At first insights, patterns in benthic fauna of RGR are comparable to some trends found in other seamounts (but see discussion below). Despite these similarities, closed circulations above seamounts and internal wave formation may act to trap or provide

a mechanism for the downward transport of phytoplankton and particulate organic carbon (POC) (Read & Pollard, 2017; Turnewitsch et al., 2016; Vilas et al., 2009; White et al., 2007). However, RGR is in the oligotrophic South Atlantic Gyre, with a low concentration of organic carbon (Perez et al., 2012) and the main reservoir of new nutrients is trapped below the permanent thermocline, in the South Atlantic Central Water (Ferreira et al., 2021). Physical processes induced by RGR and their biological consequences are unknown and should be investigated in future studies to ascertain which processes are related to the ones driven by seamounts.

4.4.1 Implications for conservation

The exploitation of Fe-Mn crusts will likely lead to loss of biological diversity resulting from direct habitat destruction, reduction in habitat heterogeneity, and changes in the geochemical characteristics of seafloor sediments (Christiansen et al., 2020; Levin et al., 2016). Indirect impacts on surrounding benthic and pelagic environments are possible through toxic and particle-rich sediment plumes, noise, vibration, and light created by the mining activity (Dunn et al., 2018; Jones et al., 2020; Miller et al., 2018). This sediment plume may cause smothering and burying of animals, clogging of feeding structures, and prevent larval settlement and colonization. Effects of particle load and toxicity could take years to decades to become visible (Weaver et al., 2022). We detected a diverse and rapidly-changing habitat in Rio Grande Rise, associated with evidence of strong currents and unique communities in Fe-Mn deposits. Thus, an extensive physical and biological analysis should occur prior to deep-sea areas being considered for exploitation in order to account for all areas that may be affected by mining activities.

Understanding spatial variations in megafaunal community structure, and their correlations with environmental parameters is crucial to predict and manage the environmental impacts of mining (Amon et al., 2016). *A priori* PERMANOVA model using only the linear variables (including latitude and longitude) had 56% of unexplained variance (a difference of 21.7% from our final model), suggesting that important environmental variables for community structure were not measured. Parameters like chemical properties of the water column, current velocity, and finer bathymetric and backscatter data may provide a better understanding of what is driving community structure in RGR and better predict regions of high diversity or unique fauna

composition. The MRT analysis can present a comprehensive view of species-environment relationships, and aid contractors and governmental agencies to make better policies and management plans.

The study area contained many gardens of Vulnerable Marine Ecosystems (VMEs) indicator species, including sponges and corals. Such species are characterized as long-lived, late-maturing, slow-growing, with low larval recruitment, and dispersal potential (Ardron et al., 2014). VMEs have low resilience and slow recovery from human disturbances such as bottom-contact fishing and, in the future, deep-sea mining. Benites et al. (2020) concluded that bulk RGR crusts in the study area are enriched in Ni and Li, which are critical metals of economic interest. Some crusts and substrate rocks had high P, F, and carbonate fluorapatite (CFA) contents (Benites et al., 2020) and might be considered potential phosphate ores in deep-sea mining. *Sarostegia oculata* and *Aphrocallistes* cf. *beatrix* are examples of dominant VMEs indicator species with a high affinity for Fe-Mn crusts, which were not found in other habitats. Criteria used to identify VMEs are often based on benthic bycatch during fishing operations (Auster et al., 2011) and only recently density thresholds were used to objectively identify VMEs (S. Long et al., 2020; Rowden et al., 2020). For example, Rowden et al. (2020) applied thresholds of 0.11 – 0.85 coral head m^{-2} of *Solenosmilia variabilis*. If we roughly considerer that our videos cover 5 m wide area, we would find a maximum density of 0.71 individuals m^{-2} of *S. oculata* and 28 out of 183 segments would have a density higher than 0.11, which suggests that some areas of RGR could in fact constitute VMEs. Comprehensive studies should address the potential impacts in these communities before and during mining operations.

Assessing similarities between benthic communities from the RGR and adjacent areas in the South Atlantic is a key factor in order to assert the extent of impacts in RGR to other regions, such as the Jean Charcot Seamounts, Vitória-Trindade seamounts chain, Southeast Brazilian continental margin, Mid-Atlantic Ridge and the 'sister' Walvis Ridge. The framework-forming *Solenosmilia variabilis* and *Desmophyllum pertusum* (former *Lophelia pertusa*) were the most dominant cold-water scleractinians in the Brazilian continental slope (G. de H. Cavalcanti et al., 2017; Pires, 2007). Both corals were not recorded in our study, which suggests that communities are different in both regions. Differences in invertebrate assemblages between the Vitória-Trindade seamount chain and the Brazilian continental shelf has been recorded before (O'Hara et al., 2010), but only for above 150 m depth. In addition, *S. oculata*

and *Aphrocallistes* cf. *beatrix* are recorded in the Vitória-Trindade seamounts chain (Tabachnick et al., 2009) and *E. rostrata* is distributed off Southeast Brazil continental margin (Arantes et al., 2009; Kitahara et al., 2020). Addressing the connectivity between populations of RGR and the South Atlantic is another important element highly relevant in the context of future mineral exploration (Perez et al., 2018).

Sampling techniques using video and still imagery vary across studies by using different sampling units. Some may use photographs or a collection of photographs (Durden et al., 2021), running length (this work, Perez et al., 2018), or dives (Morgan et al., 2015; Schlacher et al., 2014). Density, richness, and diversity can be difficult to relate across these studies. When possible, the area is often calculated from photos and video images to facilitate the comparison of megafaunal data across deep-sea studies (e.g. Amon et al., 2016; Cuvelier et al., 2020; Durden et al., 2021; Simon-Lledó et al., 2019). However, RGR is a complex feature with many steep slopes and rough terrain, which would represent a strong bias in the surface estimations in some habitats. The current development and dissemination of 3D photogrammetry (Bayley et al., 2019; Lim et al., 2020; Price et al., 2021) may prove useful tools to better estimate the area and density on such topologies, and compare results across other surveys.

The limited collection of voucher specimens in our study precludes robust assessments of endemicity due to limitations of identifying organisms to species level using videos. Lima et al. (2019) recorded nine species of antipatharians in the RGR, and only one was shared with the Brazilian continental margin. Such result was only possible due to physical sampling of biological specimens and precise taxonomic identifications. In addition, a study by Delavenne et al. (2019) revealed that Fe-Mn crusts at French Polynesia EEZ are inhabited by distinct macrobenthic communities. This result would not be possible using submarine imaging techniques alone. It is critical that future studies combine imagery data with physical collection of specimens to obtain reliable estimates of species richness and species ranges (Amon et al., 2016).

4.5 Conclusions

RGR is a large and heterogeneous feature with abrupt and common changes in habitat, where little is known about its biodiversity and ecological patterns so far. Although the area studied here is very small compared to the whole RGR, our results indicate clear spatial patterns in faunal composition that are influenced by habitats and

the presence Fe-Mn crusts. We discussed a set of environmental drivers, both abiotic and biotic, that may be influencing the distribution and abundance of species, but more studies with a broader geological scale are needed to unfold what drives the community structure and to understand its ecological patterns. The life history and morphological traits of the fauna observed imply that any recovery from mining is likely to be very slow, thus affected and surrounding areas must be considered in order to implement a strategic environmental management plan and help to address biodiversity conservation in the future. RGR has heterogeneous habitats that may require more complex regulations that treat each habitat as multiple ecological units.

5 Distribution models of the branched hexactinellid *Sarostegia oculata* in Rio Grande Rise (SW Atlantic) and implications for spatial management and conservation

Abstract

The mining of ferromanganese (Fe-Mn) crusts in the deep sea have gained more attention in the last decade due to increased demand for rare earth elements that are critical for low-carbon technologies, which makes exploitation of this resource feasible and profitable. The Rio Grande Rise (RGR) is a distinct feature located in the South Atlantic and has become a region of great commercial and scientific interest because of its potential for mining Fe-Mn crusts. Extraction of Fe-Mn deposits may cause irreversible changes by removal of substrate, creation of sediment plumes, among others. Here, we use species distribution models (SDMs) to predict the occurrence of *Sarostegia oculata*, a branched hexactinellid that mimics the 3D skeletal framework of actual corals. It is the dominant organism in areas rich in Fe-Mn crusts and has relevant ecological importance in RGR. The distribution of *S. oculata* was modeled using five algorithms widely used in SDMs: Random Forest (RF), Boosted Regression Trees (BRT), MaxEnt, Generalized Additive Models (GAMs), and Artificial Neural Networks (ANN). The models had excellent or good performance statistics and a high discrimination power between presence and absence sites. The main drivers for the distribution of the sponge were depth, fine BPI, and northness. Their occurrence was predicted within the 700–1000 m bathymetric range, with peaks in response on north- and south-facing sides, and sites with positive values for fine BPI. Exceptions include ANN, with response higher in sites facing south, and MaxEnt, with response higher for negative fine BPI values. We merged all predictions using an ensemble model approach, in which low uncertainty was found in the same areas with a high likelihood of *S. oculata* on the rift borders. The same area is aimed for the exploration of Fe-Mn crusts, and our results support the relationship between *S. oculata*, the Fe-Mn crusts, and the rift at RGR. Our results contribute toward understanding the distribution and environmental drivers of a key species in RGR, and help to create a management plan and preserve unique marine habitats and biodiversity from the deep sea.

Keywords: Hexactinellid. Sponge gardens. Species distribution models. Deep-sea mining. Fe-Mn crusts.

5.1 Introduction

Deep-sea sponges have importance as organisms that can provide multiple ecosystem goods and services, and thus have increasingly been mentioned in the literature in recent years (Beazley et al., 2018). Habitats dominated by sponges are globally distributed, forming structurally complex and often highly diverse communities, along with corals (Hogg et al., 2010; Maldonado et al., 2016). They have key roles in ecosystem functions, including habitat provision for associated fauna (Cook et al., 2008; Klitgaard, 1995), increasing biodiversity (Beazley et al., 2015; Bett & Rice, 1992; Bo et al., 2012; Marliave et al., 2009), promoting silicon and organic carbon cycling (Cathalot et al., 2015; Maldonado et al., 2011; Pile & Young, 2006), and potentially acting as nursery habitat for many species (Rossi, 2013).

Vulnerable Marine Ecosystems (VMEs) are characterized as areas with low resilience and slow recovery from anthropogenic disturbances such as bottom trawling and mining (extraction of fossil fuels, gas, or minerals) (Ramirez-Llodra et al., 2011). Some taxonomic groups, including sponges, are considered indicators of VMEs as a consequence of having slow growth rates, longevity, late maturity, fragility, as they form three-dimensional structures associated with diverse communities (Rowden et al., 2017). They have been used to assist agencies responsible for the protection of particular ocean regions, such as slopes, seamounts, and canyons (FAO, 2009). Increasing knowledge of the distribution and biology of species is necessary to create a consistent network of marine protected areas (MPAs), which can diminish human impacts on the ocean and prevent loss of biodiversity.

The Rio Grande Rise (RGR) is a major positive feature in the South Atlantic, between the parallels 28°–35° South and meridians 28°–39° West, located about 1200 km east off the Brazilian coast, and forming a volcanic plateau that rises from depths of about 5000 m to above 1000 m in some areas (Mohriak, 2020). The western region of RGR (WRGR) forms an elliptical bulge of 500 km × 300 km that includes seamounts and guyots towering over or juxtaposing with this massive platform (J. A. D. Cavalcanti et al., 2015); it is intersected by a NW-SE trending submarine rift between 20-40 km wide (also referred to as ‘graben’ or Cruzeiro do Sul Lineament). RGR has gained

special attention from researchers and the Brazilian government in recent years (da Silva, 2021; Montserrat et al., 2019) due to prospecting surveys that revealed its potential for the mining of Fe-Mn crusts . Impacts created by mining activities may range from direct destruction of habitats and formation of toxic and particle-rich sediment plumes (Christiansen et al., 2020; Levin et al., 2016; Schmidt, 2015) to noise, vibration, and light, which may lead to significant (potentially irreversible) damage to deep-sea communities and ecosystems and loss of biodiversity on mining sites and surrounding areas (Dunn et al., 2018; Jones et al., 2020; M. W. Lodge & Verlaan, 2018; Miller et al., 2018; Montserrat et al., 2019).

Sarostegia oculata is a branched hexactinellid that forms an erect, complex surface, similar to the shape of a stony coral. It has a close association with a zoanthid (likely *Thoractis topsenti*, cf. Gravier, 1918), growing on and within the skeleton in a similar way to coral polyps, thus mimicking the 3D skeletal framework of actual corals (Hajdu et al., 2017). It was first described at Cape Verde by Topsent (1904), and further sampled throughout the Atlantic (Dohrmann et al., 2011; Tabachnick et al., 2009) and Indian (Reiswig, 2002) oceans. More recently, Hajdu et al. (2017) recorded extensive sponge gardens in RGR, being the dominant organism in areas rich in Fe-Mn crusts that play a fundamental role in supporting communities in the area (Chapter 4).

Species distribution models (SDMs; also known as habitat suitability models) are a method to predict the likelihood of a species to occur in a given location, based on their observed relationship with environmental conditions. SDM is widely used in ecology and conservation, especially in the deep sea where data is scarce, and such models are useful for the development of conservation measures and marine ecosystem management by predicting species distributions beyond surveyed areas (Howell et al., 2016; Marshall et al., 2014; Reiss et al., 2015).

In the present study, we built such models to predict the distribution of *S. oculata* in two areas with available high-resolution multibeam data at RGR, surrounding the rift within the bulge of WRGR. The growing use of mineral resources in our global economy will surely lead to future commercial extraction of mineral resources in the deep sea, including, but not limited to, Fe-Mn crusts (Guilhon et al., 2021; Wedding et al., 2013, 2015). Such models can be used to inform spatial management planning for protecting VMEs and environmental impact assessments that minimize the effects of mining on deep-sea ecosystems (Kenchington et al., 2019; Ramiro-Sánchez et al., 2019).

5.2 Methods

5.2.1 Data collection

Two surveyed areas near the center of WRGR were used in this study. The first area (here named Area 1) was delimited between latitudes 30º35'S–31°03'S and longitudes 35º36'W–36°16'W (Fig. 5.1a). This area is ~2,000 km², ranging from 600 m to 1,800 m depth, and encompasses a small segment of the rift and a plateau on both sides, here named NE and SW plateaus (Fig. 5.1b). It also contains a terrace in the NE plateau, which runs almost parallel to the rift border, a slide south of the SW plateau, and a canyon that splits a section of the SW plateau in two, one next to the rift border and another named the inner SW plateau. The south and west of the SW plateau are neighbored by a lower plane, which extends beyond the MBES data. The second area (Area 2) is smaller, located about 30 km northwest of Area 1, delimited between

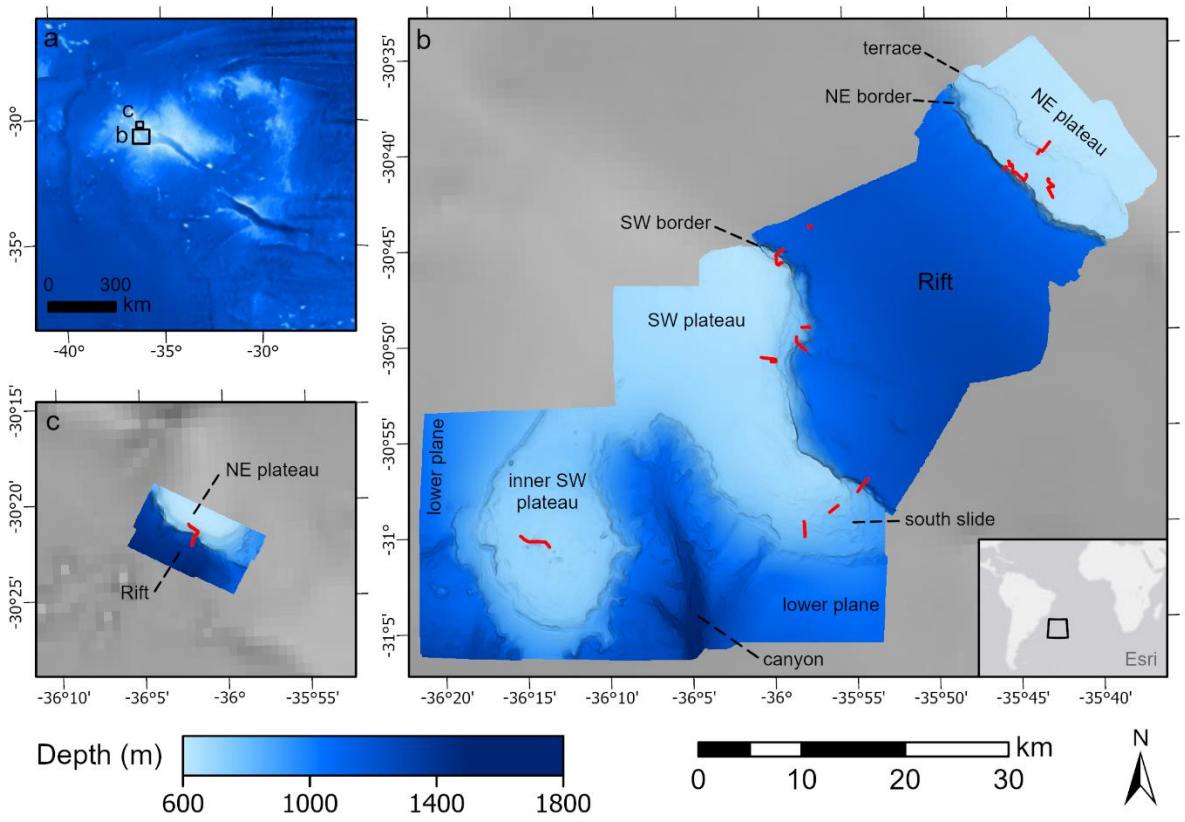

Figure 5.1. (a) Rio Grande Rise, showing the locations of panels (b) and (c). **(b)** MBES of Area 1, used for model training and validation. **(c)** MBES of Area 2, used for model testing. Red lines represent dives from (a) *HyBIS* and (c) *Shinkai*. Maps (b) and (c) are in the same scale.

latitudes 30°19’S–30°25’S and longitudes 35°57’W–36°06’W, is ~77 km², ranging from 600 to 1400 m depth. It encompasses a small area of the northeastern plateau and the rift (Fig. 5.1c).

Area 1 (Figs. 5.1b and 5.2) was surveyed with the *N/Oc. Alpha Crucis*, from January 30 to February 21, 2018, and *RSS Discovery*, from October 26 to November 8, 2018, as part of the FAPESP/RCUK funded project Marine E-Tech. *N/Oc. Alpha Crucis* used the Reason 7160 multibeam echosounder (MBES) operating at 41 kHz. *RSS Discovery* was equipped with a ship-mounted Kongsberg EM122, and multibeam was processed using Caris HIPS and SIPS v9.1.8. The data in both products were gridded at 25 m using NaviModel Producer 4.3.2, then fused with ArcGIS Pro 2.9, using the Mosaic tool with the “Blend” mosaic operator. The survey in the *RSS Discovery* included 13 dives (codes HY31–43) of the Robotic Underwater Vehicle, *RUV HyBIS* (Hydraulic Benthic Interactive Sampler). *HyBIS* was equipped with a Sony Full HD camera that recorded over 36 hours and 26 km of video footage of the seafloor and it was connected to the ship's USBL system to record its position (latitude, longitude, and depth).

Area 2 (Figs. 5.1c and 5.3) was surveyed with the submersible *Shinkai 6500* and *Yokosuka* support vessel, from April 13 to May 5, 2013, as part of the ‘Iata-Piuna’ expedition. Yokosuka was equipped with multibeam Sea Beam 2112.004, operating at 12 kHz. The data was also gridded at 25 m using NaviModel Producer. *Shinkai* 6500 was equipped with two HD video cameras. One of them was fixed at the bow, which recorded 4.5 hours and 2,282 m of footage from the seabed during the dive 6K1338. The other video camera was mobile and was ignored in this study so the analysis would be more consistent with the *RUV HyBIS*.

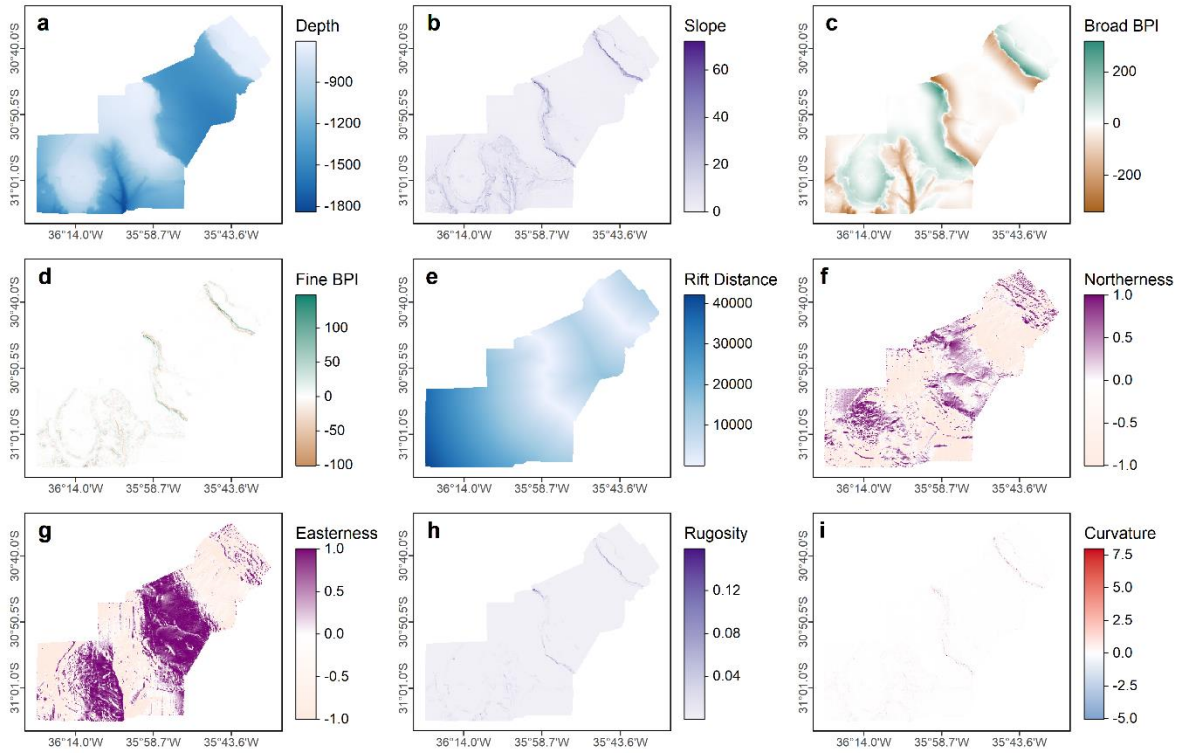

Figure 5.2. The bathymetry-derived variables in Area 1, which were used as explanatory variables in the models for training and validation. **(a)** Depth. **(b)** Slope. **(c)** Broad-scale Bathymetric Position Index (BPI). **(d)** Fine-scale BPI. **(e)** Euclidian distance from the border of the rift. **(f)** Northness. **(g)** Eastness. **(h)** Rugosity. **(i)** Curvature**.**

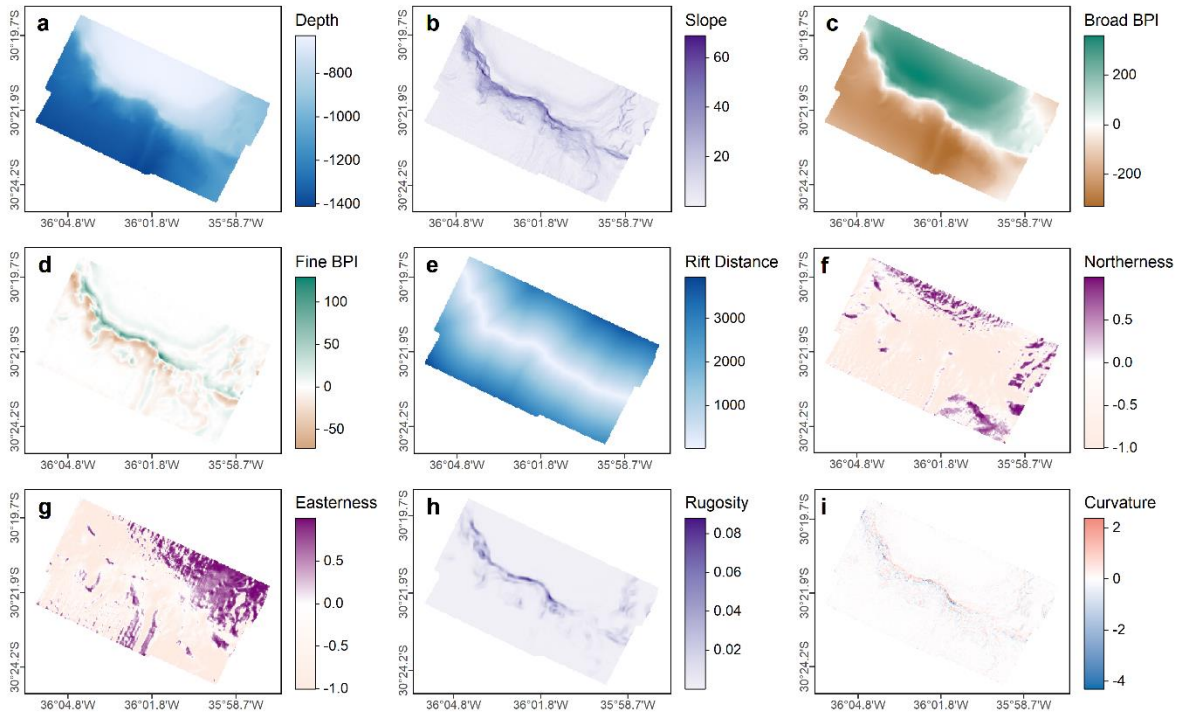

Figure 5.3. The bathymetry-derived variables in Area 2, which were used as explanatory variables in the models for testing. **(a)** Depth. **(b)** Slope. **(c)** Broad-scale Bathymetric Position Index (BPI). **(d)** Fine-scale BPI. **(e)** Euclidian distance from the border of the rift. **(f)** Northness. **(g)** Eastness. **(h)** Rugosity. **(i)** Curvature**.**

The *HyBIS* and *Shinkai* videos were annotated and counted for benthic fauna while classifying them to the lowest possible taxonomic group. The branched hexactinellid *Sarostegia oculata* was the most commonly observed habitat-forming VME indicator species in both Area 1 (Chapter 4) and Area 2 (Hajdu et al., 2017). The timestamp of the video was used to obtain the coordinates of the observations from the *HyBIS* and *Shinkai* track data. Grid cells where at least one individual of *S. oculata* were classified as “presence”, and grid cells with overlapping track and no observations of *S. oculata* were classified as “absence”. Each of these grid cells are hereafter called records or sites, used to train and evaluate the models.

A set of additional seafloor variables (Figs. 5.2 and 5.3) was derived from the bathymetric data using the Benthic Terrain Model 3.0 tool (Walbridge et al., 2018) in ArcGIS. These variables were slope, aspect (measured in terms of northness and eastness), roughness (11 neighborhood size), curvature, fine-scale (3/30 radius) Bathymetric Position Index (BPI), and broad-scale (20/200 radius) BPI. The rift is a major feature in both areas that may play an important role in the distribution of the species in RGR. As such, we included the distance from the rift border as another environment variable in our analysis. This was achieved by creating a contour at value 0 from the broad-scale BPI raster. This will result in two contours outlining the NE and SW rift borders, which were used as source for the “Euclidean Distance” tool in ArcGIS. Before data analysis, collinearity between variables was checked using Pearson’s correlation coefficient and the Variance Inflation Factors (VIFs) (Guisan et al., 2017) using the *usdm* package (Naimi et al., 2014).

5.2.2 Modeling methods

The distribution of *S. oculata* was modeled using five algorithms widely used in species distribution models: Random Forest (RF), Boosted Regression Trees (BRT), MaxEnt, Generalized Additive Models (GAMs), and Artificial Neural Networks (ANN). In general, these models differ in the way they determine the fitted function, and how they handle interactions, model complexity, and overfitting (Merow et al., 2014). Models were developed using R (R Core Team, 2020) with the framework caret (Kuhn, 2008). The caret package is a set of functions that streamline the process of creating predictive models and provides a uniform interface for data splitting, variable selection, and model tuning. It uses other packages internally to create the models. We used

default parameters for each package, except when stated in the text below or Table 5.1. The function *rfe* was used to perform recursive feature elimination in the models, but no advantage was gained in model performance from removing variables from the models, so we kept all variables in the final models.

RF builds multiple classification trees by taking many bootstrap samples from the training data and making an average prediction over all fitted trees (Strobl et al., 2009). RF uses only a randomly smaller set of the predictor variables (parameter **mtry**) on each split while growing each tree, which reduces the variance of the final model, with subsequent gains for predictive performance. We set the number of trees to grow (parameter **ntree**) as 1000.

BRT builds several regression trees (parameter **n.trees**) in a forward stagewise fashion. At each step of model fitting, the algorithm fits each new tree to the residuals of the previously fitted trees and uses only a random subset of data (Elith et al., 2008). This gradually increases emphasis on observations modeled poorly by the existing collection of trees. The contribution of each tree is controlled by the **shrinkage** parameter, as the model-building process usually performs best if it moves slowly down the gradient. **Interaction.depth** controls the maximum depth of the individual trees and **n.minobsinnode** controls the minimum number of observations in terminal nodes.

Maxent estimates species distribution by minimizing the relative entropy between two probability densities (Elith et al., 2011; Phillips et al., 2006). Although it was initially developed as a machine-learning algorithm, MaxEnt has known links to Poisson point process models (Renner & Warton, 2013) and it can be categorized as a “regression-based” model. MaxEnt has the ability to fit complex models, controlled by the use of transformed features of the predictor covariates (parameter **feature types**). **Regularization multiplier** can also be used to smooth and avoid fitting overly complex models. In this work, we employed real absences derived from the dives instead of more commonly used pseudo-absences and used the Java implementation to train the MaxEnt models, version 3.4.4.

GAMs are an extension of General Linear Models (GLMs) but use nonparametric smoothing functions which allow modeling of non-linear relationships between the response and explanatory functions. Multiple smoothing parameter estimation methods are available in the package (parameter **method**) (Wood, 2011). It can also add an extra penalty to each term (parameter **select**), meaning that the smoothing parameter estimation can completely remove terms from the model. We

used a binomial distribution with the logit function and thin plate regression splines for the smoothing basis of all terms.

ANNs are a deep learning approach that consist of a large number of nodes and connections, typically organized in layers (Basheer & Hajmeer, 2000). The input layer contains the environmental data, with each input node representing one environmental variable. The information from each input node is fed into the hidden layers, which may contain multiple layers with a variable number of nodes. Data from the last hidden layer is then fed to the output layer which represents the result of the model. The connections between the nodes from one layer to the next, also known as weights, are optimized using a back-propagation process. Our model has a single hidden layer, with 1 to 21 nodes (parameter **size**). **Decay** is used as a penalty for these connections that both help the optimization process and avoid over-fitting. The feed-forward and back-propagation processes are repeated until the model reaches a pre-defined accuracy, or a maximum set number of runs controlled by the parameter maxit (in our model we set **maxit** as 500).

Table 5.1. Modeling methods, their implementations during tuning, and the tuned parameters used in the final models.

Method	R package	Parameter	Values	Tuned
RF	randomForest	mtry	1–9	1
BRT	gbm	n.trees	from 100 to 3,000 by 50	2600
		interaction.depth	from 1 to 16 by 3	10
		shrinkage	10^{-1}, 10^{-2}, 10^{-3}, 10^{-4}	10^{-3}
		n.minobsinnode	5, 15	5
Maxent	custom[1]	feature types	l, lq, lqp, lqph, lqh, lqpt, lqt, lqpth[2]	lqpth
		regularization multiplier	from 0.2 to 2 by 0.2, 2.5, 3, 3.5, 4, 4.5, 5	1
GAM	mgcv	method	REML, ML	ML
		select	TRUE, FALSE	TRUE
ANN	nnet	size	1, 3, 5, 7, 9, 11, 13, 21	21
		decay	0, 10^{-1}, 10^{-2}, 10^{-3}, 10^{-4}, 10^{-5}	0.1

[1] Custom script was used to run the MaxEnt java application and read its output within caret.
[2] l = linear, q = quadratic, h = hinge, p = product and t = threshold.

The relationship between the environmental layers and the predicted probability of presence was analyzed using response curves produced using the methodology

described by Elith et al. (2005). All variables were held constant at their mean except the target variable, which varied at 100 points across its range. Then, the prediction of each algorithm was computed for each of the 100 values of the target variable and used to produce the response curves. The advantage of this method is that it can be applied to any model and be compared against different model techniques, but it does not account for interactions between variables. The importance of each variable in the final output was computed using the methodology described by Thuiller et al. (2009). The target variable was shuffled, while the others were left untouched. The Pearson's correlation coefficient between the reference and shuffled predictions was calculated and the score *1 - correlation* is returned. Scores near one mean the variable has a high influence on the model, and a score of zero assumes no influence of the variable on the model. The process was repeated 100 times for each variable.

An ensemble model is a popular technique for reducing the uncertainty of model predictions (Dormann et al., 2018). They may reduce prediction errors and decrease mean bias due to the choice of method (Araújo & New, 2007). This is usually achieved by computing the weighted or unweighted averages of the different model outputs. Ensemble models also permit uncertainty caused by the different predictions to be calculated. In this study, all model predictions were rescaled between 0 and 1, and their unweighted average was used to build the ensemble model. Spatial measures of uncertainty were calculated using a bootstrap technique (O. F. Anderson et al., 2016; Rowden et al., 2017). A random sample of the presence-absence data, of equal size, was drawn with replacement, and the five models were constructed with the same settings as the originals. Predictions were then made to the study area, and this process was repeated 200 times. Model uncertainty was represented as the coefficient of variation (CV) of the bootstrap output, i.e, the standard deviation divided by the mean.

5.2.3 Model evaluation

The data in this study was divided into train, validation (also referred to as development in the literature), and test sets. The train set is used to train the model, while the validation set is used to evaluate the model during tuning. After the best parameters are selected, both train and validation sets are used to train a final model, which is evaluated using the test set. Data obtained from Area 1 with *HyBIS* was used as train and validation sets. Such data inherits a high spatial dependency, as records

are available next to each other throughout each dive, and can lead to overestimation of model performance (Fourcade et al., 2018). To provide a larger level of spatial independence between the training and the validation data, the first or last 20% records in each dive were selected to be used as a validation set. Consequently, the remaining 80% were used to train the model. The region of the dive which was cut from training, whether from the beginning or towards the end, was selected at random for each dive, and this process was repeated 25 times. During model tuning, the AUC_{ROC} metric was used to select the best models. Data obtained from Area 2 with *Shinkai* is completely independent from Area 1 and was used exclusively as a test set for the final model. The evaluation was performed 25 times using a random selection of 70% of the test data (subsampling) in each interaction.

Models were evaluated using five metrics to cover different aspects of the modeling performance: (1) area under the receiver operating characteristic curve (AUC_{ROC}), (2) area under the precision-recall gain curve (AUC_{PRG}), (3) Sensitivity, (4) Specificity, and (5) True Skill Statistics (TSS). AUC_{ROC} and AUC_{PRG} are threshold-independent measures, while Sensitivity, Specificity, and TSS need to convert the predicted likelihood of the model (a value between 0 and 1) into a presence/absence classification using a threshold. Here we used the threshold which balances sensitivity and specificity, which minimizes both commission and omission errors, and is recommended for SDMs model (Liu et al., 2005). Note that thresholds were selected using the validation data set.

AUC_{ROC} assesses the ability of models to discriminate presence from absence sites and is widely used in species distribution models. The ROC curve is created by calculating the true positive rate (the proportion of presences correctly predicted, also known as sensitivity or recall) and the false positive rate (the proportion of absences falsely predicted, also calculated as 1 - specificity) at various threshold settings. AUC_{ROC} ranges from 0 to 1, where values above 0.9 indicate excellent performance, values between 0.7 and 0.9 indicate good performance, and a value of 0.5 or below indicates no better discrimination than a random classification.

The area under the precision-recall curve (AUC_{PR}) measures the ability to capture true presences and does not include false positives or absences in its calculation. AUC_{PR} is recommended when the user is more interested in an accurate prediction of the presences or when the number of absences is much larger than presences (Valavi et al., 2022). Like the ROC curve, the precision-recall curve

calculates precision (the proportion between correctly predicted presences and all predicted presences) and recall across multiple thresholds. The baseline in the AUC_{PR} depends on the prevalence in the testing data (Saito & Rehmsmeier, 2015), making it difficult to compare between species or studies. As such, the precision-recall curve is plotted in a new coordinate system, called the precision-recall gain curve, as described by Flach and Kull (2015). AUC_{PRG} values from 0 to 1 indicate a performance better than random, where 1 is a perfect discrimination model. Negative values indicate predictions worse than random.

Specificity is the proportion of absences correctly predicted. Both sensitivity and specificity are considered high with values above 0.8 (Liu et al., 2005). TSS normalizes the overall accuracy and accounts for both omission and commission errors (Allouche et al., 2006). TSS is calculated as sensitivity plus specificity minus one and ranges from -1 to 1, where +1 indicates perfect agreement and values of zero or less indicate a performance no better than random. TSS is also considered less sensitive to prevalence compared to Cohen's Kappa statistic.

Because we used presence-absence data to train the models, we also produced calibration plots to evaluate the agreement between predicted probabilities of occurrence and observation of presence and absence. If the plotted tend is lined up close to the diagonal, we conclude that the model is well-calibrated. Calibration plots were drawn using the scripts in Phillips and Elith (2010). Statistical significance of differences between the models for the five statistics were tested using Friedman's Aligned Rank test ($p < 0.05$) (García et al., 2010), using the R package *scmamp* v0.2.55 (Calvo & Santafé, 2016). We also applied the post hoc test to conduct pairwise comparisons for each metric, using the Shaffer correction.

5.3 Results

From the 1193 records (grid cells) that were observed by *HyBIS* in Area 1, 231 had the presence of at least one *Sarostegia oculata*. In Area 2, 29 out of 255 records were observed with the presence of *S. oculata* by *Shinkai*. The hexactinellid showed a higher abundance near the rift walls in both areas and was found only on hard substrates, of which the majority had a ferromanganese crust.

The performance of the models was good for each metric calculated, for both validation and test data. AUC_{ROC} (Fig. 5.4a) values were > 0.9, except for ANN which

performed slightly lower. All models had good AUC_{PRG} scores > 0.8 (Fig. 5.4b) and the RF, BRT, MaxEnt, GAM, and Ensemble models had nearly perfect values close to one for the test data, indicating a good discrimination ability to detect presence records. Similarly, all models showed high values for Sensitivity (Fig. 5.4c) and Specificity (Fig. 5.4d) for the validation data, suggesting a high proportion of observed presences and absences correctly predicted, respectively. Models RF, BRT, MaxEnt, and Ensemble had a higher sensitivity for the test data compared to the validation data. In contrast, GAM and ANN models had lower performance. Models had high specificity for test data as well, although the RF model was below 0.8. For the TSS metric, the ANN model had the overall lowest performance, while models BRT, MaxEnt, and Ensemble had the highest values for test data (Fig. 5.4e). Friedman's Aligned Rank test showed a significant difference between models for the five statistics. The post-hoc test showed that the most significant differences were found when comparing GAM and ANN with other models (Appendix D). The threshold values used to discriminate between presence and absence were 0.248, 0.126, 0.304, 0.121, 0.187, and 0.225 for the RF, BRT, MaxEnt, ANN, GAM, and Ensemble models, respectively.

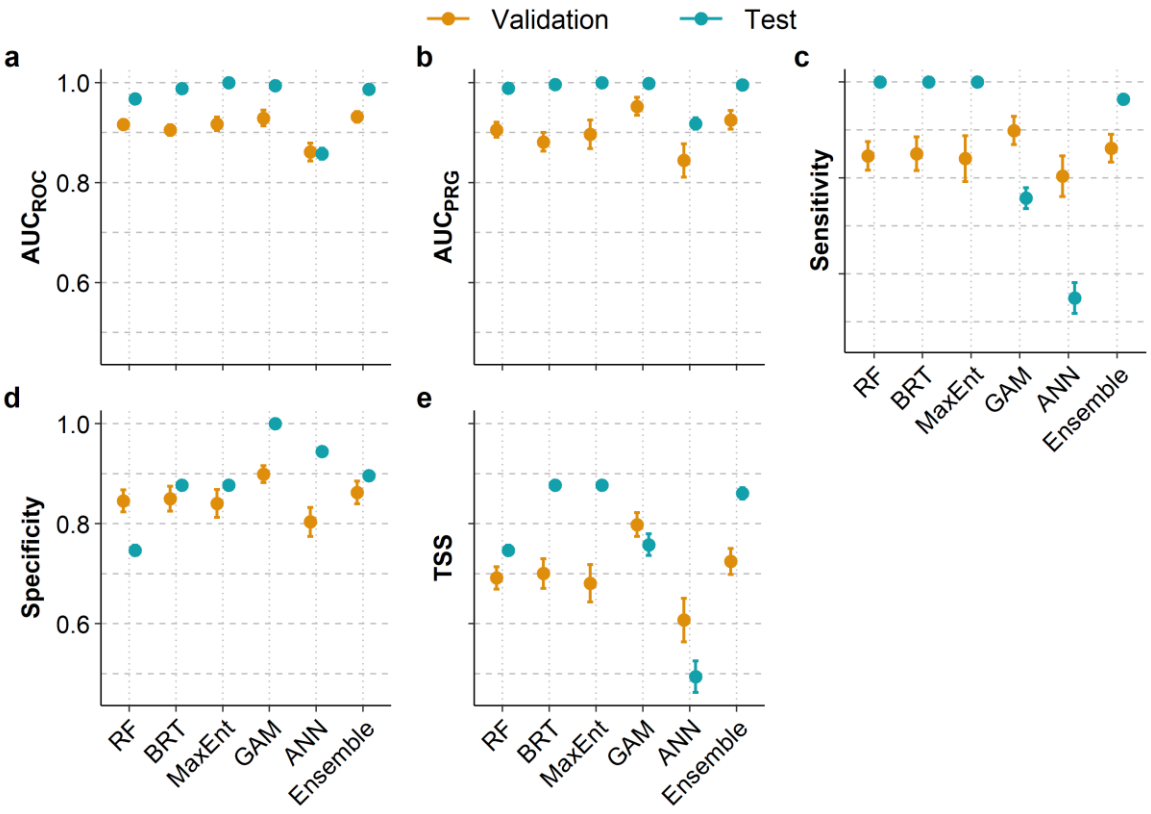

Figure 5.4. Mean and standard error of model performance statistics for both validation (orange) and test (blue) data across replicates. **(a)** AUC_{ROC}, **(b)** AUC_{PRG}, **(c)** Sensitivity, **(d)** Specificity and **(e)** TSS.

The calibration plots show that the true probability of presence compared to the predicted presence of the five models are badly calibrated (Fig. 5.5). The ideal curve (dotted line) is below the lower confidence interval of the fitted calibration curve, indicating that the true probability of presence is much larger than the estimate given by the models. Only models RF (Fig. 5.5a) and MaxEnt (Fig. 5.5c) had the ideal curves above the higher confidence interval for low probability values. These results indicate models have a high discrimination power, i.e. the ability of a model to correctly distinguish between occupied and unoccupied sites, but the model output should not be interpreted as estimates of *conditional* probability of presence.

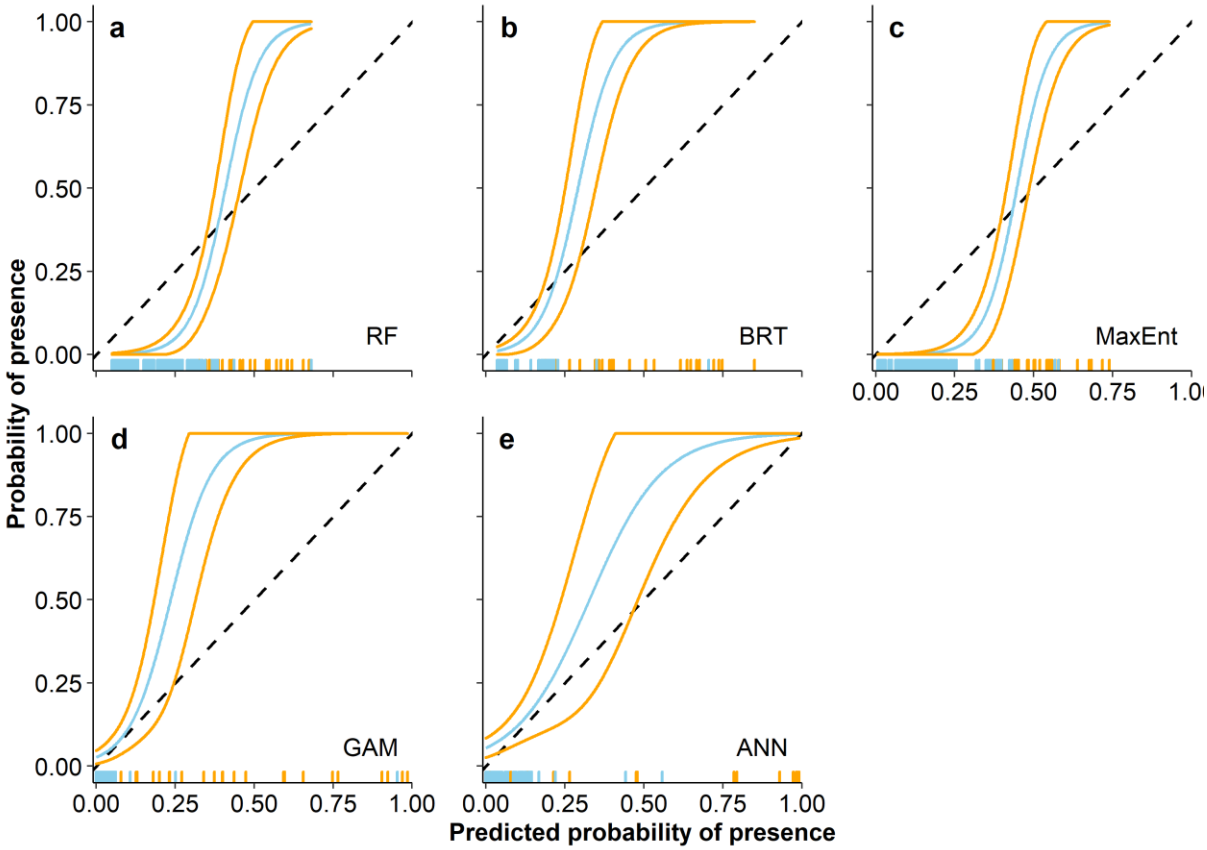

Figure 5.5. Presence-absence calibration plots for each model fitted with natural splines. **(a)** Random Forest, **(b)** Boosted Regression Trees, **(c)** MaxEnt, **(d)** Generalized Additive Models, and **(e)** Artificial Neural Networks. The calibration curve is in blue and a confidence interval of ± 2 SD is in orange. The rug plots show model predictions at presences (orange) and absences (blue). The dotted line indicates a 1:1 relationship representing 'perfect' calibration.

Generally, all models predicted a suitable habitat along with the full extent of both NE and SW rift borders in Area 1, and the NE rift border in Area 2. For Area 1 (Fig. 5.6), RF model predicted the distribution to be more extensive, with a relatively higher likelihood on the bottom of the rift compared to the middle of the plateaus. Other

models had a relatively low (< 0.1) likelihood on the bottom of the rift, on top of the plateaus, on the south canyon, and the lower plane regions at southwest.

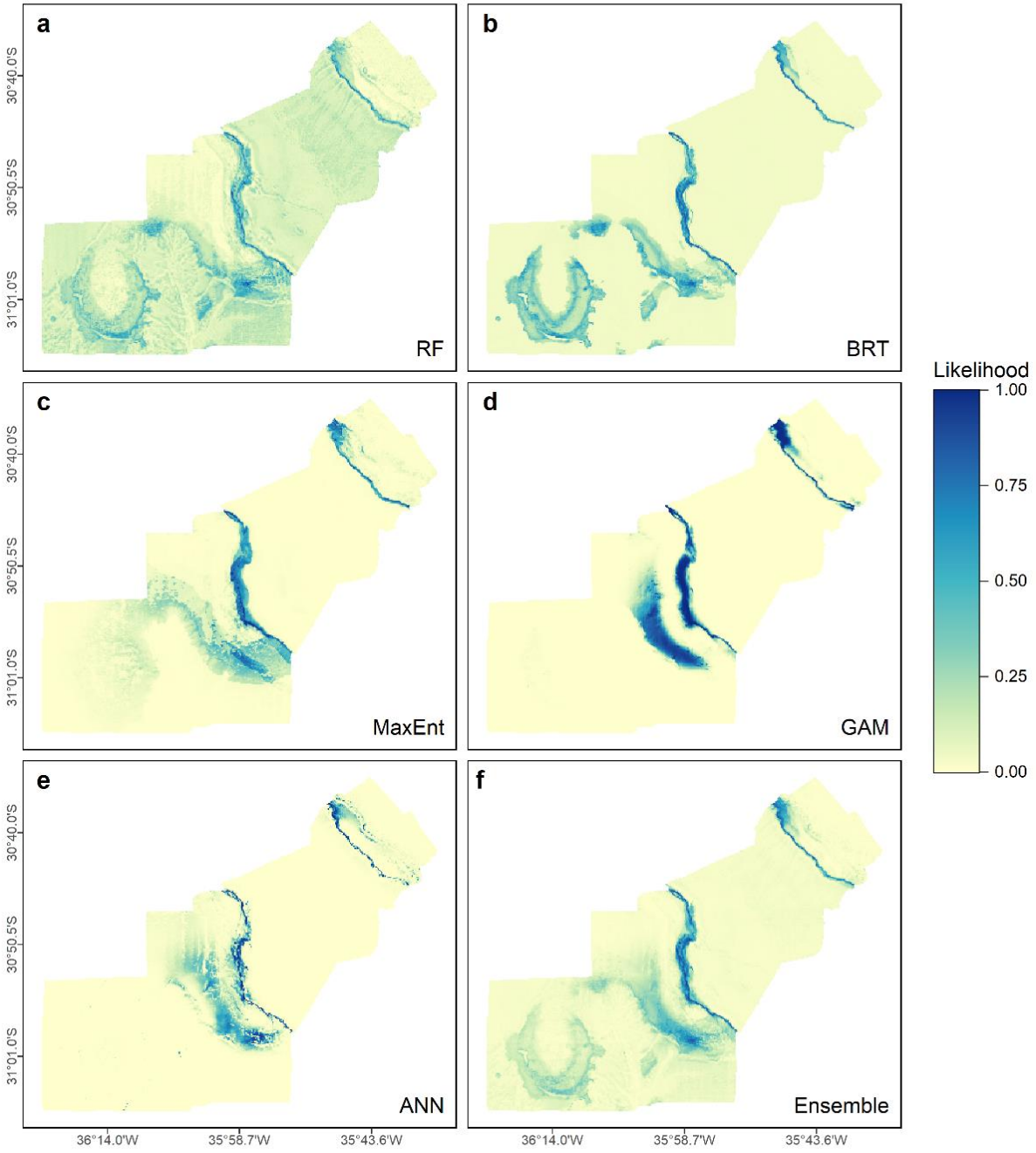

Figure 5.6. Prediction maps of *Sarostegia oculata* in Area 1, using **(a)** Random Forest, **(b)** Boosted Regression Trees, **(c)** MaxEnt, **(d)** Generalized Additive Models, **(e)** Artificial Neural Networks, and **(f)** Ensemble models.

All models predicted a larger area with a high likelihood around the north end of the NE rift border. However, only models RF and ANN extended this area throughout the small terrace at the NE plateau. Models predicted high suitability nearby the area between the east side of the canyon and the SW plateau. The predicted likelihood

extended to the other side of the canyon for the MaxEnt model, and even further around the inner SW plateau for models RF and BRT. The south slide of the SW plateau showed high predicted suitability as well, except for the GAM model. For Area 2 (Fig. 5.7), models predicted a high likelihood near the slope of the NE rift border, between 700 and 1000 m. All models, except for RF, showed low (< 0.1) suitability at the rift bottom and the top to the plateau.

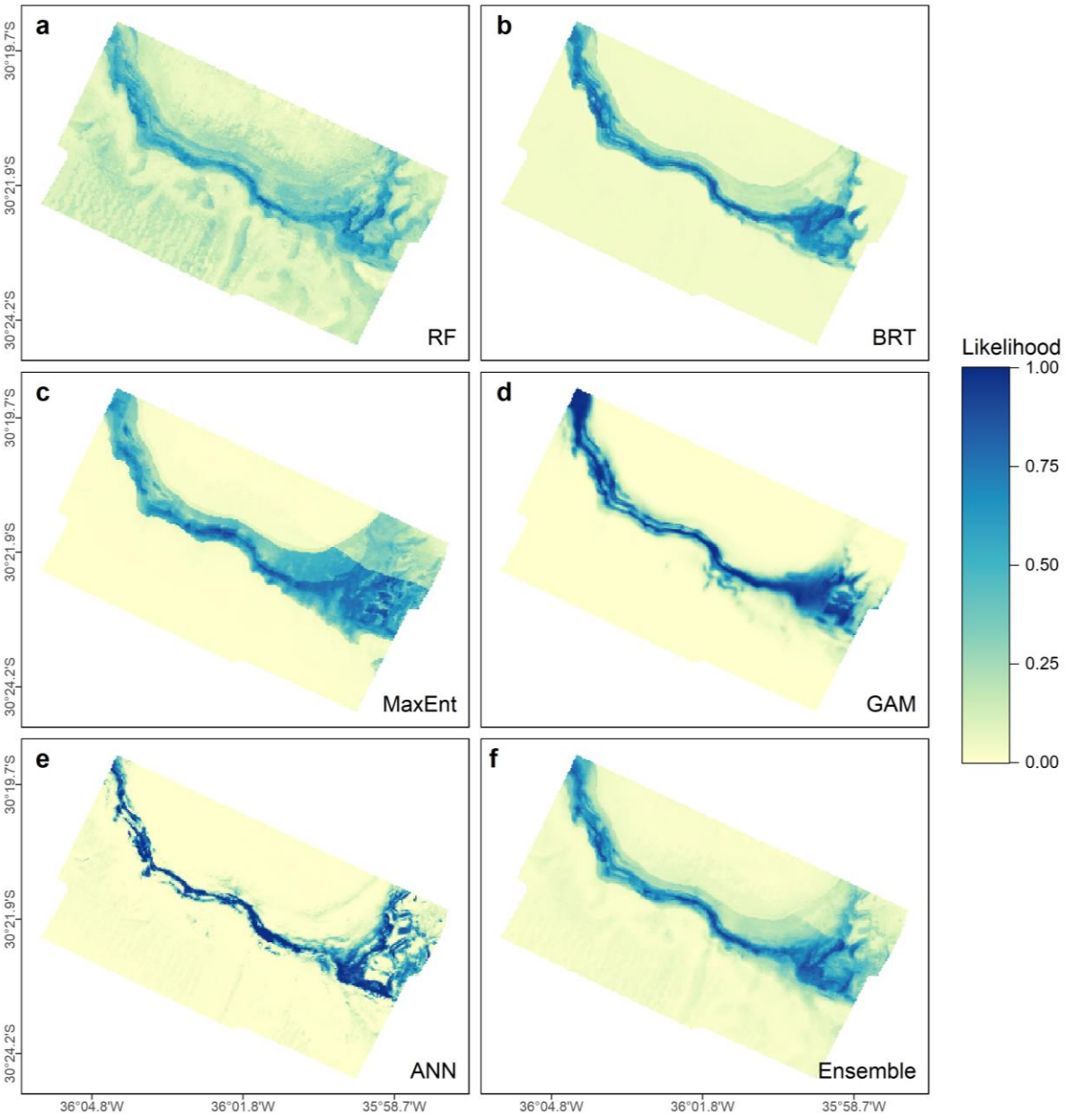

Figure 5.7. Prediction maps of *Sarostegia oculata* in Area 2, using **(a)** Random Forest, **(b)** Boosted Regression Trees, **(c)** MaxEnt, **(d)** Generalized Additive Models, **(e)** Artificial Neural Networks, and **(f)** Ensemble models.

The predicted suitable habitat by the ensemble model reflected the average of all five models accordingly. This predicted distribution reflected environmental variables included in the model, namely depth and slope. The region with bottom depths between 700 and 1000 m that had nearby slopes > 20 degrees contained a continuous band of high prediction of suitable habitat. The spatial patterns of low-modeled uncertainty corresponded to the main areas predicted as highly suitable on the rift borders in both Area 1 and Area 2 (Fig. 5.8), together with the majority of the SW plateau and around the inner SW plateau. Regions of high uncertainty were obtained for the rift bottom, the canyon, the lower plane regions, and in some areas on top of the plateaus.

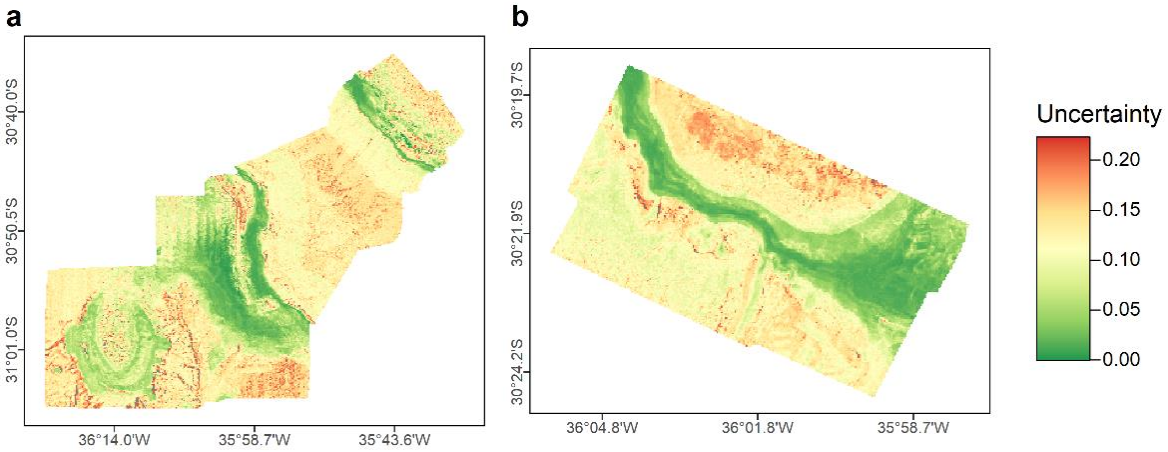

Figure 5.8. Uncertainty (CV) for the ensemble distribution model of **(a)** Area 1 and **(b)** Area 2.

The importance of the environmental variables varied across the modeling algorithms, but depth, fine BPI, and northness usually had a high influence across all models (Table 5.2). For the RF model, the variables showed a low importance index (< 0.1), indicating that this model uses all variables to predict the presence of *S. oculata*, and changing a single variable has little effect on its output. Only depth and fine BPI had higher importance relative to other variables. For BRT, MaxEnt, and GAM models, the variables depth, fine BPI, northness, and curvature had a high influence in the likelihood of *S. oculata*. However, depth had a higher influence for BRT and GAM compared to MaxEnt, and northness had a higher influence for MaxEnt and GAM compared to BRT models. For the ANN model, most variables showed a high influence in its output, except for broad BPI and eastness.

Table 5.2. Mean index of the importance of each predictor variable across 100 permutations in the training dataset, for the Random Forest (RF), Boosted Regression Trees (BRT), MaxEnt, Generalized Additive Models (GAM), and Artificial Neural Networks (ANN) models.

Variables	RF	BRT	MaxEnt	GAM	ANN
depth	0.09	0.388	0.113	0.572	0.553
slope	0.035	0.009	0.034	0.051	0.183
broad BPI	0.016	0.002	0.000	0.000	0.066
fine BPI	0.072	0.296	0.441	0.588	0.44
rift distance	0.049	0.008	0.004	0.000	0.349
northness	0.044	0.112	0.435	0.762	0.338
eastness	0.031	0.003	0.007	0.000	0.081
rugosity	0.036	0.011	0.008	0.000	0.19
curvature	0.037	0.046	0.106	0.094	0.304

In general, models showed similar response patterns across the gradient of each environmental variable. Depth (Fig. 5.9a): MaxEnt, GAM, and ANN models showed a low response at higher depths below ~1000 m and shallower waters above ~700 m, but showed a peak in the predicted likelihood of *S. oculata* within ~700–1000 m. For RF and BRT models, the response remained high from deeper sites until ~800 m where it reached a peak, and then the response was low at shallow depths. Slope (Fig. 5.9b): models had a low response at flat sites, which increased at steeper slopes. The biggest variation in the response for slope was found in the ANN model. Broad BPI (Fig. 5.9c): it had a high response around 70 for RF, BRT, and MaxEnt models, but GAM and ANN predicted likelihood was higher at lower broad BPI values (< 0), and lower at broad BPI > 100. Fine BPI (Fig. 5.9d): RF, BRT, and ANN showed a lower response at fine BPI < 0, and a higher response at values > 0, with a larger variation produced by the ANN model. MaxEnt response was higher with negative fine BPI, while GAM was unresponsive for this variable, characterized by a flat horizontal line in the plot. Rift distance (Fig. 5.9e): All models except ANN showed a similar pattern for the rift distance. A peak in response near the rift (< 2000 m) and from 4500 to 7000 m, along with low response between 2000 and 4500 m and regions more distant than 7000 m. The ANN model was different, with a high response near the rift, lowering constantly as it moves away until 10,000 m. The MaxEnt, GAM, and ANN had very low predicted outputs when far away from the rift (> 20,000 m). Northness (Fig. 5.9f): peaks in response were produced at sides facing north and south in models RF, BRT, and MaxEnt. GAM generated a slightly higher response in sites facing north than south.

ANN, instead, generated a higher response in sites facing south than north. Eastness (Fig. 5.9g): models predicted a slightly higher response on sites facing either east or west. However, the GAM was unresponsive for this variable as well. Rugosity (Fig. 5.9h): models had a low response at sites with low rugosity, that increased at areas with higher values. Curvature (Fig. 5.9i): only ANN model had a large variation in response for curvature, with a peak in sites with curvature close to zero. RF and BRT, instead, showed a smaller response in these sites. MaxEnt and GAM were unresponsive for this variable.

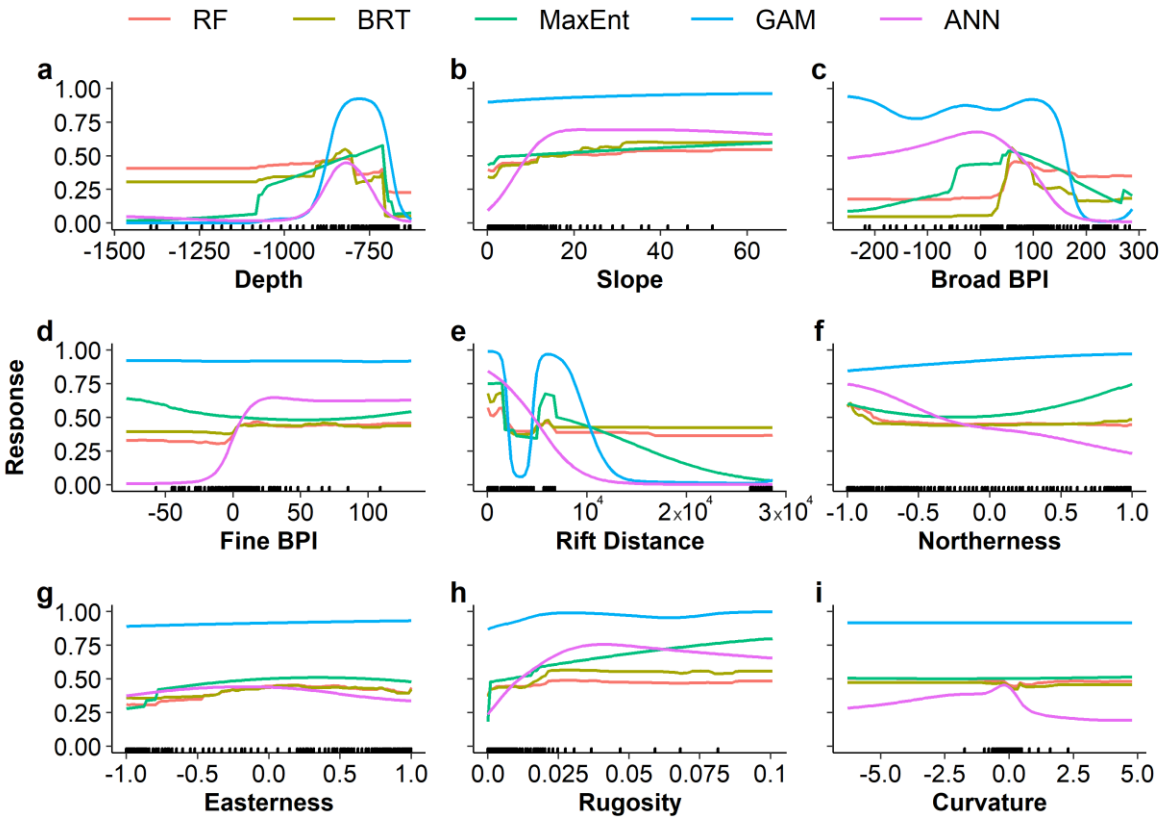

Figure 5.9. Response curves of the likelihood of presence of *Sarostegia oculata* for each predictor variable for the Random Forest (RF), Boosted Regression Trees (BRT), MaxEnt, Generalized Additive Models (GAM), and Artificial Neural Networks (ANN) models. Rug plot inside bottom of each panel show distribution of sites across that variable, in percentiles.

5.4 Discussion

The Rio Grande Rise contains diverse benthic communities which include several VME indicator species such as sponges, scleractinians, octocorals, and black corals (Chapter 4). Although RGR is located in oligotrophic waters, this diversity is likely related to strong currents and complex geomorphology with multiple habitats

(Montserrat et al., 2019). Our study provides high-resolution Distribution Maps (DM) for an important VME indicator species recorded in RGR, the branched hexactinellid *Sarostegia oculata*. This sponge was the most abundant species found in the footage near the rift (Chapter 4) (Hajdu et al., 2017), closely associated with Fe-Mn crust substrates. A few fragments of *S. oculata* sampled by dredges revealed 18 species associated with this sponge (Chapter 3), the most notorious being a zoanthid and an annelid: *Thoracactis topsenti* and *Hermadion fauveli cf.* Gravier (1918), respectively, which also emphasize the importance *S. oculata* has in this environment. Our work is the first to create a species distribution model of *S. oculata*, and the first to produce high-resolution DMs at RGR, with potential use for deep-sea conservation and management in this area.

Deep-sea sponges have a high conservation and management significance because of their low resilience (Ramiro-Sánchez et al., 2019). These species and their associated fauna are particularly vulnerable to anthropogenic impacts such as fishing and deep-sea mining due to their slow growth rates and low or unpredictable recruitment (Gollner et al., 2017), proving to have a very slow or nonexistent recovery (Klitgaard, 1995). For being suspension filters, they will likely suffer from sediment loads caused by deep-sea mining (Miller et al., 2018). The water canal system of such sponges is at risk of becoming clogged (Wahab et al., 2017) by high loads of suspended particulate matter. These mining plumes can be of low or no nutritional value, further threatening the maintenance of these animals. Hence, *S. oculata* not only will be primarily affected by crust removal, but also in the area surrounding mining operations

High-resolution distribution models of benthic species, using seafloor camera imagery and bathymetric data obtained from multibeam surveys, have proven useful in the last two decades. Similar models for VME indicator taxa have been developed for conservation and management of areas of interest in the deep sea (Dolan et al., 2008; Howell et al., 2011; Ramiro-Sánchez et al., 2019; Rengstorf et al., 2013, 2014; Robert et al., 2016; Rodríguez-Basalo et al., 2021; Rowden et al., 2017; Tong et al., 2013). Such models are able to provide expert advice on the occurrence of VME indicator taxa in efforts to limit anthropogenic threats from future marine resource exploitation

5.4.1 Species distribution model

The five models trained in this study predicted a high likelihood of *S. oculata* along with all extent of both rift borders in the multibeam survey. These findings reinforce the idea that *S. oculata* distribution is highly related to the NE-SW rift border that runs throughout RGR, as suggested by Hajdu et al. (2017) and in Chapter 4. This area is known to be an optimal place for Fe-Mn crusts formation (Montserrat et al., 2019), highly supported by the first claims by CPRM to ISA, which consists of 150 blocks of 20 km^2 each, the maximum allowed by Regulations on Prospecting and Exploration for Fe-Mn crusts (da Silva, 2021). The majority of the blocks are situated along the plateaus of WRGR, on both sides of the rift (Montserrat et al., 2019, fig. 1), where CPRM likely prospected areas of high Fe-Mn deposits before submitting the claim. In addition, *S. oculata* is somehow more closely associated with Fe-Mn crusts pavements in the plateaus near the rift and along the rift walls compared to other substrates (Chapter 4) (Hajdu et al., 2017). Our study reinforces this relationship between *S. oculata*, Fe-Mn crusts, and the rift at RGR. A second notable suitable area was predicted between the southwestern of the SW plateau and on the top northeastern canyon side. However, we have no footage of this area that can confirm or not the presence of *S. oculata* there.

Sampled Fe-Mn crusts near the rift suggest that they were eroded by the strong currents that impacted the RGR plateau (Benites et al., 2020), and bottom currents of more than 0.2 m/s may be capable of eroding Fe-Mn crust surfaces (Yeo et al., 2019). These currents may provide a high food supply for the development of *S. oculata*, and can be an important key factor in the development of this organism. Unfortunately, we do not have a hydrodynamic model in the study area that could provide current velocities and directions, which could be used as predictors in the distribution models. Future studies should focus on obtaining and applying such variables in the models, as they likely play an important role in the distribution of species in RGR. The complex outlines of the rift walls may generate vortices (Hajdu et al., 2017) and areas of slope may facilitate the propagation of internal tidal waves (Beazley et al., 2018; Klitgaard & Tendal, 2004), which can cause resuspensions favoring greater development of sponges. This may explain the importance and response of rift distance and fine BPI in the distribution of *Sarostegia*. Steeper slopes also predicted higher response in the models, although this variable did not output great importance in the bootstrapped

correlation test. The aspect of the seabed, in terms of northness, predicted the highest likelihood on the northern and southern slopes, which may correspond with the direction of currents in RGR as well.

Another variable considered important in our results was depth. The prediction of *S. oculata* was restricted between ~700–1000 m, which corresponds to the plateaus and upper rift walls. Depth is usually an important variable that predicts the occurrence of VME indicator species and can act as a surrogate for other important variables such as temperature, salinity, oxygen, nutrients, water masses, exported surface production, and aragonite saturation (Leathwick et al., 2006; Rowden et al., 2017; Thresher et al., 2014). *S. oculata* was collected/observed at 598–1311 m depth in Cape Verde (Topsent, 1904), at 745 m in east of Miami Terrace, south-west of Bimini (Dohrmann et al., 2011), at 790–900 m in the Vitória Trindade seamounts chain (Tabachnick et al., 2009), at 738–1040 m in RGR by Hajdu el al. (2017), and in our study, from 681 to 1203 m. The similarity in depth ranges in the Atlantic between these records suggests that this sponge occurs in bathymetrically constrained bands. However, it is important to note that this bathymetric range alone is not sufficient to predict the distribution, as the inner SW plateau is within this range, but the models had a low likelihood in this region.

There are a few global distribution models of VME indicator taxa, namely scleractinians, octocorals, and black corals, that predicted their occurrence on RGR (A. J. Davies & Guinotte, 2011; Montserrat et al., 2019, fig. 9; Yesson et al., 2012, 2015). Similar models were built using data exclusively from the Brazilian continental margin by Barbosa et al. (2020), who addressed the distribution of scleractinians and octocorals in RGR. Overall, they predicted a high suitability of VME indicator taxa on the plateau of RGR, especially in regions near the rift, somewhat similar to the predicted output of our models. However, these models use coarse resolution data (>= 0.0083°, ~1 km) as environmental predictors, and none had access to biological records from RGR to train or evaluate the model. High-resolution bathymetric data can better represent seabed physiographic features and improve regional and local suitability models (Ross et al., 2015).

5.4.2 Implications for Spatial Management and Conservation

There is a growing number of examples in the literature that demonstrate the potential of using species distribution models to predict the occurrence of deep-sea sponges for their conservation and management from impacts caused by anthropogenic activities such as bottom trawling and mining (Beazley et al., 2018; Rowden et al., 2017). They provide fundamental ecosystem functions, and even in low densities, hexactinellid sponges may create a suitable substrate for colonization and development of several invertebrate taxa, serving as island habitats on the deep-sea floor (Beaulieu, 2001). Thus, increasing knowledge of their distribution and environmental conditions responsible for their formation and persistence are key factors to ensure the protection of the marine environment, especially from harmful effects resulting from human activities.

The models performance were excellent or good in most cases, correctly identifying 85.4% of sites for validation and 88.8% for testing. Our study uses a completely different dataset to test the models (Area 2), independent from the data used to train and validate the model (Area 1). This method was intended to simulate how models would perform in case they were used to predict the distribution of *S. oculata* in a neighboring, unexplored region compared to the original area where models were built. The high performance models had in the test dataset suggests they could be used to predict the distribution of *S. oculata* in unsurveyed areas, at least to some extent. In addition, our study suggests an overlap in the potential distribution of Fe-Mn crusts and *S. oculata*, which should be addressed in the management of mining to minimize impacts in this community and diminish the loss of biodiversity in RGR.

There are a few limitations that should be considered during the modeling approach. Species occurrence in different areas can be difficult to model, as SDMs can fail to account for biotic processes, such as competition and predator-prey interactions, and due to shortfalls in the available data, such as sampling bias and lack of key drivers of habitat suitability (Vierod et al., 2014). The absolute uncertainty of the model prediction is unknown, but the bootstrap procedures provided a measure of internal consistency across the models (O. F. Anderson et al., 2016). Uncertainty maps are a key resource when applying predictions of distribution models to management measures. The uncertainty of the ensemble model was the lowest near the rift border on both sides, and higher below 1,000 m depth or in some areas on top of the plateaus.

Predictions in the rift border had more confidence, which could be explained by a higher sampling effort in this region. Thus, it is advised to use our models carefully to predict areas away from the rift. Increase in model performance and reduction in uncertainty may be achieved with (a) a regularly spaced sampling regime that covers the entirety of the environmental conditions observed in the region of interest (Hirzel & Guisan, 2002), (b) inclusion of key environmental drivers for sponges, such as sediment type, current regimes, and nutrients (Rengstorf et al., 2013, 2014), (c) and broader high-resolution surveys, that are still scarce for the area (Jovane et al., 2019).

Rio Grande Rise had been treated as an area beyond national jurisdictions (ABNJ) and under regulations of the International Seabed Authority (ISA). In December 2018, Brazil presented a partial revised submission to the Commission on Limits of The Continental Shelf (CLCS), which includes RGR as part of its continental margin (da Silva, 2021). If approved, RGR will become a region under the jurisdiction and sovereign rights of Brazil, along with its mineral resources. This creates unforeseen implications for the management of RGR, as the regulations that will govern this area are still uncertain. Nevertheless, this issue should not undermine research that produces data and results which could be used to inform management and conservation planning in the area.

5.5 Conclusions

Our study is the first to create a high-resolution species distribution model of a VME indicator species in Rio Grande Rise. *Sarostegia oculata* is a dominant organism on substrates rich in Fe-Mn crusts, which play a fundamental role to support communities and provide key ecosystem functions in RGR. The five models built here predicted a high likelihood of *S. oculata* along with the rift borders with a low degree of uncertainty, in an area aimed at exploration of Fe-Mn crust deposits. This reinforces the relationship between *S. oculata*, the Fe-Mn crusts, and the rift, implicating that direct destruction of habitats caused by the mining of Fe-Mn crusts could lead to a severe impact in the communities sustained by *S. oculata*, which should be addressed in the management and MPA network design for RGR. There are still large gaps in the knowledge of the benthic fauna distribution and ecosystem functions on RGR, but our study provides expert advice on the occurrence of deep-sea sponges in the area and represents initial steps to guide future surveys and conservation plans in the region.

6 Closing Remarks

The Rio Grande Rise is a complex and massive positive feature located in the middle of the Southwest Atlantic. Its distance from Brazil's shoreline makes it difficult and expensive to reach and collect samples in this area. Hence, the fauna and ecological patterns remain mostly unknown to science. This situation is starting to change, due to the prospect of ferromanganese crusts in RGR. Many surveys were made in the area with the objective to understand the genesis of Fe-Mn crusts, the locations where they are more concentrated, and evaluate its potential for mining, and more are expected until the next decade. These cruises are an excellent opportunity to investigate the diversity and understand biological processes there, filling a huge gap about its knowledge.

While sampling and describing most communities found across all habitats at RGR was not the main object of the MARINE E-TECH project (and such feat would take decades of studies), the results presented in this thesis give us some perception into how and where species are distributed in this region, important ecosystem functions they provide and how they relate with the environment. Rock dredges are not the ideal sampling gear to collect biological samples. They are a semi-qualitative method and can damage the animals during dredging, resulting in a loss of animals and hindering the identification of these specimens. This effect was evident, as large organisms often were sampled in fragments. But they can be used in hard and scarp substrate, which is the case in many areas of RGR, and are cheap, compared to other methods like ROVs (Remotely Operated Vehicles). The collected samples revealed a diverse macro and megafauna attached to the rocks, and many specimens were found associated with larger organisms. Such findings would not be possible by using video analysis alone, as many collected morphotypes were not seen in the images. In addition, many individuals were only identified to genus or species level because they were collected in the dredges as well, meaning that these sampling methods complement each other.

The seabed videos and bathymetric data revealed highly heterogeneous and rapidly changing habitats in RGR, ranging from pavements, terraces, sinkholes, and scarps. The videos recorded during the dive provide more detailed information on how the fauna is distributed in these places. From them, we found variations in the community structure at regional scales and related to distinct habitats. Hence, we may

conclude that heterogeneity in geomorphology and substrates in RGR reflects the variety in communities. In addition, only a small area of RGR was sampled in this study, meaning that the number of species and variations in community structure could be much higher. *Sarostegia oculata* marked a distinct community in the video analysis, likely providing important ecosystem functions based on collected fragments by dredging. The species distribution models suggest that *S. oculata* occurs along both sides of the rift, on the upper slope of the rift and in the plateaus, adjacent to the rift. Its predicted area is targeted for mining of Fe-Mn crusts, which could lead to a severe impact on the communities sustained by this sponge.

Assessing the environmental impacts of FE-Mn crusts exploitation is necessary to build a strategy for the conservation of biodiversity in the deep sea. Do biologically rich ecosystems and Fe-Mn crusts coincide? Are these ecosystems supported by the same environmental processes that are thought to enhance Fe-Mn deposit thickness and grade? What is the potential impact of sediment plumes on deep-sea ecosystems? The results of this thesis contribute to answering these questions and provide insights into the diversity, how they are distributed, and which environmental variables drive their occurrence. While there are still many gaps and more research should be conducted in RGR to fully answer these questions, the data here suggest that acute conflict between benthic fauna and Fe-Mn crusts mining will arise in the following decades. These results may help to establish a network of conservation areas and will facilitate more informed management regarding mining activities in the future.

References

Alberoni, A. A. L., Jeck, I. K., Silva, C. G., & Torres, L. C. (2020). The new Digital Terrain Model (DTM) of the Brazilian Continental Margin: Detailed morphology and revised undersea feature names. *Geo-Marine Letters*, *40*(6), 949–964. https://doi.org/10.1007/s00367-019-00606-x

Allouche, O., Tsoar, A., & Kadmon, R. (2006). Assessing the accuracy of species distribution models: Prevalence, kappa and the true skill statistic (TSS): Assessing the accuracy of distribution models. *Journal of Applied Ecology*, *43*(6), 1223–1232. https://doi.org/10.1111/j.1365-2664.2006.01214.x

Amon, D. J., Ziegler, A. F., Dahlgren, T. G., Glover, A. G., Goineau, A., Gooday, A. J., Wiklund, H., & Smith, C. R. (2016). Insights into the abundance and diversity of abyssal megafauna in a polymetallic-nodule region in the eastern Clarion-Clipperton Zone. *Scientific Reports*, *6*(1), 30492. https://doi.org/10.1038/srep30492

Anderson, M. J. (2001). A new method for non-parametric multivariate analysis of variance: Non-parametric manova for ecology. *Austral Ecology*, *26*(1), 32–46. https://doi.org/10.1111/j.1442-9993.2001.01070.pp.x

Anderson, M. J. (2006). Distance-Based Tests for Homogeneity of Multivariate Dispersions. *Biometrics*, *62*(1), 245–253.

Anderson, O. F., Guinotte, J. M., Rowden, A. A., Tracey, D. M., Mackay, K. A., & Clark, M. R. (2016). Habitat suitability models for predicting the occurrence of vulnerable marine ecosystems in the seas around New Zealand. *Deep Sea Research Part I: Oceanographic Research Papers*, *115*, 265–292. https://doi.org/10.1016/j.dsr.2016.07.006

Arantes, R., Castro, C., Pires, D., & Seoane, J. (2009). Depth and water mass zonation and species associations of cold-water octocoral and stony coral communities in the southwestern Atlantic. *Marine Ecology Progress Series*, *397*, 71–79. https://doi.org/10.3354/meps08230

Araújo, M. B., & New, M. (2007). Ensemble forecasting of species distributions. *Trends in Ecology & Evolution*, *22*(1), 42–47. https://doi.org/10.1016/j.tree.2006.09.010

Ardron, J. A., Clark, M. R., Penney, A. J., Hourigan, T. F., Rowden, A. A., Dunstan, P. K., Watling, L., Shank, T. M., Tracey, D. M., Dunn, M. R., & Parker, S. J. (2014). A systematic approach towards the identification and protection of vulnerable marine ecosystems. *Marine Policy*, *49*, 146–154. https://doi.org/10.1016/j.marpol.2013.11.017

Ashford, O. S., Kenny, A. J., Barrio Froján, C. R. S., Downie, A.-L., Horton, T., & Rogers, A. D. (2019). On the Influence of Vulnerable Marine Ecosystem Habitats on Peracarid Crustacean Assemblages in the Northwest Atlantic Fisheries

Organisation Regulatory Area. *Frontiers in Marine Science*, *6*. https://doi.org/10.3389/fmars.2019.00401

Auster, P. J., Gjerde, K., Heupel, E., Watling, L., Grehan, A., & Rogers, A. D. (2011). Definition and detection of vulnerable marine ecosystems on the high seas: Problems with the “move-on” rule. *ICES Journal of Marine Science*, *68*(2), 254–264. https://doi.org/10.1093/icesjms/fsq074

Baker, E., & Beaudoin, Y. (2013). *Cobalt-rich Ferromanganese Crusts: A physical, biological, environmental, and technical review* (Vol. 1C). Secretariat of the Pacific Community.

Baker, P. F. (1983). Tectonic evolution and subsidence history of the Rio Grande Rise. In P. F. Baker, R. L. Carlson, & D. A. Johnson, *Initial Reports of the Deep Sea Drilling Project* (Vol. 72, pp. 953–976). US Government Printing Office. http://www.deepseadrilling.org/72/volume/dsdp72_51.pdf

Barbosa, R. V., Davies, A. J., & Sumida, P. Y. G. (2020). Habitat suitability and environmental niche comparison of cold-water coral species along the Brazilian continental margin. *Deep Sea Research Part I: Oceanographic Research Papers*, *155*, 103147. https://doi.org/10.1016/j.dsr.2019.103147

Bart, M. C., de Kluijver, A., Hoetjes, S., Absalah, S., Mueller, B., Kenchington, E., Rapp, H. T., & de Goeij, J. M. (2020). Differential processing of dissolved and particulate organic matter by deep-sea sponges and their microbial symbionts. *Scientific Reports*, *10*(1), 17515. https://doi.org/10.1038/s41598-020-74670-0

Basheer, I. A., & Hajmeer, M. (2000). Artificial neural networks: Fundamentals, computing, design, and application. *Journal of Microbiological Methods*, *43*(1), 3–31. https://doi.org/10.1016/S0167-7012(00)00201-3

Bax, N. J., Cleary, J., Donnelly, B., Dunn, D. C., Dunstan, P. K., Fuller, M., & Halpin, P. N. (2016). Results of efforts by the Convention on Biological Diversity to describe ecologically or biologically significant marine areas: EBSAs in the High Seas. *Conservation Biology*, *30*(3), 571–581. https://doi.org/10.1111/cobi.12649

Bayley, D. T. I., Mogg, A. O. M., Koldewey, H., & Purvis, A. (2019). Capturing complexity: Field-testing the use of ‘structure from motion’ derived virtual models to replicate standard measures of reef physical structure. *PeerJ*, *7*, e6540. https://doi.org/10.7717/peerj.6540

Beaulieu, S. E. (2001). Life on glass houses: Sponge stalk communities in the deep sea. *Marine Biology*, *138*(4), 803–817. https://doi.org/10.1007/s002270000500

Beazley, L., Kenchington, E., Yashayaev, I., & Murillo, F. J. (2015). Drivers of epibenthic megafaunal composition in the sponge grounds of the Sackville Spur, northwest Atlantic. *Deep Sea Research Part I: Oceanographic Research Papers*, *98*, 102–114. https://doi.org/10.1016/j.dsr.2014.11.016

Beazley, L., Wang, Z., Kenchington, E., Yashayaev, I., Rapp, H. T., Xavier, J. R., Murillo, F. J., Fenton, D., & Fuller, S. (2018). Predicted distribution of the glass sponge Vazella pourtalesi on the Scotian Shelf and its persistence in the face of climatic variability. *PLOS ONE*, *13*(10), e0205505. https://doi.org/10.1371/journal.pone.0205505

Becker, J. J., Sandwell, D. T., Smith, W. H. F., Braud, J., Binder, B., Depner, J., Fabre, D., Factor, J., Ingalls, S., Kim, S.-H., Ladner, R., Marks, K., Nelson, S., Pharaoh, A., Trimmer, R., Von Rosenberg, J., Wallace, G., & Weatherall, P. (2009). Global Bathymetry and Elevation Data at 30 Arc Seconds Resolution: SRTM30_PLUS. *Marine Geodesy*, *32*(4), 355–371. https://doi.org/10.1080/01490410903297766

Behrenfeld, M. J., & Falkowski, P. G. (1997). Photosynthetic rates derived from satellite-based chlorophyll concentration. *Limnology and Oceanography*, *42*(1), 1–20. https://doi.org/10.4319/lo.1997.42.1.0001

Benites, M., Hein, J. R., Mizell, K., Blackburn, T., & Jovane, L. (2020). Genesis and Evolution of Ferromanganese Crusts from the Summit of Rio Grande Rise, Southwest Atlantic Ocean. *Minerals*, *10*(4), 349. https://doi.org/10.3390/min10040349

Benites, M., Hein, J. R., Mizell, K., & Jovane, L. (2021). Miocene Phosphatization of Rocks From the Summit of Rio Grande Rise, Southwest Atlantic Ocean. *Paleoceanography and Paleoclimatology*, *36*(9), e2020PA004197. https://doi.org/10.1029/2020PA004197

Bergo, N. M., Bendia, A. G., Ferreira, J. C. N., Murton, B. J., Brandini, F. P., & Pellizari, V. H. (2021). Microbial Diversity of Deep-Sea Ferromanganese Crust Field in the Rio Grande Rise, Southwestern Atlantic Ocean. *Microbial Ecology*. https://doi.org/10.1007/s00248-020-01670-y

Bett, B. J., & Rice, A. L. (1992). The influenceof hexactinellid sponge (Pheronema carpenteri) spicules on the patchy distribution of macrobenthos in the porcupine seabight (bathyal ne atlantic). *Ophelia*, *36*(3), 217–226. https://doi.org/10.1080/00785326.1992.10430372

Bo, M., Bertolino, M., Bavestrello, G., Canese, S., Giusti, M., Angiolillo, M., Pansini, M., & Taviani, M. (2012). Role of deep sponge grounds in the Mediterranean Sea: A case study in southern Italy. In M. Maldonado, X. Turon, M. Becerro, & M. Jesús Uriz (Eds.), *Ancient Animals, New Challenges: Developments in Sponge Research* (pp. 163–177). Springer Netherlands. https://doi.org/10.1007/978-94-007-4688-6_14

Borcard, D., Gillet, F., & Legendre, P. (2018). *Numerical Ecology with R* (2nd ed.). Springer International Publishing. https://doi.org/10.1007/978-3-319-71404-2

Boyer, T. P., Antonov, J. I., Baranova, O. K., Coleman, C., Garcia, H. E., Grodsky, A., Johnson, D. R., Locarnini, R. A., Mishonov, A. V., O'Brien, T. D., Paver, C. R.,

Reagan, J. R., Seidov, D., Smolyar, I. V., & Zweng, M. M. (2013). *World Ocean Database 2013*. http://doi.org/10.7289/V5NZ85MT

Brown, C. J., Smith, S. J., Lawton, P., & Anderson, J. T. (2011). Benthic habitat mapping: A review of progress towards improved understanding of the spatial ecology of the seafloor using acoustic techniques. *Estuarine, Coastal and Shelf Science*, *92*(3), 502–520. https://doi.org/10.1016/j.ecss.2011.02.007

Cáceres, M. D., & Legendre, P. (2009). Associations between species and groups of sites: Indices and statistical inference. *Ecology*, *90*(12), 3566–3574. https://doi.org/10.1890/08-1823.1

Calvo, B., & Santafé, G. (2016). scmamp: Statistical Comparison of Multiple Algorithms in Multiple Problems. *The R Journal*, *8*(1), 248–256.

Cardoso, I. A., Perez, J. A. A., & Kitazato, H. (2018). Deep-sea decapods sampled or observed with a manned submersible at the Rio Grande Rise (SW Atlantic), including the first record of four species from this region. *Marine Biodiversity*, *48*(1), 695–702. https://doi.org/10.1007/s12526-017-0836-7

Carton, J. A., Chepurin, G. A., & Chen, L. (2018). SODA3: A New Ocean Climate Reanalysis. *Journal of Climate*, *31*(17), 6967–6983. https://doi.org/10.1175/JCLI-D-18-0149.1

Cathalot, C., Van Oevelen, D., Cox, T. J. S., Kutti, T., Lavaleye, M., Duineveld, G., & Meysman, F. J. R. (2015). Cold-water coral reefs and adjacent sponge grounds: Hotspots of benthic respiration and organic carbon cycling in the deep sea. *Frontiers in Marine Science*, *2*. https://www.frontiersin.org/article/10.3389/fmars.2015.00037

Cavalcanti, G. de H., Arantes, R. C. M., Falcão, A. P. da C., Curbelo-Fernandez, M. P., Silveira, M. A. da S., Politano, A. T., Viana, A. R., Hercos, C. M., & Brasil, A. C. dos S. (2017). Ecossistemas de corais de águas profundas da Bacia de Campos. In Curbelo-Fernandez, M. P. & Braga, A. C., *Comunidades Demersais e Bioconstrutores* (Vol. 4, pp. 43–85). Elsevier. https://doi.org/10.1016/B978-85-352-7295-6.50003-8

Cavalcanti, J. A. D., Santos, R. V., Lacasse, C. M., Rojas, J. N. L., & Nobrega, M. (2015). Potential Mineral Resources of Phosphates and Trace Elements on the Rio Grande Rise, South Atlantic Ocean. *44th Underwater Mining Conference*. https://www.researchgate.net/profile/Jose_Dias_Cavalcanti/publication/284178203_Potential_Mineral_Resources_of_Phosphates_and_Trace_Elements_on_the_Rio_Grande_Rise_South_Atlantic_Ocean/links/564e257908aeafc2aab19e2f.pdf

Christiansen, B., Denda, A., & Christiansen, S. (2020). Potential effects of deep seabed mining on pelagic and benthopelagic biota. *Marine Policy*, *114*, 103442. https://doi.org/10.1016/j.marpol.2019.02.014

CIRM. (2009). *Resolução n° 3/2009*. Comissão Interministerial Para Recursos Do Mar. https://www.mar.mil.br/secirm/portugues/proarea.html

CIRM. (2016). *PROAREA - Projetos*. Comissão Interministerial Para Recursos Do Mar. https://www.mar.mil.br/secirm/portugues/proarea.html

Clark, M. R., Schlacher, T. A., Rowden, A. A., Stocks, K. I., & Consalvey, M. (2012). Science Priorities for Seamounts: Research Links to Conservation and Management. *PLOS ONE*, *7*(1), e29232. https://doi.org/10.1371/journal.pone.0029232

Clark, M. R., Vinnichenko, V. I., Gordon, J. D. M., Beck-Bulat, G. Z., Kukharev, N. N., & Kakora, A. F. (2007). Large-Scale Distant-Water Trawl Fisheries on Seamounts. In T. J. Pitcher, T. Morato, P. J. B. Hart, M. R. Clark, N. Haggan, & R. S. Santos, *Seamounts: Ecology, Fisheries & Conservation* (pp. 361–399). Blackwell Publishing Ltd. https://doi.org/10.1002/9780470691953.ch17

Claus, S., Hauwere, N. D., Vanhoorne, B., Dias, F. S., García, P. O., Hernandez, F., & Mees, J. (2017). *Marine Regions*. http://www.marineregions.org/

Constantino, R. R., Hackspacher, P. C., de Souza, I. A., & Lima Costa, I. S. (2017). Basement structures over Rio Grande Rise from gravity inversion. *Journal of South American Earth Sciences*, *75*, 85–91. https://doi.org/10.1016/j.jsames.2017.02.005

Cook, S. E., Conway, K. W., & Burd, B. (2008). Status of the glass sponge reefs in the Georgia Basin. *Marine Environmental Research*, *66*, S80–S86. https://doi.org/10.1016/j.marenvres.2008.09.002

Costello, M. J., & Chaudhary, C. (2017). Marine Biodiversity, Biogeography, Deep-Sea Gradients, and Conservation. *Current Biology*, *27*(11), R511–R527. https://doi.org/10.1016/j.cub.2017.04.060

Cuvelier, D., Ribeiro, P. A., Ramalho, S. P., Kersken, D., Martinez Arbizu, P., & Colaço, A. (2020). Are seamounts refuge areas for fauna from polymetallic nodule fields? *Biogeosciences*, *17*(9), 2657–2680. https://doi.org/10.5194/bg-17-2657-2020

da Silva, A. P. (2021). Brazil advances over the Area: The inclusion of the Rio Grande Rise within the Brazilian outer continental shelf and its consequences for other states and for the common heritage of mankind. *Marine Policy*, *125*, 104399. https://doi.org/10.1016/j.marpol.2021.104399

da Silveira, I. C. A., Napolitano, D. C., & Farias, I. U. (2020). Water Masses and Oceanic Circulation of the Brazilian Continental Margin and Adjacent Abyssal Plain. In P. Y. G. Sumida, A. F. Bernardino, & F. C. De Léo (Eds.), *Brazilian Deep-Sea Biodiversity* (pp. 7–36). Springer International Publishing. https://doi.org/10.1007/978-3-030-53222-2_2

Davies, A. J., & Guinotte, J. M. (2011). Global Habitat Suitability for Framework-Forming Cold-Water Corals. *PLoS ONE*, *6*(4), e18483. https://doi.org/10.1371/journal.pone.0018483

Davies, J. S., Stewart, H. A., Narayanaswamy, B. E., Jacobs, C., Spicer, J., Golding, N., & Howell, K. L. (2015). Benthic Assemblages of the Anton Dohrn Seamount (NE Atlantic): Defining Deep-Sea Biotopes to Support Habitat Mapping and Management Efforts with a Focus on Vulnerable Marine Ecosystems. *PLOS ONE*, *10*(5), e0124815. https://doi.org/10.1371/journal.pone.0124815

De'ath, G. (2002). Multivariate Regression Trees: A New Technique for Modeling Species-Environment Relationships. *Ecology*, *83*(4), 1105. https://doi.org/10.2307/3071917

Delavenne, J., Keszler, L., Castelin, M., Lozouet, P., Maestrati, P., & Samadi, S. (2019). Deep-sea benthic communities in the largest oceanic desert are structured by the presence of polymetallic crust. *Scientific Reports*, *9*(1), 6977. https://doi.org/10.1038/s41598-019-43325-0

Dohrmann, M., Göcke, C., Janussen, D., Reitner, J., Lüter, C., & Wörheide, G. (2011). Systematics and spicule evolution in dictyonal sponges (Hexactinellida: Sceptrulophora) with description of two new species. *Zoological Journal of the Linnean Society*, *163*(4), 1003–1025. https://doi.org/10.1111/j.1096-3642.2011.00753.x

Dolan, M. F. J., Grehan, A. J., Guinan, J. C., & Brown, C. (2008). Modelling the local distribution of cold-water corals in relation to bathymetric variables: Adding spatial context to deep-sea video data. *Deep Sea Research Part I: Oceanographic Research Papers*, *55*(11), 1564–1579. https://doi.org/10.1016/j.dsr.2008.06.010

Dormann, C. F., Calabrese, J. M., Guillera-Arroita, G., Matechou, E., Bahn, V., Bartoń, K., Beale, C. M., Ciuti, S., Elith, J., Gerstner, K., Guelat, J., Keil, P., Lahoz-Monfort, J. J., Pollock, L. J., Reineking, B., Roberts, D. R., Schröder, B., Thuiller, W., Warton, D. I., … Hartig, F. (2018). Model averaging in ecology: A review of Bayesian, information-theoretic, and tactical approaches for predictive inference. *Ecological Monographs*, *88*(4), 485–504. https://doi.org/10.1002/ecm.1309

Dufrêne, M., & Legendre, P. (1997). Species Assemblages and Indicator Species: The need for a flexible asymmetrical approach. *Ecological Monographs*, *67*(3), 345–366. https://doi.org/10.1890/0012-9615(1997)067[0345:SAAIST]2.0.CO;2

Dunn, D. C., Dover, C. L. V., Etter, R. J., Smith, C. R., Levin, L. A., Morato, T., Colaço, A., Dale, A. C., Gebruk, A. V., Gjerde, K. M., Halpin, P. N., Howell, K. L., Johnson, D., Perez, J. A. A., Ribeiro, M. C., Stuckas, H., Weaver, P., & Participants, S. W. (2018). A strategy for the conservation of biodiversity on mid-ocean ridges from deep-sea mining. *Science Advances*, *4*(7), eaar4313. https://doi.org/10.1126/sciadv.aar4313

Durden, J. M., Putts, M., Bingo, S., Leitner, A. B., Drazen, J. C., Gooday, A. J., Jones, D. O. B., Sweetman, A. K., Washburn, T. W., & Smith, C. R. (2021). Megafaunal

Ecology of the Western Clarion Clipperton Zone. *Frontiers in Marine Science*, *8*, 671062. https://doi.org/10.3389/fmars.2021.671062

Dutkiewicz, A., Müller, R. D., O'Callaghan, S., & Jónasson, H. (2015). Census of seafloor sediments in the world's ocean. *Geology*, *43*(9), 795–798. https://doi.org/10.1130/G36883.1

Elith, J., Ferrier, S., Huettmann, F., & Leathwick, J. (2005). The evaluation strip: A new and robust method for plotting predicted responses from species distribution models. *Ecological Modelling*, *186*(3), 280–289. https://doi.org/10.1016/j.ecolmodel.2004.12.007

Elith, J., Leathwick, J. R., & Hastie, T. (2008). A working guide to boosted regression trees. *Journal of Animal Ecology*, *77*(4), 802–813. https://doi.org/10.1111/j.1365-2656.2008.01390.x

Elith, J., Phillips, S. J., Hastie, T., Dudík, M., Chee, Y. E., & Yates, C. J. (2011). A statistical explanation of MaxEnt for ecologists: Statistical explanation of MaxEnt. *Diversity and Distributions*, *17*(1), 43–57. https://doi.org/10.1111/j.1472-4642.2010.00725.x

FAO. (2009). *International Guidelines for the Management of Deep-Sea Fisheries in the High-Seas*. Food and Agriculture Organization of the United Nations.

Ferreira, J. C. N., Bergo, N. M., Tura, P. M., Chuqui, M. G., Brandini, F. P., Jovane, L., & Pellizari, V. H. (2021). *Abundance and Microbial Diversity from Surface to Deep Water Layers Over the Rio Grande Rise, South Atlantic* [Preprint]. Microbiology. https://doi.org/10.1101/2021.04.22.441028

Fisher, N. I. (1995). *Statistical analysis of circular data*. Cambridge University Press. https://doi.org/10.1017/CBO9780511564345

Flach, P., & Kull, M. (2015). Precision-Recall-Gain Curves: PR Analysis Done Right. In C. Cortes, N. Lawrence, D. Lee, M. Sugiyama, & R. Garnett (Eds.), *Advances in Neural Information Processing Systems* (Vol. 28, pp. 838–846). Massachusetts Institute of Technology (MIT) Press. https://papers.nips.cc/paper/5867- precision-recall-gain-curves-pr-analysis-done-right

Florindo, F., Gennari, R., Persico, D., Turco, E., Villa, G., Lurcock, P. C., Roberts, A. P., Winkler, A., Carter, L., & Pekar, S. F. (2015). New magnetobiostratigraphic chronology and paleoceanographic changes across the Oligocene-Miocene boundary at DSDP Site 516 (Rio Grande Rise, SW Atlantic). *Paleoceanography*, *30*(6), 659–681. https://doi.org/10.1002/2014PA002734

Folmer, O., Black, M., Hoeh, W., Lutz, R., & Vrijenhoek, R. (1994). DNA primers for amplification of mitochondrial cytochrome c oxidase subunit I from diverse metazoan invertebrates. *Molecular Marine Biology and Biotechnology*, *3*(5), 294–299.

Fourcade, Y., Besnard, A. G., & Secondi, J. (2018). Paintings predict the distribution of species, or the challenge of selecting environmental predictors and evaluation statistics. *Global Ecology and Biogeography*, *27*(2), 245–256. https://doi.org/10.1111/geb.12684

Gage, J. D., & Tyler, P. A. (1991). *Deep-Sea Biology: A Natural History of Organisms at the Deep-Sea Floor*. Cambridge University Press.

Gamboa, L. A. P., & Rabinowitz, P. D. (1984). The evolution of the Rio Grande Rise in the southwest Atlantic Ocean. *Marine Geology*, *58*(1–2), 35–58.

Garcia, H. E., Boyer, T. P., Locarnini, R. A., Antonov, J. I., Mishonov, A. V., Baranova, O. K., Zweng, M. M., Reagan, J. R., & Johnson, D. R. (2013). *World ocean atlas 2013. Volume 3, Dissolved oxygen, apparent oxygen utilization, and oxygen saturation*. https://doi.org/10.7289/V5XG9P2W

Garcia, H. E., Locarnini, R. A., Boyer, T. P., Antonov, J. I., Baranova, O. K., Zweng, M. M., Reagan, J. R., & Johnson, D. R. (2013). *World ocean atlas 2013. Volume 4, Dissolved inorganic nutrients (phosphate, nitrate, silicate)*. https://doi.org/10.7289/V5J67DWD

García, S., Fernández, A., Luengo, J., & Herrera, F. (2010). Advanced nonparametric tests for multiple comparisons in the design of experiments in computational intelligence and data mining: Experimental analysis of power. *Information Sciences*, *180*(10), 2044–2064. https://doi.org/10.1016/j.ins.2009.12.010

García-Alegre, A., Sánchez, F., Gómez-Ballesteros, M., Hinz, H., Serrano, A., & Parra, S. (2014). Modelling and mapping the local distribution of representative species on the Le Danois Bank, El Cachucho Marine Protected Area (Cantabrian Sea). *Deep Sea Research Part II: Topical Studies in Oceanography*, *106*, 151–164. https://doi.org/10.1016/j.dsr2.2013.12.012

Genin, A., & Boehlert, G. W. (1985). Dynamics of temperature and chlorophyll structures above a seamount: An oceanic experiment. *Journal of Marine Research*, *43*(4), 907–924. https://doi.org/10.1357/002224085788453868

Genin, A., Noble, M., & Lonsdale, P. F. (1989). Tidal currents and anticyclonic motions on two North Pacific seamounts. *Deep Sea Research Part A. Oceanographic Research Papers*, *36*(12), 1803–1815. https://doi.org/10.1016/0198-0149(89)90113-1

Glover, A. G., & Smith, C. R. (2003). The deep-sea floor ecosystem: Current status and prospects of anthropogenic change by the year 2025. *Environmental Conservation*, *30*(3), 219–241. https://doi.org/10.1017/S0376892903000225

Gollner, S., Kaiser, S., Menzel, L., Jones, D. O. B., Brown, A., Mestre, N. C., van Oevelen, D., Menot, L., Colaço, A., Canals, M., Cuvelier, D., Durden, J. M., Gebruk, A., Egho, G. A., Haeckel, M., Marcon, Y., Mevenkamp, L., Morato, T., Pham, C. K., … Martinez Arbizu, P. (2017). Resilience of benthic deep-sea

fauna to mining activities. *Marine Environmental Research*, *129*, 76–101. https://doi.org/10.1016/j.marenvres.2017.04.010

Graça, M. C., Kusznir, N., & Gomes Stanton, N. S. (2019). Crustal thickness mapping of the central South Atlantic and the geodynamic development of the Rio Grande Rise and Walvis Ridge. *Marine and Petroleum Geology*, *101*, 230–242. https://doi.org/10.1016/j.marpetgeo.2018.12.011

Gräler, B., Pebesma, E., & Heuvelink, G. (2016). Spatio-Temporal Interpolation using gstat. *The R Journal*, *8*(1), 204–218.

Grassle, J. F., & Maciolek, N. J. (1992). Deep-sea species richness: Regional and local diversity estimates from quantitative bottom samples. *American Naturalist*, *139*(2), 313–341. https://doi.org/10.1086/285329

Gravier, Ch. (1918). Note sur une Actinie (*Thoracactis* n. G., *Topsenti* n. Sp.) et un Annélide Polychète (*Hermadion Faiweli* n. Sp.), commensaux d'une Éponge siliceuse (*Sarostegia oculata* Topsent). *Bulletin Du Musée Océanographique de Monaco*, *344*, 1–20.

Greene, H. G., Bizzarro, J. J., O'Connell, V. M., & Brylinsky, C. K. (2007). *Construction of Digital Potential Marine Benthic Habitat Maps using a Coded Classification Scheme and its Application*. 16.

Greene, H. G., Yoklavich, M. M., Starr, R. M., O'Connell, V. M., Wakefield, W. W., Sullivan, D. E., McRea, J. E., & Cailliet, G. M. (1999). A classification scheme for deep seafloor habitats. *Oceanologica Acta*, *22*(6), 663–678. https://doi.org/10.1016/S0399-1784(00)88957-4

Guilhon, M., Montserrat, F., & Turra, A. (2021). Recognition of ecosystem-based management principles in key documents of the seabed mining regime: Implications and further recommendations. *ICES Journal of Marine Science*, *78*(3), 884–899. https://doi.org/10.1093/icesjms/fsaa229

Guinotte, J. M., & Davies, A. J. (2014). Predicted Deep-Sea Coral Habitat Suitability for the U.S. West Coast. *PLOS ONE*, *9*(4), e93918. https://doi.org/10.1371/journal.pone.0093918

Guisan, A., Thuiller, W., & Zimmermann, N. E. (2017). *Habitat Suitability and Distribution Models: With Applications in R*. Cambridge University Press. https://doi.org/10.1017/9781139028271

Hajdu, E., Castello-Branco, C., Lopes, D. A., Sumida, P. Y. G., & Perez, J. A. A. (2017). Deep-sea dives reveal an unexpected hexactinellid sponge garden on the Rio Grande Rise (SW Atlantic). A mimicking habitat? *Deep Sea Research Part II: Topical Studies in Oceanography*, *146*, 93–100. https://doi.org/10.1016/j.dsr2.2017.11.009

Halpern, B. S., Frazier, M., Potapenko, J., Casey, K. S., Koenig, K., Longo, C., Lowndes, J. S., Rockwood, R. C., Selig, E. R., Selkoe, K. A., & Walbridge, S. (2015). Spatial and temporal changes in cumulative human impacts on the

world?s ocean. *Nature Communications*, *6*, 7615. https://doi.org/10.1038/ncomms8615

Harlamov, V., Lisniowski, M., Frazao, E., Pessoa, J., Aguiar, R., Lopes, V., Nobrega, M., Lisboa, M., Simoes, H., Cavalacanti, J., & Pessanha, I. (2015). Preliminary results onmid-depth circulation features on Rio Grande Rise. *2015 IEEE/OES Acoustics in Underwater Geosciences Symposium (RIO Acoustics)*, 1–8. https://doi.org/10.1109/RIOAcoustics.2015.7473647

Harris, P. T., Heap, A. D., Whiteway, T., & Post, A. (2008). Application of biophysical information to support Australia's representative marine protected area program. *Ocean & Coastal Management*, *51*(10), 701–711. https://doi.org/10.1016/j.ocecoaman.2008.07.007

Harris, P. T., & Whiteway, T. (2009). High seas marine protected areas: Benthic environmental conservation priorities from a GIS analysis of global ocean biophysical data. *Ocean & Coastal Management*, *52*(1), 22–38. https://doi.org/10.1016/j.ocecoaman.2008.09.009

Hein, J. (2004). Cobalt-Rich Ferromanganese Crusts: Global Distribution, Composition, Origin and Research Activities. In *Study* (Vol. 2, pp. 188–256).

Hein, J., Conrad, T., & Staudigel, H. (2010). Seamount Mineral Deposits: A Source of Rare Metals for High-Technology Industries. *Oceanography*, *23*(1), 184–189. https://doi.org/10.5670/oceanog.2010.70

Hein, J., & Koschinsky, A. (2014). Deep-Ocean Ferromanganese Crusts and Nodules. In S. Scott, *Treatise on Geochemistry* (Vol. 13, pp. 273–291). Elsevier. https://doi.org/10.1016/B978-0-08-095975-7.01111-6

Herzig, P. M., & Hannington, M. D. (1995). Polymetallic massive sulfides at the modern seafloor A review. *Ore Geology Reviews*, *10*(2), 95–115. https://doi.org/10.1016/0169-1368(95)00009-7

Hirzel, A., & Guisan, A. (2002). Which is the optimal sampling strategy for habitat suitability modelling. *Ecological Modelling*, *157*(2), 331–341. https://doi.org/10.1016/S0304-3800(02)00203-X

Hofierka, J., Mitášová, H., & Neteler, M. (2009). Chapter 17 Geomorphometry in GRASS GIS. In *Developments in Soil Science* (Vol. 33, pp. 387–410). Elsevier. https://doi.org/10.1016/S0166-2481(08)00017-2

Hogg, M. M., Tendal, O. S., Conway, K. W., Pomponi, S. A., van Soest, R. W. M., Gutt, J., Krautter, M., & Roberts, J. M. (2010). *Deep-sea Sponge Grounds: Reservoirs of Biodiversity*. UNEP-WCMC. https://wedocs.unep.org/xmlui/handle/20.500.11822/8579

Howell, K. L., Hilário, A., Allcock, A. L., Bailey, D., Baker, M., Clark, M. R., Colaço, A., Copley, J., Cordes, E. E., Danovaro, R., Dissanayake, A., Escobar, E., Esquete, P., Gallagher, A. J., Gates, A. R., Gaudron, S. M., German, C. R., Gjerde, K. M., Higgs, N. D., … Xavier, J. R. (2021). A decade to study deep-sea life. *Nature*

Ecology & Evolution, *5*(3), 265–267. https://doi.org/10.1038/s41559-020-01352-5

Howell, K. L., Holt, R., Endrino, I. P., & Stewart, H. (2011). When the species is also a habitat: Comparing the predictively modelled distributions of Lophelia pertusa and the reef habitat it forms. *Biological Conservation*, *144*(11), 2656–2665. https://doi.org/10.1016/j.biocon.2011.07.025

Howell, K. L., Piechaud, N., Downie, A.-L., & Kenny, A. (2016). The distribution of deep-sea sponge aggregations in the North Atlantic and implications for their effective spatial management. *Deep Sea Research Part I: Oceanographic Research Papers*, *115*, 309–320. https://doi.org/10.1016/j.dsr.2016.07.005

Hughes, D. J., Shimmield, T. M., Black, K. D., & Howe, J. A. (2015). Ecological impacts of large-scale disposal of mining waste in the deep sea. *Scientific Reports*, *5*, 9985. https://doi.org/10.1038/srep09985

ISA (Ed.). (2007). *Polymetallic sulphides and cobalt-rich ferromanganese crusts deposits: Establishment of environmental baselines and an associated monitoring programme during exploration*. International Seabed Authority.

ISA. (2008). *Rationale and recommendations for the establishment of preservation reference areas for nodule mining in the Clarion-Clipperton Zone. ISBA/14/LTC/2*. International Seabed Authority. https://www.isa.org.jm/files/documents/EN/14Sess/LTC/ISBA-14LTC-2.pdf

ISA. (2011). *Environmental Management Plan for the Clarion-Clipperton Zone. ISBA/17/LTC/7*. International Seabed Authority. https://www.isa.org.jm/files/documents/EN/17Sess/LTC/ISBA-17LTC-7.pdf

ISA. (2013). *Recommendations for the guidance of contractors for the assessment of the possible environmental impacts arising from exploration for marine minerals in the Area. ISBA/19/LTC/8*. International Seabed Authority. https://www.isa.org.jm/sites/default/files/files/documents/isba-19ltc-8_0.pdf

ISA. (2014). *Decision of the Council relating to an application for the approval of a plan of work for exploration for cobalt-rich ferromanganese crusts by Companhia de Pesquisa de Recursos Minerais. ISBA/20/C/30*. International Seabed Authority. http://www.isa.org.jm/files/documents/EN/20Sess/Council/ISBA-20C-30.pdf

Jones, D. O. B., Ardron, J. A., Colaço, A., & Durden, J. M. (2020). Environmental considerations for impact and preservation reference zones for deep-sea polymetallic nodule mining. *Marine Policy*, *118*. https://doi.org/10.1016/j.marpol.2018.10.025

Jovane, L., Hein, J. R., Yeo, I. A., Benites, M., Bergo, N. M., Corrêa, P. V. F., Couto, D. M., Guimarães, A. D., Howarth, S. A., Miguel, H. R., Mizell, K. L., Moura, D. S., Vicentini Neto, F. L., Pompeu, M., Rodrigues, I. M. M., Santana, F. R., Serrao, P. F., Silva, T. E., Tura, P. M., … Brandini, F. P. (2019). Multidisciplinary

Scientific Cruise to the Rio Grande Rise. *Frontiers in Marine Science*, *6*, 252. https://doi.org/10.3389/fmars.2019.00252

Kenchington, E. L., Callery, O., Davidson, F., Grehan, A., Morato, T., Appiott, J., Davis, A., Dunstan, P., Preez, C. D., Finney, J., González-Irusta, J. M., Howell, K., Knudby, A., Lacharité, M., Lee, J., Murillo, F. J., Beazley, L., Roberts, J. M., Roberts, M., … Yesson, C. (2019). Use of Species Distribution Modeling in the Deep Sea. *Canadian Technical Report of Fisheries and Aquatic Sciences*, *3296*, 1–76. https://doi.org/10.13140/RG.2.2.12433.28003

Key, R. M., Olsen, A., Van Heuven, S., Lauvset, S. K., Velo, A., Lin, X., Schirnick, C., Kozyr, A., Tanhua, T., Hoppema, M., Jutterstrom, S., Steinfeldt, R., Jeansson, E., Ishi, M., Perez, F. F., & Suzuki, T. (2015). *Global Ocean Data Analysis Project, Version 2 (GLODAPv2), ORNL/CDIAC-162, ND-P093*. Carbon Dioxide Information Analysis Center (CDIAC). https://doi.org/10.3334/CDIAC/OTG.NDP093_GLODAPv2

Key, R. M., Tanhua, T., Olsen, A., Hoppema, M., Jutterström, S., Schirnick, C., Van Heuven, S., Lin, X., Wallace, D. W., & Mintrop, L. (2010). The CARINA data synthesis project: Introduction and overview. *Earth System Science Data*, *2*, 105–121.

Kfouri, L. O., Millo, C., de Lima, A. E., Silveira, C. S., Sant'Anna, L. G., Marino, E., González, F. J., Sayeg, I. J., Hein, J. R., Jovane, L., Bernardini, S., Lusty, P. A. J., & Murton, B. J. (2021). Growth of ferromanganese crusts on bioturbated soft substrate, Tropic Seamount, northeast Atlantic ocean. *Deep Sea Research Part I: Oceanographic Research Papers*, *175*, 103586. https://doi.org/10.1016/j.dsr.2021.103586

Kitahara, M. V., Cordeiro, R. T. S., Barbosa, R. V., Pires, D. de Oliveira, & Sumida, P. Y. G. (2020). Brazilian Deep-Sea Corals. In P. Y. G. Sumida, A. F. Bernardino, & F. C. De Léo (Eds.), *Brazilian Deep-Sea Biodiversity* (pp. 73–107). Springer International Publishing. https://doi.org/10.1007/978-3-030-53222-2_4

Klitgaard, A. B. (1995). The fauna associated with outer shelf and upper slope sponges (Porifera, Demospongiae) at the Faroe Islands, northeastern Atlantic. *Sarsia*, *80*(1), 1–22. https://doi.org/10.1080/00364827.1995.10413574

Klitgaard, A. B., & Tendal, O. S. (2004). Distribution and species composition of mass occurrences of large-sized sponges in the northeast Atlantic. *Progress in Oceanography*, *61*(1), 57–98. https://doi.org/10.1016/j.pocean.2004.06.002

Kruskal, W. H., & Wallis, W. A. (1952). Use of Ranks in One-Criterion Variance Analysis. *Journal of the American Statistical Association*, *47*(260), 583–621. https://doi.org/10.1080/01621459.1952.10483441

Kuhn, M. (2008). Building Predictive Models in *R* Using the **caret** Package. *Journal of Statistical Software*, *28*(5). https://doi.org/10.18637/jss.v028.i05

Lauvset, S. K., Key, R. M., Olsen, A., Heuven, S. van, Velo, A., Lin, X., Schirnick, C., Kozyr, A., Tanhua, T., Hoppema, M., Jutterström, S., Steinfeldt, R., Jeansson, E., Ishii, M., Perez, F. F., Suzuki, T., & Watelet, S. (2016). A new global interior ocean mapped climatology: The 1° × 1° GLODAP version 2. *Earth System Science Data*, *8*(2), 325–340. https://doi.org/10.5194/essd-8-325-2016

Le, J. T., Levin, L. A., & Carson, R. T. (2017). Incorporating ecosystem services into environmental management of deep-seabed mining. *Deep Sea Research Part II: Topical Studies in Oceanography*, *137*, 486–503. https://doi.org/10.1016/j.dsr2.2016.08.007

Leathwick, J. R., Elith, J., Francis, M. P., Hastie, T., & Taylor, P. (2006). Variation in demersal fish species richness in the oceans surrounding New Zealand: An analysis using boosted regression trees. *Marine Ecology Progress Series*, *321*, 267–281. https://doi.org/10.3354/meps321267

LEPLAC. (2018). *Executive Summary: Brazilian Partial Revised Submission to the Commission on the Limits of the Continental Shelf*. Brazillian Continental Shelf Survey Program. https://www.un.org/depts/los/clcs_new/submissions_files/bra02_rev18/BR-OMM-ExecutiveSummary.pdf

Levin, L. A., Etter, R. J., Rex, M. A., Gooday, A. J., Smith, C. R., Pineda, J., Stuart, C. T., Hessler, R. R., & Pawson, D. (2001). Environmental Influences on Regional Deep-Sea Species Diversity. *Annual Review of Ecology and Systematics*, *32*(1), 51–93. https://doi.org/10.1146/annurev.ecolsys.32.081501.114002

Levin, L. A., Mengerink, K., Gjerde, K. M., Rowden, A. A., Van Dover, C. L., Clark, M. R., Ramirez-Llodra, E., Currie, B., Smith, C. R., Sato, K. N., Gallo, N., Sweetman, A. K., Lily, H., Armstrong, C. W., & Brider, J. (2016). Defining “serious harm” to the marine environment in the context of deep-seabed mining. *Marine Policy*, *74*, 245–259. https://doi.org/10.1016/j.marpol.2016.09.032

Lim, A., Wheeler, A. J., Price, D. M., O’Reilly, L., Harris, K., & Conti, L. (2020). Influence of benthic currents on cold-water coral habitats: A combined benthic monitoring and 3D photogrammetric investigation. *Scientific Reports*, *10*(1), 19433. https://doi.org/10.1038/s41598-020-76446-y

Lima, M. M., Cordeiro, R. T. S., & Perez, C. D. (2019). Black Corals (Anthozoa: Antipatharia) from the Southwestern Atlantic. *Zootaxa*, *4692*(1), 1–67. https://doi.org/10.11646/zootaxa.4692.1.1

Liu, C., Berry, P. M., Dawson, T. P., & Pearson, R. G. (2005). Selecting thresholds of occurrence in the prediction of species distributions. *Ecography*, *28*(3), 385–393. https://doi.org/10.1111/j.0906-7590.2005.03957.x

Locarnini, R. A., Mishonov, A. V., Antonov, J. I., Boyer, T. P., Garcia, H. E., Baranova, O. K., Zweng, M. M., Paver, C. R., Reagan, J. R., Johnson, D. R., Hamilton, M.,

& Seidov, D. (2013). *World ocean atlas 2013. Volume 1, Temperature*. https://doi.org/10.7289/V55X26VD

Lodge, M., Johnson, D., Le Gurun, G., Wengler, M., Weaver, P., & Gunn, V. (2014). Seabed mining: International Seabed Authority environmental management plan for the Clarion–Clipperton Zone. A partnership approach. *Marine Policy*, *49*, 66–72. https://doi.org/10.1016/j.marpol.2014.04.006

Lodge, M. W., & Verlaan, P. A. (2018). Deep-Sea Mining: International Regulatory Challenges and Responses. *Elements*, *14*(5), 331–336. https://doi.org/10.2138/gselements.14.5.331

Long, D. J., & Baco, A. R. (2014). Rapid change with depth in megabenthic structure-forming communities of the Makapu'u deep-sea coral bed. *Deep Sea Research Part II: Topical Studies in Oceanography*, *99*, 158–168. https://doi.org/10.1016/j.dsr2.2013.05.032

Long, S., Sparrow-Scinocca, B., Blicher, M. E., Hammeken Arboe, N., Fuhrmann, M., Kemp, K. M., Nygaard, R., Zinglersen, K., & Yesson, C. (2020). Identification of a Soft Coral Garden Candidate Vulnerable Marine Ecosystem (VME) Using Video Imagery, Davis Strait, West Greenland. *Frontiers in Marine Science*, *7*. https://www.frontiersin.org/article/10.3389/fmars.2020.00460

Lundsten, L., Barry, J., Cailliet, G., Clague, D., DeVogelaere, A., & Geller, J. (2009). Benthic invertebrate communities on three seamounts off southern and central California, USA. *Marine Ecology Progress Series*, *374*, 23–32. https://doi.org/10.3354/meps07745

Lutz, M. J., Caldeira, K., Dunbar, R. B., & Behrenfeld, M. J. (2007). Seasonal rhythms of net primary production and particulate organic carbon flux to depth describe the efficiency of biological pump in the global ocean. *Journal of Geophysical Research*, *112*(C10). https://doi.org/10.1029/2006JC003706

Magurran, A. E. (2004). *Measuring Biological Diversity*. Blackwell Publishing. https://nbn-resolving.org/urn:nbn:de:101:1-2014122012826

Maldonado, M., Aguilar, R., Bannister, R. J., Bell, J. J., Conway, K. W., Dayton, P. K., Díaz, C., Gutt, J., Kelly, M., Kenchington, E. L. R., Leys, S. P., Pomponi, S. A., Rapp, H. T., Rützler, K., Tendal, O. S., Vacelet, J., & Young, C. M. (2016). Sponge Grounds as Key Marine Habitats: A Synthetic Review of Types, Structure, Functional Roles, and Conservation Concerns. In S. Rossi, L. Bramanti, A. Gori, & C. Orejas Saco del Valle (Eds.), *Marine Animal Forests: The Ecology of Benthic Biodiversity Hotspots* (pp. 1–39). Springer International Publishing. https://doi.org/10.1007/978-3-319-17001-5_24-1

Maldonado, M., Navarro, L., Grasa, A., Gonzalez, A., & Vaquerizo, I. (2011). Silicon uptake by sponges: A twist to understanding nutrient cycling on continental margins. *Scientific Reports*, *1*(1), 30. https://doi.org/10.1038/srep00030

Manceau, A., Lanson, M., & Takahashi, Y. (2014). Mineralogy and crystal chemistry of Mn, Fe, Co, Ni, and Cu in a deep-sea Pacific polymetallic nodule. *American Mineralogist*, *99*(10), 2068–2083. https://doi.org/10.2138/am-2014-4742

Marliave, J. B., Conway, K. W., Gibbs, D. M., Lamb, A., & Gibbs, C. (2009). Biodiversity and rockfish recruitment in sponge gardens and bioherms of southern British Columbia, Canada. *Marine Biology*, *156*(11), 2247–2254. https://doi.org/10.1007/s00227-009-1252-8

Marshall, C. E., Glegg, G. A., & Howell, K. L. (2014). Species distribution modelling to support marine conservation planning: The next steps. *Marine Policy*, *45*, 330–332. https://doi.org/10.1016/j.marpol.2013.09.003

Mastella, A. M. (2017). *Características das Comunidades Bentônicas da Elevação Do Rio Grande, Atlântico Sul-Ocidental e suas Implicações para Exploração Mineral e Conservação* [Master's project]. Universidade do Vale do Itajaí.

McArdle, B. H., & Anderson, M. J. (2001). Fitting Multivariate Models to Community Data: A Comment on Distance-Based Redundancy Analysis. *Ecology*, *82*(1), 290–297. https://doi.org/10.1890/0012-9658(2001)082[0290:FMMTCD]2.0.CO;2

McClain, C. R., & Hardy, S. M. (2010). The dynamics of biogeographic ranges in the deep sea. *Proceedings of the Royal Society B: Biological Sciences*, *277*(1700), 3533–3546. https://doi.org/10.1098/rspb.2010.1057

Merow, C., Smith, M. J., Edwards Jr, T. C., Guisan, A., McMahon, S. M., Normand, S., Thuiller, W., Wüest, R. O., Zimmermann, N. E., & Elith, J. (2014). What do we gain from simplicity versus complexity in species distribution models? *Ecography*, *37*(12), 1267–1281. https://doi.org/10.1111/ecog.00845

Miller, K. A., Thompson, K. F., Johnston, P., & Santillo, D. (2018). An Overview of Seabed Mining Including the Current State of Development, Environmental Impacts, and Knowledge Gaps. *Frontiers in Marine Science*, *4*, 418. https://doi.org/10.3389/fmars.2017.00418

Millo, C., Vieira do Nascimento e Silva, M. H., de Mello, R. M., Leckie, R. M., Benites, M., Fonseca Giannini, P. C., Boggiani, P. C., Bosence, D., Lusty, P. A. J., Murton, B. J., & Jovane, L. (2022). Discovery of enigmatic toroidal carbonate concretions on the Rio Grande Rise (Southwestern Atlantic Ocean). *Marine Geology*, *443*, 106665. https://doi.org/10.1016/j.margeo.2021.106665

Mohriak, W. U. (2020). Genesis and evolution of the South Atlantic volcanic islands offshore Brazil. *Geo-Marine Letters*, *40*(1), 1–33. https://doi.org/10.1007/s00367-019-00631-w

Mohriak, W. U., Nobrega, M., Odegard, M. E., Gomes, B. S., & Dickson, W. G. (2010). Geological and geophysical interpretation of the Rio Grande Rise, south-eastern Brazilian margin: Extensional tectonics and rifting of continental and

oceanic crusts. *Petroleum Geoscience*, *16*(3), 231–245. https://doi.org/10.1144/1354-079309-910

Montserrat, F., Guilhon, M., Corrêa, P. V. F., Bergo, N. M., Signori, C. N., Tura, P. M., Santos Maly, M. de los, Moura, D., Jovane, L., Pellizari, V., Sumida, P. Y. G., Brandini, F. P., & Turra, A. (2019). Deep-sea mining on the Rio Grande Rise (Southwestern Atlantic): A review on environmental baseline, ecosystem services and potential impacts. *Deep Sea Research Part I: Oceanographic Research Papers*, *145*, 31–58. https://doi.org/10.1016/j.dsr.2018.12.007

Mora, C., Tittensor, D. P., Adl, S., Simpson, A. G. B., & Worm, B. (2011). How Many Species Are There on Earth and in the Ocean? *PLOS Biology*, *9*(8), e1001127. https://doi.org/10.1371/journal.pbio.1001127

Morato, T., Cleary, J., Taranto, G. H., Bilan, M., Barros, I., Vandeperre, F., Pham, C. K., Dunn, D. C., Colaço, A., & Halpin, P. N. (2016). *Data report: Towards development of a strategic Environmental Management Plan for deep seabed mineral exploitation in the Atlantic basin*. IMAR & MGEL. https://www.eu-midas.net/sites/default/files/Workshops/SEMPIA/SEMPIA_Data_Report_lowres.pdf

Morato, T., Hoyle, S. D., Allain, V., & Nicol, S. J. (2010). Seamounts are hotspots of pelagic biodiversity in the open ocean. *Proceedings of the National Academy of Sciences*, *107*(21), 9707–9711. https://doi.org/10.1073/pnas.0910290107

Morel, A., & Berthon, J.-F. (1989). Surface pigments, algal biomass profiles, and potential production of the euphotic layer: Relationships reinvestigated in view of remote-sensing applications. *Limnology and Oceanography*, *34*(8), 1545–1562. https://doi.org/10.4319/lo.1989.34.8.1545

Morgan, N. B., Cairns, S., Reiswig, H., & Baco, A. R. (2015). Benthic megafaunal community structure of cobalt-rich manganese crusts on Necker Ridge. *Deep Sea Research Part I: Oceanographic Research Papers*, *104*, 92–105. https://doi.org/10.1016/j.dsr.2015.07.003

Mourato, B. L., Arfelli, C. A., Amorim, A. F., Hazin, H. G., Carvalho, F. C., & Hazin, F. H. V. (2011). Spatio-temporal distribution and target species in a longline fishery off the southeastern coast of Brazil. *Brazilian Journal of Oceanography*, *59*(2), 185–194. https://doi.org/10.1590/S1679-87592011000200007

Murton, B. J., Huhnerbach, V., & Garrard, J. (2012). HyBIS: A new concept in versatile, 6000-m rated robotic underwater vehicles. In G. N. Roberts & R. Sutton (Eds.), *Further Advances in Unmanned Marine Vehicles* (pp. 45–67). Institution of Engineering and Technology. https://doi.org/10.1049/PBCE077E_ch3

Naimi, B., Hamm, N. A. S., Groen, T. A., Skidmore, A. K., & Toxopeus, A. G. (2014). Where is positional uncertainty a problem for species distribution modelling? *Ecography*, *37*(2), 191–203. https://doi.org/10.1111/j.1600-0587.2013.00205.x

NASA Goddard Space Flight Center, O. E. L. (2014). *MODIS-Aqua Ocean Color Data*. NASA Goddard Space Flight Center, Ocean Ecology Laboratory, Ocean Biology Processing Group. https://doi.org/10.5067/AQUA/MODIS_OC.2014.0

NIWA. (2016, February 3). *Vulnerable marine ecosystems in the South Pacific Ocean region*. National Institute of Water and Atmospheric Research (NIWA), Wellington, New Zealand, 202873 Records. https://nzobisipt.niwa.co.nz/resource?r=vme_inverts

O'Connor, J. M., & Duncan, R. A. (1990). *Evolution of the Walvis Ridge-Rio Grande rise hot spot systen: Implications for African and South American plate motions over plumes*. http://ir.library.oregonstate.edu/xmlui/handle/1957/17329

O'Hara, T. D., Consalvey, M., Lavrado, H. P., & Stocks, K. I. (2010). Environmental predictors and turnover of biota along a seamount chain: Assemblage composition along a seamount chain. *Marine Ecology*, *31*, 84–94. https://doi.org/10.1111/j.1439-0485.2010.00379.x

O'Hara, T. D., & Tittensor, D. P. (2010). Environmental drivers of ophiuroid species richness on seamounts: Ophiuroid seamount species richness. *Marine Ecology*, *31*, 26–38. https://doi.org/10.1111/j.1439-0485.2010.00373.x

Oksanen, J., Blanchet, F. G., Friendly, M., Kindt, R., Legendre, P., McGlinn, D., Minchin, P. R., O'Hara, R. B., Simpson, G. L., Solymos, P., Stevens, M. H. H., Szoecs, E., & Wagner, H. (2019). *vegan: Community Ecology Package*. https://CRAN.R-project.org/package=vegan

Orcutt, B. N., Bradley, J. A., Brazelton, W. J., Estes, E. R., Goordial, J. M., Huber, J. A., Jones, R. M., Mahmoudi, N., Marlow, J. J., Murdock, S., & Pachiadaki, M. (2020). Impacts of deep-sea mining on microbial ecosystem services. *Limnology and Oceanography*, *65*(7), 1489–1510. https://doi.org/10.1002/lno.11403

Perez, J. A. A., dos Santos Alves, E., Clark, M., Bergstad, O. A., Gebruk, A., Azevedo Cardoso, I., & Rogacheva, A. (2012). Patterns of Life on the Southern Mid-Atlantic Ridge: Compiling What is Known and Addressing Future Research. *Oceanography*, *25*(4), 16–31. https://doi.org/10.5670/oceanog.2012.102

Perez, J. A. A., Kitazato, H., Sumida, P. Y. G., Sant'Ana, R., & Mastella, A. M. (2018). Benthopelagic megafauna assemblages of the Rio Grande Rise (SW Atlantic). *Deep Sea Research Part I: Oceanographic Research Papers*, *134*, 1–11. https://doi.org/10.1016/j.dsr.2018.03.001

Peterson, R. G., & Whitworth, T. (1989). The subantarctic and polar fronts in relation to deep water masses through the southwestern Atlantic. *Journal of Geophysical Research*, *94*(C8), 10817. https://doi.org/10.1029/JC094iC08p10817

Phillips, S. J., Anderson, R. P., & Schapire, R. E. (2006). Maximum entropy modeling of species geographic distributions. *Ecological Modelling*, *190*(3–4), 231–259. https://doi.org/10.1016/j.ecolmodel.2005.03.026

Phillips, S. J., & Elith, J. (2010). POC plots: Calibrating species distribution models with presence-only data. *Ecology*, *91*(8), 2476–2484. https://doi.org/10.1890/09-0760.1

Pielou, E. C. (1966). The measurement of diversity in different types of biological collections. *Journal of Theoretical Biology*, *13*, 131–144. https://doi.org/10.1016/0022-5193(66)90013-0

Pile, A. J., & Young, C. M. (2006). The natural diet of a hexactinellid sponge: Benthic–pelagic coupling in a deep-sea microbial food web. *Deep Sea Research Part I: Oceanographic Research Papers*, *53*(7), 1148–1156. https://doi.org/10.1016/j.dsr.2006.03.008

Pires, D. de O. (2007). The azooxanthellate coral fauna of Brazil. *Bulletin of Marine Science*, *81*(3), 265–272.

Price, D. M., Lim, A., Callaway, A., Eichhorn, M. P., Wheeler, A. J., Lo Iacono, C., & Huvenne, V. A. I. (2021). Fine-Scale Heterogeneity of a Cold-Water Coral Reef and Its Influence on the Distribution of Associated Taxa. *Frontiers in Marine Science*, *8*. https://doi.org/10.3389/fmars.2021.556313

R Core Team. (2020). *R: A Language and Environment for Statistical Computing*. R Foundation for Statistical Computing. https://www.R-project.org/

Ramirez-Llodra, E., Brandt, A., Danovaro, R., De Mol, B., Escobar, E., German, C. R., Levin, L. A., Martinez Arbizu, P., Menot, L., Buhl-Mortensen, P., Narayanaswamy, B. E., Smith, C. R., Tittensor, D. P., Tyler, P. A., Vanreusel, A., & Vecchione, M. (2010). Deep, diverse and definitely different: Unique attributes of the world's largest ecosystem. *Biogeosciences*, *7*(9), 2851–2899. https://doi.org/10.5194/bg-7-2851-2010

Ramirez-Llodra, E., Tyler, P. A., Baker, M. C., Bergstad, O. A., Clark, M. R., Escobar, E., Levin, L. A., Menot, L., Rowden, A. A., Smith, C. R., & Dover, C. L. V. (2011). Man and the Last Great Wilderness: Human Impact on the Deep Sea. *PLOS ONE*, *6*(8), e22588. https://doi.org/10.1371/journal.pone.0022588

Ramiro-Sánchez, B., González-Irusta, J. M., Henry, L.-A., Cleland, J., Yeo, I., Xavier, J. R., Carreiro-Silva, M., Sampaio, Í., Spearman, J., Victorero, L., Messing, C. G., Kazanidis, G., Roberts, J. M., & Murton, B. (2019). Characterization and Mapping of a Deep-Sea Sponge Ground on the Tropic Seamount (Northeast Tropical Atlantic): Implications for Spatial Management in the High Seas. *Frontiers in Marine Science*, *6*. https://doi.org/10.3389/fmars.2019.00278

Ratnasingham, S., & Hebert, P. D. N. (2007). bold: The Barcode of Life Data System (http://www.barcodinglife.org). *Molecular Ecology Notes*, *7*(3), 355–364. https://doi.org/10.1111/j.1471-8286.2007.01678.x

Read, J., & Pollard, R. (2017). An introduction to the physical oceanography of six seamounts in the southwest Indian Ocean. *Deep Sea Research Part II: Topical Studies in Oceanography*, *136*, 44–58. https://doi.org/10.1016/j.dsr2.2015.06.022

Rees, H. L., Bergman, M. J. N., Birchenough, S., Borja, A., & Boois, I. (2009). Guidelines for the study of the epibenthos of subtidal environments. *ICES Techniques in Marine Environmental Sciences*, *42*, 88 p.

Reiss, H., Birchenough, S., Borja, A., Buhl-Mortensen, L., Craeymeersch, J., Dannheim, J., Darr, A., Galparsoro, I., Gogina, M., Neumann, H., Populus, J., Rengstorf, A. M., Valle, M., van Hoey, G., Zettler, M. L., & Degraer, S. (2015). Benthos distribution modelling and its relevance for marine ecosystem management. *ICES Journal of Marine Science*, *72*(2), 297–315. https://doi.org/10.1093/icesjms/fsu107

Reiswig, H. M. (2002). Family Farreidae Gray, 1872. In J. N. A. Hooper, R. W. M. Van Soest, & P. Willenz (Eds.), *Systema Porifera: A guide to the classification of sponges* (pp. 1332–1340). Springer. https://doi.org/10.1007/978-1-4615-0747-5_136

Rengstorf, A. M., Mohn, C., Brown, C., Wisz, M. S., & Grehan, A. J. (2014). Predicting the distribution of deep-sea vulnerable marine ecosystems using high-resolution data: Considerations and novel approaches. *Deep Sea Research Part I: Oceanographic Research Papers*, *93*, 72–82. https://doi.org/10.1016/j.dsr.2014.07.007

Rengstorf, A. M., Yesson, C., Brown, C., & Grehan, A. J. (2013). High-resolution habitat suitability modelling can improve conservation of vulnerable marine ecosystems in the deep sea. *Journal of Biogeography*, *40*(9), 1702–1714. https://doi.org/10.1111/jbi.12123

Renner, I. W., & Warton, D. I. (2013). Equivalence of MAXENT and Poisson Point Process Models for Species Distribution Modeling in Ecology. *Biometrics*, *69*(1), 274–281. https://doi.org/10.1111/j.1541-0420.2012.01824.x

Rex, M. A., & Etter, R. J. (2010). *Deep-sea biodiversity: Pattern and scale*. Harvard University Press.

Richer de Forges, B., Koslow, J. A., & Poore, G. C. B. (2000). Diversity and endemism of the benthic seamount fauna in the southwest Pacific. *Nature*, *405*(6789), 944–947. https://doi.org/10.1038/35016066

Robert, K., Jones, D. O. B., Roberts, J. M., & Huvenne, V. A. I. (2016). Improving predictive mapping of deep-water habitats: Considering multiple model outputs and ensemble techniques. *Deep Sea Research Part I: Oceanographic Research Papers*, *113*, 80–89. https://doi.org/10.1016/j.dsr.2016.04.008

Rodríguez-Basalo, A., Prado, E., Sánchez, F., Ríos, P., Gómez-Ballesteros, M., & Cristobo, J. (2021). High Resolution Spatial Distribution for the Hexactinellid

Sponges Asconema setubalense and Pheronema carpenteri in the Central Cantabrian Sea. *Frontiers in Marine Science*, *8*, 612761. https://doi.org/10.3389/fmars.2021.612761

Rogers, A. D. (2018). Chapter Four - The Biology of Seamounts: 25 Years on. In C. Sheppard (Ed.), *Advances in Marine Biology* (Vol. 79, pp. 137–224). Academic Press. https://doi.org/10.1016/bs.amb.2018.06.001

Ross, L. K., Ross, R. E., Stewart, H. A., & Howell, K. L. (2015). The Influence of Data Resolution on Predicted Distribution and Estimates of Extent of Current Protection of Three 'Listed' Deep-Sea Habitats. *PLOS ONE*, *10*(10), e0140061. https://doi.org/10.1371/journal.pone.0140061

Rossi, S. (2013). The destruction of the 'animal forests' in the oceans: Towards an over-simplification of the benthic ecosystems. *Ocean & Coastal Management*, *84*, 77–85. https://doi.org/10.1016/j.ocecoaman.2013.07.004

Rowden, A. A., Anderson, O. F., Georgian, S. E., Bowden, D. A., Clark, M. R., Pallentin, A., & Miller, A. (2017). High-Resolution Habitat Suitability Models for the Conservation and Management of Vulnerable Marine Ecosystems on the Louisville Seamount Chain, South Pacific Ocean. *Frontiers in Marine Science*, *4*, 335. https://doi.org/10.3389/fmars.2017.00335

Rowden, A. A., Dower, J. F., Schlacher, T. A., Consalvey, M., & Clark, M. R. (2010). Paradigms in seamount ecology: Fact, fiction and future. *Marine Ecology*, *31*, 226–241. https://doi.org/10.1111/j.1439-0485.2010.00400.x

Rowden, A. A., Pearman, T. R. R., Bowden, D. A., Anderson, O. F., & Clark, M. R. (2020). Determining Coral Density Thresholds for Identifying Structurally Complex Vulnerable Marine Ecosystems in the Deep Sea. *Frontiers in Marine Science*, *7*, 95. https://doi.org/10.3389/fmars.2020.00095

Saito, T., & Rehmsmeier, M. (2015). The Precision-Recall Plot Is More Informative than the ROC Plot When Evaluating Binary Classifiers on Imbalanced Datasets. *PLOS ONE*, *10*(3), e0118432. https://doi.org/10.1371/journal.pone.0118432

Schlacher, T. A., Baco, A. R., Rowden, A. A., O'Hara, T. D., Clark, M. R., Kelley, C., & Dower, J. F. (2014). Seamount benthos in a cobalt-rich crust region of the central Pacific: Conservation challenges for future seabed mining. *Diversity and Distributions*, *20*(5), 491–502. https://doi.org/10.1111/ddi.12142

Schlacher, T. A., Rowden, A. A., Dower, J. F., & Consalvey, M. (2010). Seamount science scales undersea mountains: New research and outlook. *Marine Ecology*, *31*, 1–13. https://doi.org/10.1111/j.1439-0485.2010.00396.x

Schmidt, C. W. (2015). Going Deep: Cautious Steps toward Seabed Mining. *Environmental Health Perspectives*, *123*(9), A234–A241. https://doi.org/10.1289/ehp.123-A234

Simon-Lledó, E., Bett, B. J., Huvenne, V. A. I., Schoening, T., Benoist, N. M. A., Jeffreys, R. M., Durden, J. M., & Jones, D. O. B. (2019). Megafaunal variation

in the abyssal landscape of the Clarion Clipperton Zone. *Progress in Oceanography*, *170*, 119–133. https://doi.org/10.1016/j.pocean.2018.11.003

Simon-Lledó, E., Pomee, C., Ahokava, A., Drazen, J. C., Leitner, A. B., Flynn, A., Parianos, J., & Jones, D. O. B. (2020). Multi-scale variations in invertebrate and fish megafauna in the mid-eastern Clarion Clipperton Zone. *Progress in Oceanography*, *187*, 102405. https://doi.org/10.1016/j.pocean.2020.102405

Smith, A. (2017). *Environmental Features Relevant to Deep-Sea Mining along the Rio Grande Rise for the Implementation of Protected Areas* [Master's project, Duke University]. https://hdl.handle.net/10161/14148

Sousa, I. M. C., Santos, R. V., Koschinsky, A., Bau, M., Wegorzewski, A. V., Cavalcanti, J. A. D., & Dantas, E. L. (2021). Mineralogy and chemical composition of ferromanganese crusts from the Cruzeiro do Sul Lineament—Rio Grande Rise, South Atlantic. *Journal of South American Earth Sciences*, *108*, 103207. https://doi.org/10.1016/j.jsames.2021.103207

Stramma, L., & England, M. (1999). On the water masses and mean circulation of the South Atlantic Ocean. *Journal of Geophysical Research: Oceans*, *104*(C9), 20863–20883. https://doi.org/10.1029/1999JC900139

Strobl, C., Malley, J., & Tutz, G. (2009). An introduction to recursive partitioning: Rationale, application, and characteristics of classification and regression trees, bagging, and random forests. *Psychological Methods*, *14*(4), 323–348. https://doi.org/10.1037/a0016973

Sumida, P. Y. G., Yoshinaga, M. Y., Madureira, L. A. S.-P., & Hovland, M. (2004). Seabed pockmarks associated with deepwater corals off SE Brazilian continental slope, Santos Basin. *Marine Geology*, *207*(1), 159–167. https://doi.org/10.1016/j.margeo.2004.03.006

Sweetman, A. K., Thurber, A. R., Smith, C. R., Levin, L. A., Mora, C., Wei, C.-L., Gooday, A. J., Jones, D. O. B., Rex, M., Yasuhara, M., Ingels, J., Ruhl, H. A., Frieder, C. A., Danovaro, R., Würzberg, L., Baco, A., Grupe, B. M., Pasulka, A., Meyer, K. S., … Roberts, J. M. (2017). Major impacts of climate change on deep-sea benthic ecosystems. *Elem Sci Anth*, *5*(0), 4. https://doi.org/10.1525/elementa.203

Tabachnick, K. R., Menshenina, L. L., Lopes, D. A., & Hajdu, E. (2009). Two new *Hyalonema* species (Hyalonematidae: Amphidiscosida) from eastern and south-eastern Brazil, and further Hexactinellida (Porifera) collected from seamounts off south-eastern Brazil by the RV 'Marion Dufresne' MD55 expedition. *Journal of the Marine Biological Association of the United Kingdom*, *89*(6), 1243–1250. https://doi.org/10.1017/S0025315409000253

TeleGeography. (2017). *Submarine Cable Map*. https://www.submarinecablemap.com/

Thompson, K. F., Miller, K. A., Currie, D., Johnston, P., & Santillo, D. (2018). Seabed Mining and Approaches to Governance of the Deep Seabed. *Frontiers in Marine Science*, *5*. https://doi.org/10.3389/fmars.2018.00480

Thresher, R., Althaus, F., Adkins, J., Gowlett-Holmes, K., Alderslade, P., Dowdney, J., Cho, W., Gagnon, A., Staples, D., McEnnulty, F., & Williams, A. (2014). Strong Depth-Related Zonation of Megabenthos on a Rocky Continental Margin (~700–4000 m) off Southern Tasmania, Australia. *PLOS ONE*, *9*(1), e85872. https://doi.org/10.1371/journal.pone.0085872

Thuiller, W., Lafourcade, B., Engler, R., & Araújo, M. B. (2009). BIOMOD – a platform for ensemble forecasting of species distributions. *Ecography*, *32*(3), 369–373. https://doi.org/10.1111/j.1600-0587.2008.05742.x

Thurber, A. R., Sweetman, A. K., Narayanaswamy, B. E., Jones, D. O. B., Ingels, J., & Hansman, R. L. (2014). Ecosystem function and services provided by the deep sea. *Biogeosciences*, *11*(14), 3941–3963. https://doi.org/10.5194/bg-11-3941-2014

Tittensor, D. P., Baco, A. R., Brewin, P. E., Clark, M. R., Consalvey, M., Hall-Spencer, J., Rowden, A. A., Schlacher, T., Stocks, K. I., & Rogers, A. D. (2009). Predicting global habitat suitability for stony corals on seamounts. *Journal of Biogeography*, *36*(6), 1111–1128. https://doi.org/10.1111/j.1365-2699.2008.02062.x

Tong, R., Purser, A., Guinan, J., & Unnithan, V. (2013). Modeling the habitat suitability for deep-water gorgonian corals based on terrain variables. *Ecological Informatics*, *13*, 123–132. https://doi.org/10.1016/j.ecoinf.2012.07.002

Topsent, E. (1904). *Sarostegia oculata*, Hexactinellide nouvelle des îles du Cap-Vert. *Bulletin Du Musée Océanographique de Monaco*, *10*, 1–8.

Turnewitsch, R., Dumont, M., Kiriakoulakis, K., Legg, S., Mohn, C., Peine, F., & Wolff, G. (2016). Tidal influence on particulate organic carbon export fluxes around a tall seamount. *Progress in Oceanography*, *149*, 189–213. https://doi.org/10.1016/j.pocean.2016.10.009

Ussami, N., Chaves, C. A. M., Marques, L. S., & Ernesto, M. (2013). Origin of the Rio Grande Rise-Walvis Ridge reviewed integrating palaeogeographic reconstruction, isotope geochemistry and flexural modelling. *Geological Society, London, Special Publications*, *369*(1), 129–146. https://doi.org/10.1144/SP369.10

Valavi, R., Guillera-Arroita, G., Lahoz-Monfort, J. J., & Elith, J. (2022). Predictive performance of presence-only species distribution models: A benchmark study with reproducible code. *Ecological Monographs*, *92*(1), e01486. https://doi.org/10.1002/ecm.1486

Van Dover, C. L., Ardron, J. A., Escobar, E., Gianni, M., Gjerde, K. M., Jaeckel, A., Jones, D. O. B., Levin, L. A., Niner, H. J., Pendleton, L., Smith, C. R., Thiele, T., Turner, P. J., Watling, L., & Weaver, P. P. E. (2017). Biodiversity loss from deep-

sea mining. *Nature Geoscience*, *10*(7), 464–465. https://doi.org/10.1038/ngeo2983

Victorero, L., Robert, K., Robinson, L. F., Taylor, M. L., & Huvenne, V. A. I. (2018). Species replacement dominates megabenthos beta diversity in a remote seamount setting. *Scientific Reports*, *8*(1), 4152. https://doi.org/10.1038/s41598-018-22296-8

Vierod, A. D. T., Guinotte, J. M., & Davies, A. J. (2014). Predicting the distribution of vulnerable marine ecosystems in the deep sea using presence-background models. *Deep Sea Research Part II: Topical Studies in Oceanography*, *99*, 6–18. https://doi.org/10.1016/j.dsr2.2013.06.010

Vilas, J. C., Arístegui, J., Kiriakoulakis, K., Wolff, G. A., Espino, M., Polo, I., Montero, M. F., & Mendonça, A. (2009). Seamounts and organic matter—Is there an effect? The case of Sedlo and Seine Seamounts: Part 1. Distributions of dissolved and particulate organic matter. *Deep Sea Research Part II: Topical Studies in Oceanography*, *56*(25), 2618–2630. https://doi.org/10.1016/j.dsr2.2008.12.023

Wahab, M. A. A., Fromont, J., Gomez, O., Fisher, R., & Jones, R. (2017). Comparisons of benthic filter feeder communities before and after a large-scale capital dredging program. *Marine Pollution Bulletin*, *122*(1–2), 176–193. https://doi.org/10.1016/j.marpolbul.2017.06.041

Walbridge, S., Slocum, N., Marjean Pobuda, & Wright, D. (2018). Unified Geomorphological Analysis Workflows with Benthic Terrain Modeler. *Geosciences*, *8*(3), 94. https://doi.org/10.3390/geosciences8030094

Weaver, P. P. E., Aguzzi, J., Boschen-Rose, R. E., Colaço, A., de Stigter, H., Gollner, S., Haeckel, M., Hauton, C., Helmons, R., Jones, D. O. B., Lily, H., Mestre, N. C., Mohn, C., & Thomsen, L. (2022). Assessing plume impacts caused by polymetallic nodule mining vehicles. *Marine Policy*, *139*, 105011. https://doi.org/10.1016/j.marpol.2022.105011

Wedding, L. M., Friedlander, A. M., Kittinger, J. N., Watling, L., Gaines, S. D., Bennett, M., Hardy, S. M., & Smith, C. R. (2013). From principles to practice: A spatial approach to systematic conservation planning in the deep sea. *Proceedings of the Royal Society B: Biological Sciences*, *280*(1773), 20131684–20131684. https://doi.org/10.1098/rspb.2013.1684

Wedding, L. M., Reiter, S. M., Smith, C. R., Gjerde, K. M., Kittinger, J. N., Friedlander, A. M., Gaines, S. D., Clark, M. R., Thurnherr, A. M., Hardy, S. M., & others. (2015). Managing mining of the deep seabed. *Science*, *349*(6244), 144–145.

White, M., Bashmachnikov, I., Arístegui, J., & Martins, A. (2007). Physical Processes and Seamount Productivity. In *Seamounts: Ecology, Fisheries & Conservation* (pp. 62–84). John Wiley & Sons, Ltd. https://doi.org/10.1002/9780470691953.ch4

Whittaker, J. M., Goncharov, A., Williams, S. E., Müller, R. D., & Leitchenkov, G. (2013). Global sediment thickness data set updated for the Australian-Antarctic Southern Ocean: Technical Brief. *Geochemistry, Geophysics, Geosystems*, *14*(8), 3297–3305. https://doi.org/10.1002/ggge.20181

Wickham, H. (2016). *ggplot2: Elegant Graphics for Data Analysis*. Springer-Verlag New York. https://ggplot2.tidyverse.org

Wilson, R. R., & Kaufmann, R. (1987). Seamount biota and biogeography. *Washington DC American Geophysical Union Geophysical Monograph Series*, *43*, 355–377. https://doi.org/10.1029/GM043p0355

Wood, S. N. (2011). Fast stable restricted maximum likelihood and marginal likelihood estimation of semiparametric generalized linear models. *Journal of the Royal Statistical Society: Series B (Statistical Methodology)*, *73*(1), 3–36. https://doi.org/10.1111/j.1467-9868.2010.00749.x

Yeo, I. A., Howarth, S. A., Spearman, J., Cooper, A., Crossouard, N., Taylor, J., Turnbull, M., & Murton, B. J. (2019). Distribution of and hydrographic controls on ferromanganese crusts: Tropic Seamount, Atlantic. *Ore Geology Reviews*, *114*, 103131. https://doi.org/10.1016/j.oregeorev.2019.103131

Yesson, C., Bedford, F., Rogers, A. D., & Taylor, M. L. (2015). The global distribution of deep-water Antipatharia habitat. *Deep Sea Research Part II: Topical Studies in Oceanography*. https://doi.org/10.1016/j.dsr2.2015.12.004

Yesson, C., Clark, M. R., Taylor, M. L., & Rogers, A. D. (2011). The global distribution of seamounts based on 30 arc seconds bathymetry data. *Deep Sea Research Part I: Oceanographic Research Papers*, *58*(4), 442–453. https://doi.org/10.1016/j.dsr.2011.02.004

Yesson, C., Taylor, M. L., Tittensor, D. P., Davies, A. J., Guinotte, J., Baco, A., Black, J., Hall-Spencer, J. M., & Rogers, A. D. (2012). Global habitat suitability of cold-water octocorals: Global distribution of deep-sea octocorals. *Journal of Biogeography*, *39*(7), 1278–1292. https://doi.org/10.1111/j.1365-2699.2011.02681.x

Zweng, M. M., Reagan, J. R., Antonov, J. I., Locarnini, R. A., Mishonov, A. V., Boyer, T. P., Garcia, H. E., Baranova, O. K., Johnson, D. R., Seidov, D., & Biddle, M. M. (2013). *World ocean atlas 2013. Volume 2, Salinity*. https://doi.org/10.7289/V5251G4D

Appendix A - Enviroment variables of Rio Grande Rise obtainded from global databases

Maps elaborated by the author following the methods described in Chapter 2.2. The figures were used by Montserrat and collaborators in a review paper of Rio Grande Rise (Montserrat et al., 2019).

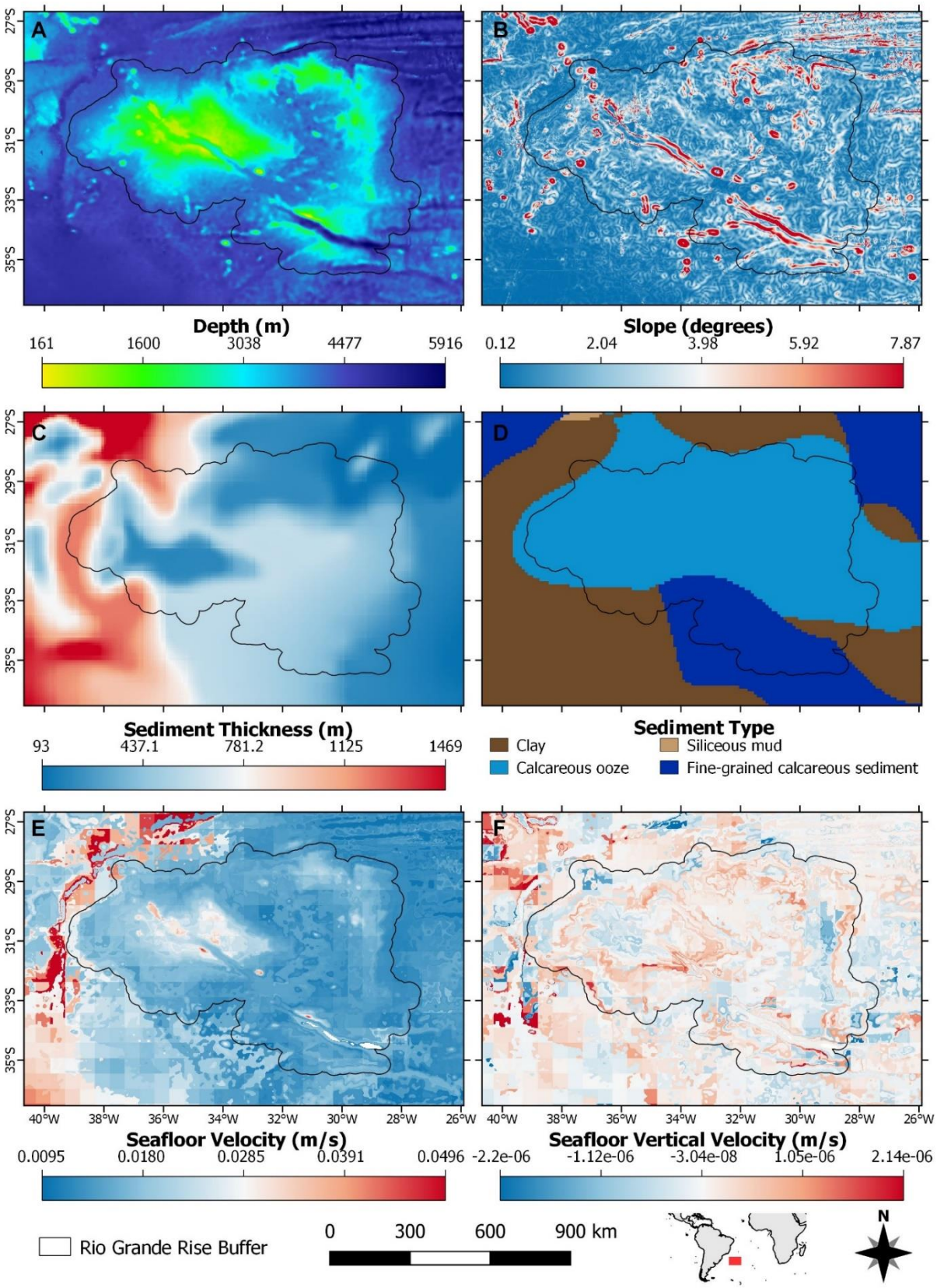

Figure S1. Maps showing time-averaged environmental data for the RGR buffer area and surroundings. **(A)** Bathymetry [m below sea level]. **(B)** Slope [degrees]. **(C)** Sediment thickness [m]. **(D)** Sediment type. **(E)** Horizontal current velocity along seafloor [m/s]. **(F)** Vertical current velocity [m/s].

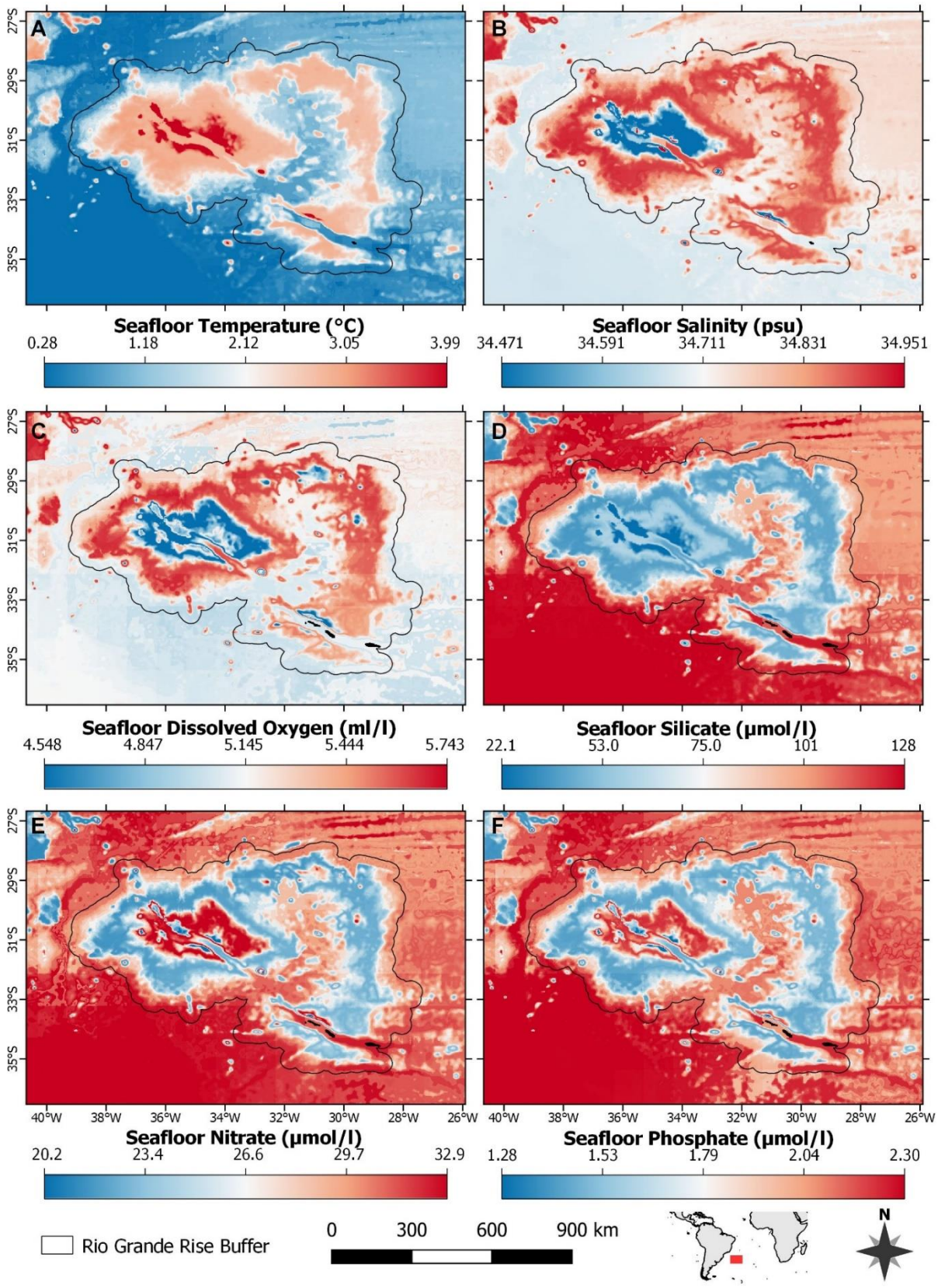

Figure S2. Maps showing time-averaged environmental data for the RGR buffer area and surroundings. **(A)** Temperature [degrees Celsius]. **(B)** Salinity [PSU]. **(C)** Bottom water dissolved oxygen [mL/L]. **(D)** Bottom water silicate concentration [µmol/L]. **(E)** Bottom water nitrate concentration [µmol/L]. **(F)** Bottom water phosphate concentration [µmol/L].

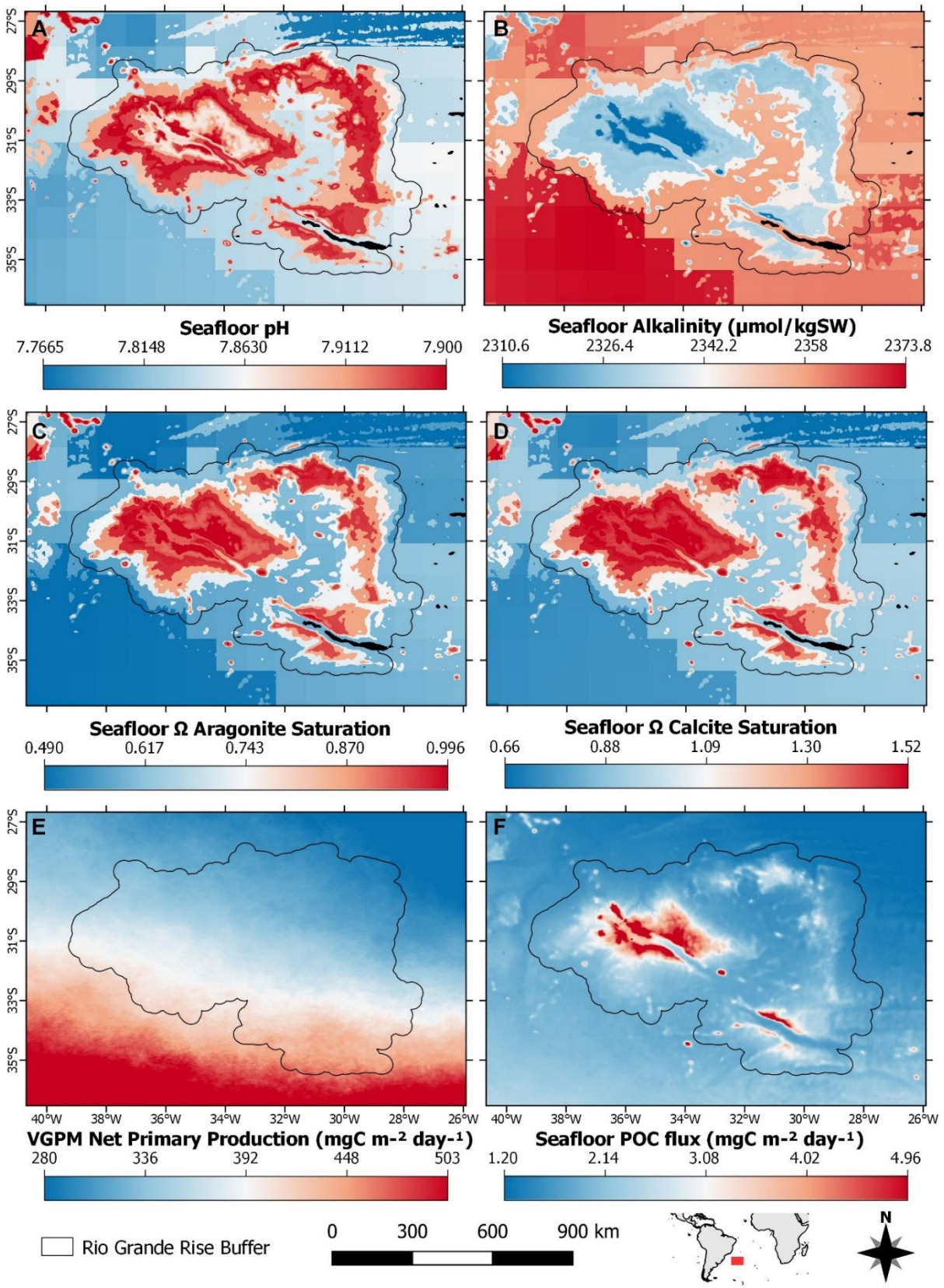

Figure S3. Maps showing time-averaged environmental data for the RGR buffer area and surroundings. **(A)** Bottom water pH. **(B)** Bottom water alkalinity [µmol / kg SW]. **(C)** Bottom water Aragonite saturation state. **(D)** Bottom water Calcite sauration state. **(E)** Surface water primary production [mgC m^{-2} day^{-1}]. **(F)** Downward flux of Particulate Organic Carbon [mgC m^{-2} day^{-1}].

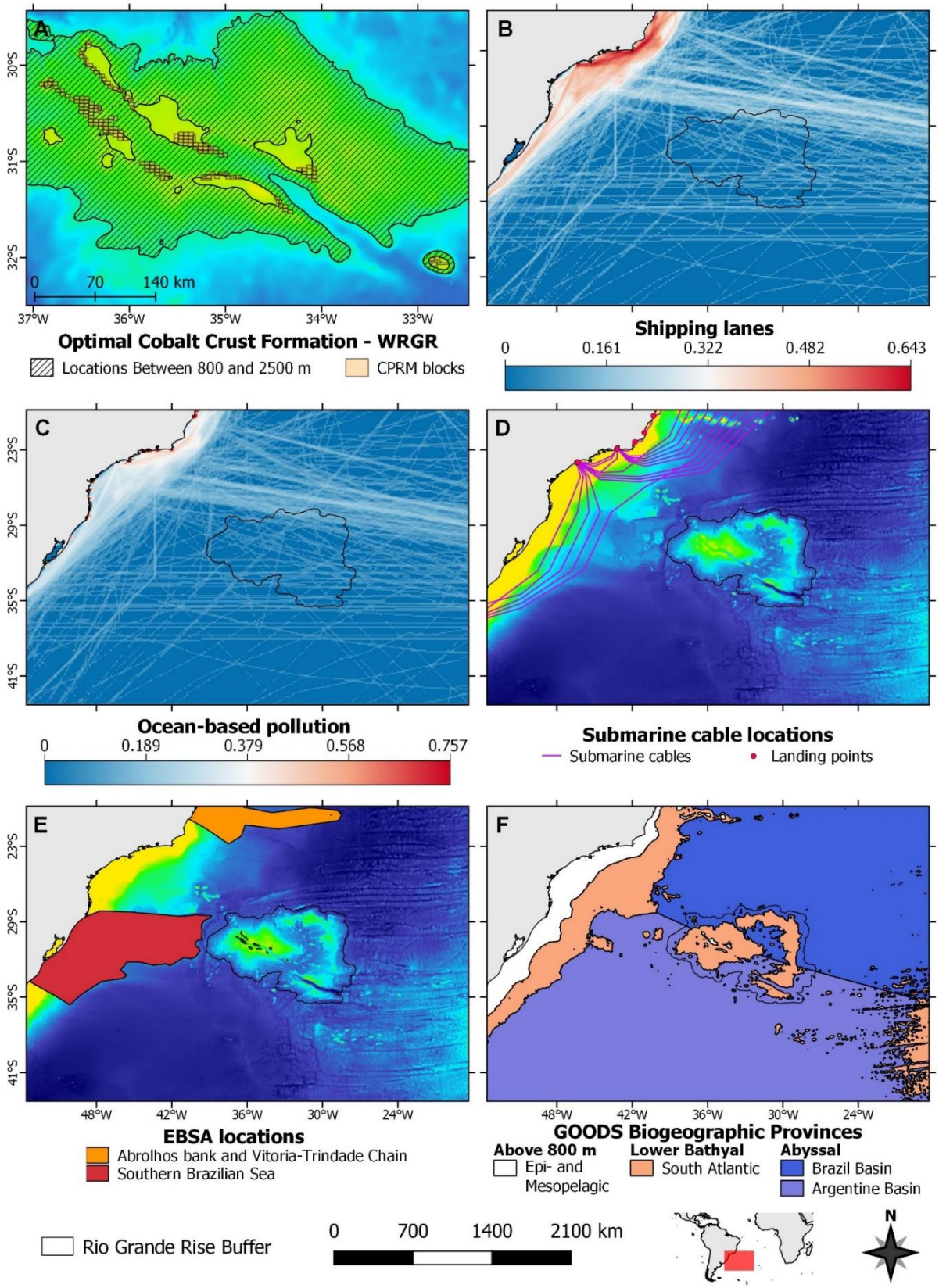

Figure S4. Maps showing biogeographic data and human uses for the RGR buffer area and surroundings. **(A)** Zonation for cobalt-rich crust (CRC) optimal formation conditions (hashed area) over the western Alpha bulge region, with overlay of the location of the CPRM blocks (yellow rectangles). **(B)** Shipping routes with traffic intensity in and around RGR. **(C)** Ocean-based pollution with intensity in and around RGR. **(D)** Submarine (data traffic cables superimposed on bathymetric chart for RGR and SE Brazil coast. **(E)** Locations of Ecologically or Biologically Significant Areas (EBSA) superimposed on

bathymetric chart of the RGR and SE Brazil coast. **(F)** Distribution of GOODS biogeographic provinces over the RGR and SE Brazil coast.

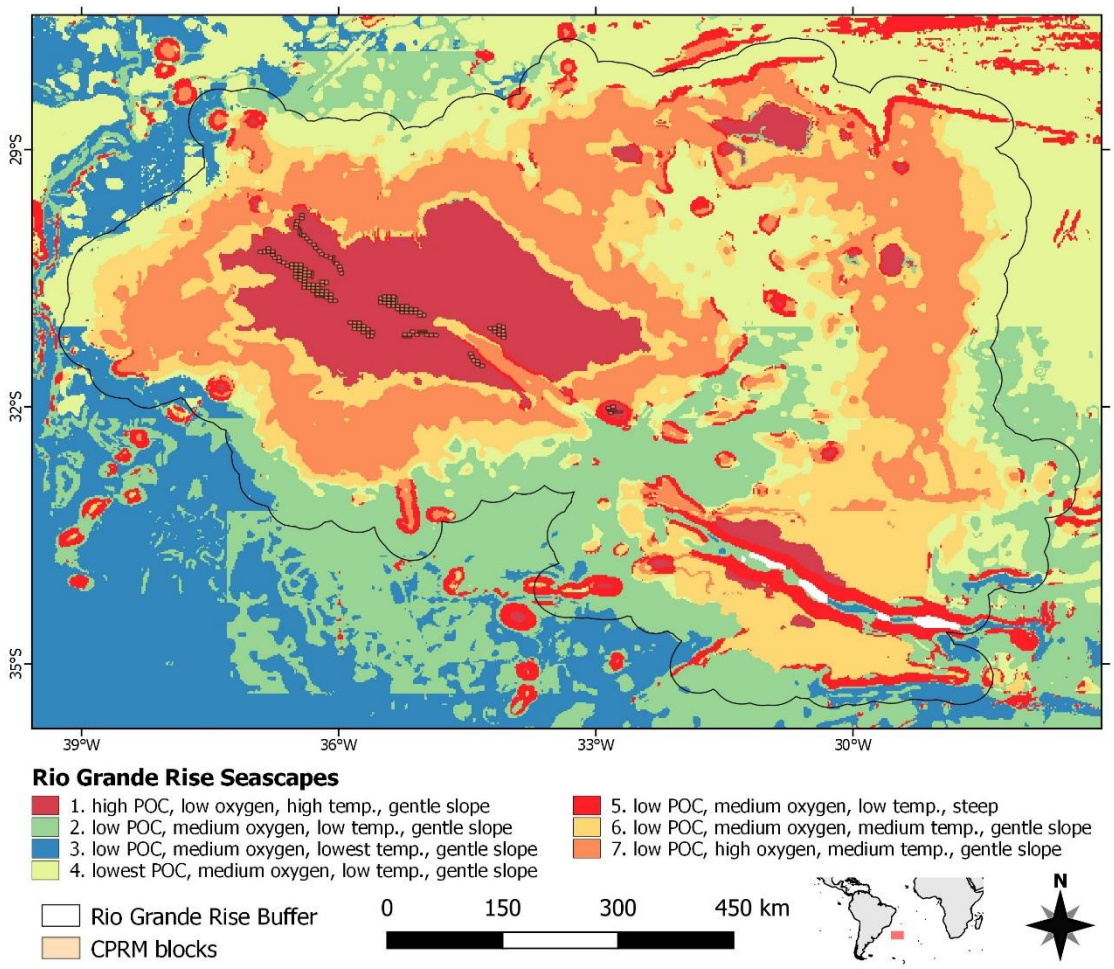

Figure S5. Map showing seascape classification of the Rio Grande Rise, using ArcGIS ISO Cluster Unsupervised Classification tool. Former figure 11 of Montserrat et al. (2019).

Appendix B - Representative images for each morphotype observed with the *RUV HyBIS* (dives HY31–43) in Rio Grande Rise (SW Atlantic).

Below each image is the lowest possible taxonomic group identified and a unique code for each morphotype created for this study, composed of four letters and one number. The appendix is divided in three sections: the first contains benthic morphotypes used in Chapter 4 of this thesis; the second contains morphotypes very small (< 5 cm), which were not included in the analysis; and third section contains pelagic morphotypes.

Benthic Fauna		
Arthropoda		
 *Projasus parkeri* Deca1	 Pleocyemata Deca2	 *Chaceon sanctaehelenae* Deca3
 Isopoda Isop1		

Chordata		
 *Chaunax suttkusi* Loph1	 *Helicolenus* sp. Scor1	

Cnidaria		
 *Paraphelliactis* sp. Acti1	 Actinoscyphiidae Acti2	 Hormathiidae Acti3
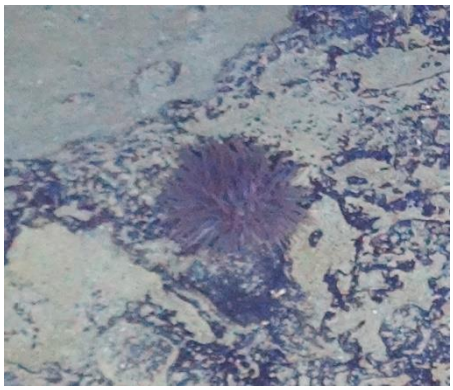 Liponematidae Acti4	 Actiniaria Acti5	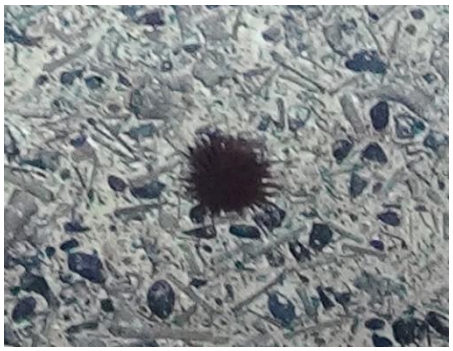 Actiniaria Acti6
 Plexauridae Alcy1	 Alcyonacea Alcy2	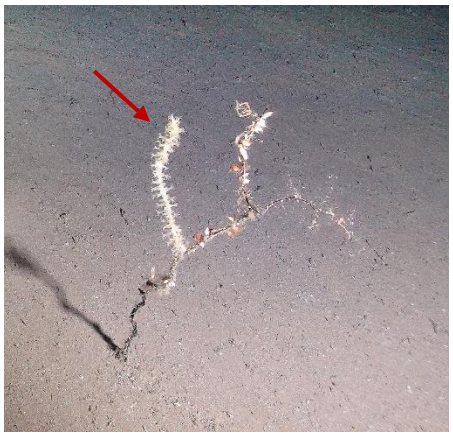 Alcyonacea Alcy3

Paragorgia sp.
Alcy4

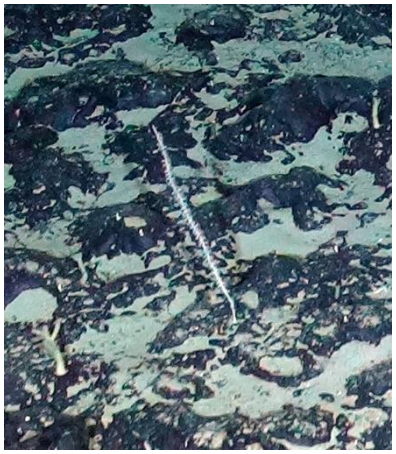

Primnoidae
Alcy5

Aphanostichopathes sp.
Anti1

Stichopathes sp.
Anti2

Bathypathes sp.
Anti3

Schizopathidae
Anti4

Leiopathidae
Anti5

Umbellapathes sp.
Anti6

Antipatharia
Anti7

Antipatharia
Anti8

Iridogorgia sp.
Chry1

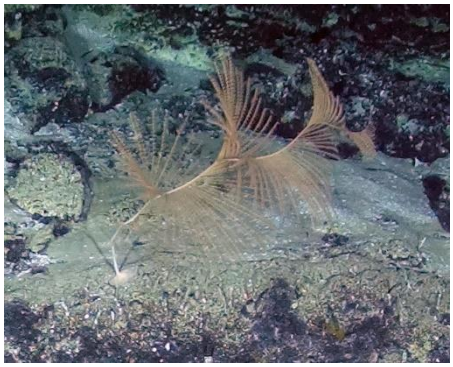

Iridogorgia sp.
Chry2

Ceriantharia
Cnid1

Anthozoa
Cnid2

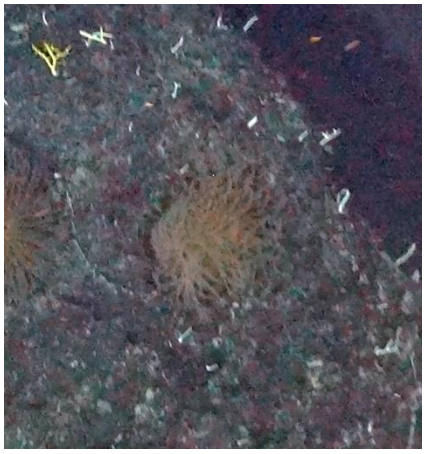

Anthozoa
Cnid3

Anthozoa
Cnid4

Corymorphidae
Hydr1

Corymorphidae
Hydr2

Isididae
Isid1

Isididae
Isid2

Isididae
Isid3

Isididae
Isid4

Isididae
Isid5

Pennatulacea
Pena1

Protoptilum sp.
Pena2

Scleroptilidae
Pena3

Enallopsammia rostrata
Scle1

Echinodermata		
 Goniasteridae Aste1	 Goniasteridae Aste2	 Valvatida Aste3
 Valvatida Aste4	 Valvatida Aste5	 Asteroidea Aste6
 Asteroidea Aste7	 Asteroidea Aste8	 Brisingidae Bris1

Freyellidae
Bris2

Comatulida
Crin1

Comatulida
Crin2

Comatulida
Crin3

Crinoidea
Crin4

Echinoida
Echi1

Gracilechinus sp.
Echi2

Echinothurioida
Echi3

Pedinoida
Echi4

Elpidiidae
Holo1

Synallactida
Holo2

Ophiuroidea
Ophi1

 Ophiuroidea Ophi2		

Mollusca		
 Octopodidae Ceph1	 Limidae Limi1	

Porifera		
 Astrophorina Desm1	 Corallistidae Desm2	 Demospongiae Desm3

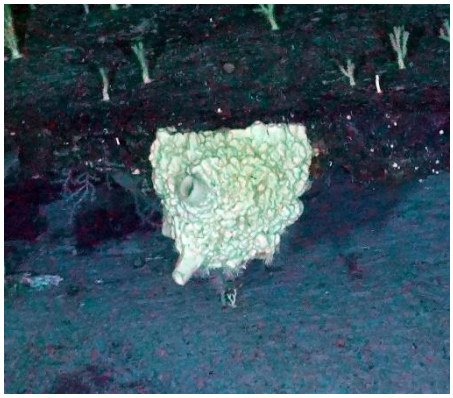

Xestospongia
Desm4

Demospongiae
Desm5

Demospongiae
Desm6

Euplectellidae
Hexa1

Hexactinellida
Hexa2

Hexactinellida
Hexa3

Hexactinellida
Hexa4

Hyalonema sp.
Hexa5

Hexactinellida
Hexa6

 Hexactinellida Hexa7	 Hexactinellida Hexa8	 *Sarostegia oculata* Scep1
 *Aphrocallistes* cf. *beatrix* Scep2	 Sceptrulophora Scep3	

Morphotypes < 5 cm		
 Actiniaria Acti7	 Zoantharia Cnid5	 Ceriantharia Cnid6
 Paguroidea Deca4	 Psolidae Holo3	 Caryophylliidae Scle2

Pelagic Fauna
Annelida
 Annelida Anne1

Arthropoda		
 Decapoda Deca5	 Nematocarcinidae Deca6	 Decapoda Deca7

Chordata		
 *Oreosoma* cf. *atlanticus* Agii1	 Alepocephalidae Agii2	 Beryciformes Agii3

Halosauridae
Agii4

Beryx splendens
Agii5

Centriscops sp.
Agii6

Actinopteri
Agii7

Synaphobranchus sp.
Angu1

Nettastoma sp.
Angu2

Bathysaurus sp.
Aulo1

Chlorophthalmus sp.
Aulo2

Chimaeridae
Chim1

Hydrolagus sp.
Chim2

Malacocephalus okamurai
Gadi1

Moridae
Gadi2

Macrouridae
Gadi3

Macrouridae
Gadi4

Coelorinchus sp.
Gadi5

Gadomus sp.
Gadi6

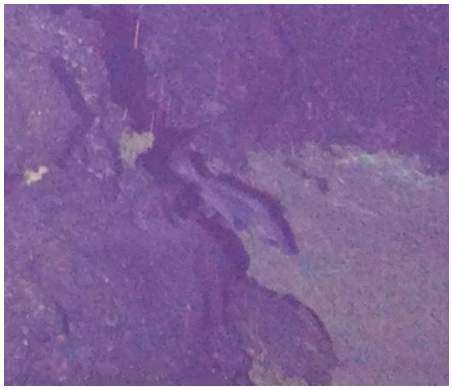

Moridae
Gadi7

Scorpaeniformes
Scor2

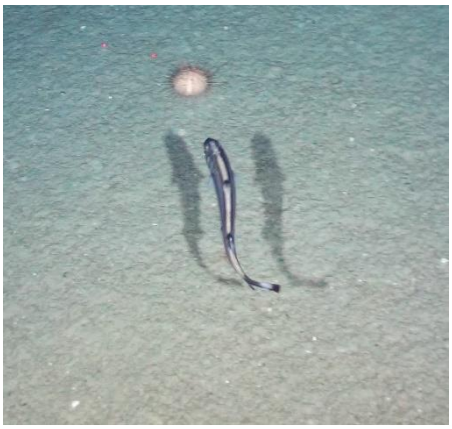

Etmopteridae
Squa1

Etmopteridae
Squa2

Squaliformes
Squa3

 Salpidae Tuni1	 Pyrosomatida Tuni2	

Cnidaria		
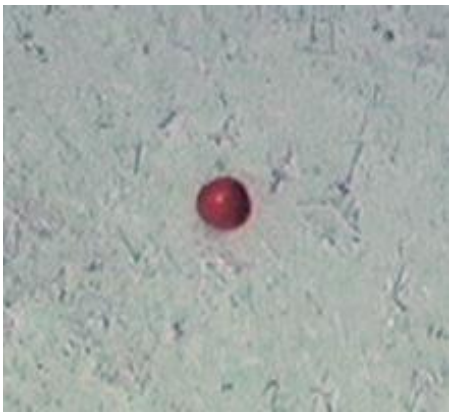 *Crossota* sp. Hydr3	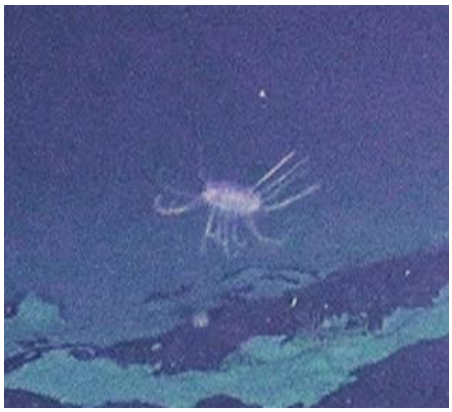 Trachymedusae Hydr4	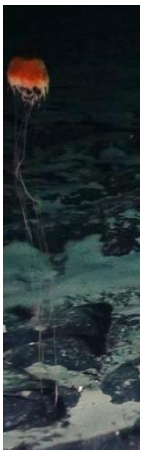 Trachymedusae Hydr5
 Trachymedusae Hydr6	 Cubozoa Medu1	

Ctenophora		
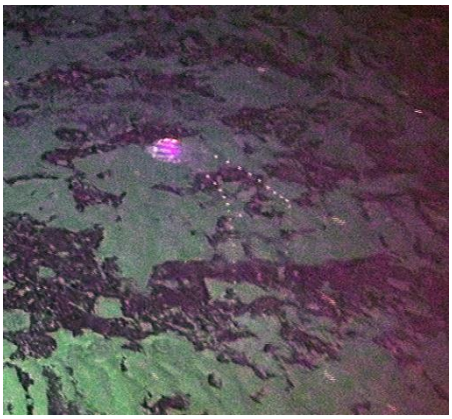 Ctenophora Cten1	 Ctenophora Cten2	 Ctenophora Cten3
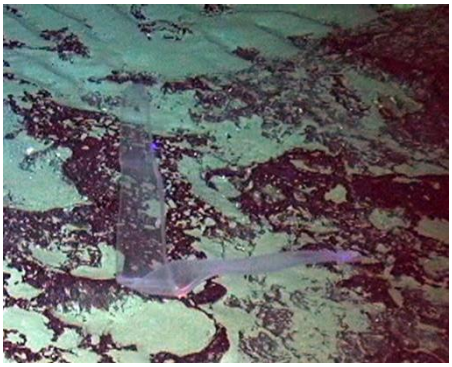 Elopomorpha Cten4		

Appendix C - Pattern analysis using indicator value indices

```
Multilevel pattern analysis
 ---------------------------

 Association function: indval.g
 Significance level (alpha): 0.05

 Total number of species: 80
 Selected number of species: 33
 Number of species associated to 1 group: 22
 Number of species associated to 2 groups: 7
 Number of species associated to 3 groups: 1
 Number of species associated to 4 groups: 3
 Number of species associated to 5 groups: 0

 List of species associated to each combination:

 Group A  #sps.  10
       stat p.value
Acti3 1.000   0.005 **
Anti8 1.000   0.005 **
Chry2 1.000   0.005 **
Crin4 1.000   0.005 **
Isid5 1.000   0.005 **
Crin3 0.997   0.005 **
Anti4 0.977   0.005 **
Anti6 0.963   0.005 **
Desm3 0.954   0.005 **
Crin2 0.930   0.005 **

 Group B  #sps.  4
       stat p.value
Pena2 0.535   0.020 *
Hexa5 0.504   0.030 *
Hexa1 0.501   0.045 *
Cnid3 0.378   0.030 *

 Group C  #sps.  1
       stat p.value
Scep1 0.986   0.005 **

 Group D  #sps.  1
      stat p.value
Echi2 0.93   0.005 **

 Group E  #sps.  4
       stat p.value
Scep2 0.876   0.015 *
Desm2 0.839   0.030 *
Bris2 0.820   0.010 **
Aste6 0.689   0.035 *

 Group F  #sps.  2
       stat p.value
Anti1 0.986   0.005 **
Alcy3 0.842   0.030 *

 Group A+B  #sps.  3
       stat p.value
Chry1 0.976   0.005 **
Cnid2 0.917   0.010 **
Isid1 0.832   0.020 *
```

```
 Group A+E  #sps.  1
       stat p.value
Anti2 0.847    0.01 **

 Group A+F  #sps.  1
       stat p.value
Anti5 0.838    0.01 **

 Group D+F  #sps.  1
       stat p.value
Echi3 0.774   0.035 *

 Group E+F  #sps.  1
       stat p.value
Desm1 0.783   0.025 *

 Group D+E+F  #sps.  1
       stat p.value
Scor1 0.712   0.015 *

 Group A+C+E+F  #sps.  1
       stat p.value
Bris1 0.713   0.045 *

 Group B+C+D+F  #sps.  1
      stat p.value
Scle1 0.84   0.005 **

 Group C+D+E+F  #sps.  1
       stat p.value
Loph1 0.721   0.015 *
---
Signif. codes:  0 ‘***’ 0.001 ‘**’ 0.01 ‘*’ 0.05 ‘.’ 0.1 ‘ ’ 1
```

Appendix D - Friedman test comparing models

Table S1. *P* values of the Friedman's Aligned Rank test for each metric. Values < 0.05 rejects the null hypothesis of equal performance of the models based on the metric.

Metric	*p* value
PRG	$2.13\ 10^{-8}$
ROC	$1.63\ 10^{-9}$
Sens	$1.69\ 10^{-4}$
Spec	$3.98\ 10^{-8}$
TSS	$1.45\ 10^{-10}$

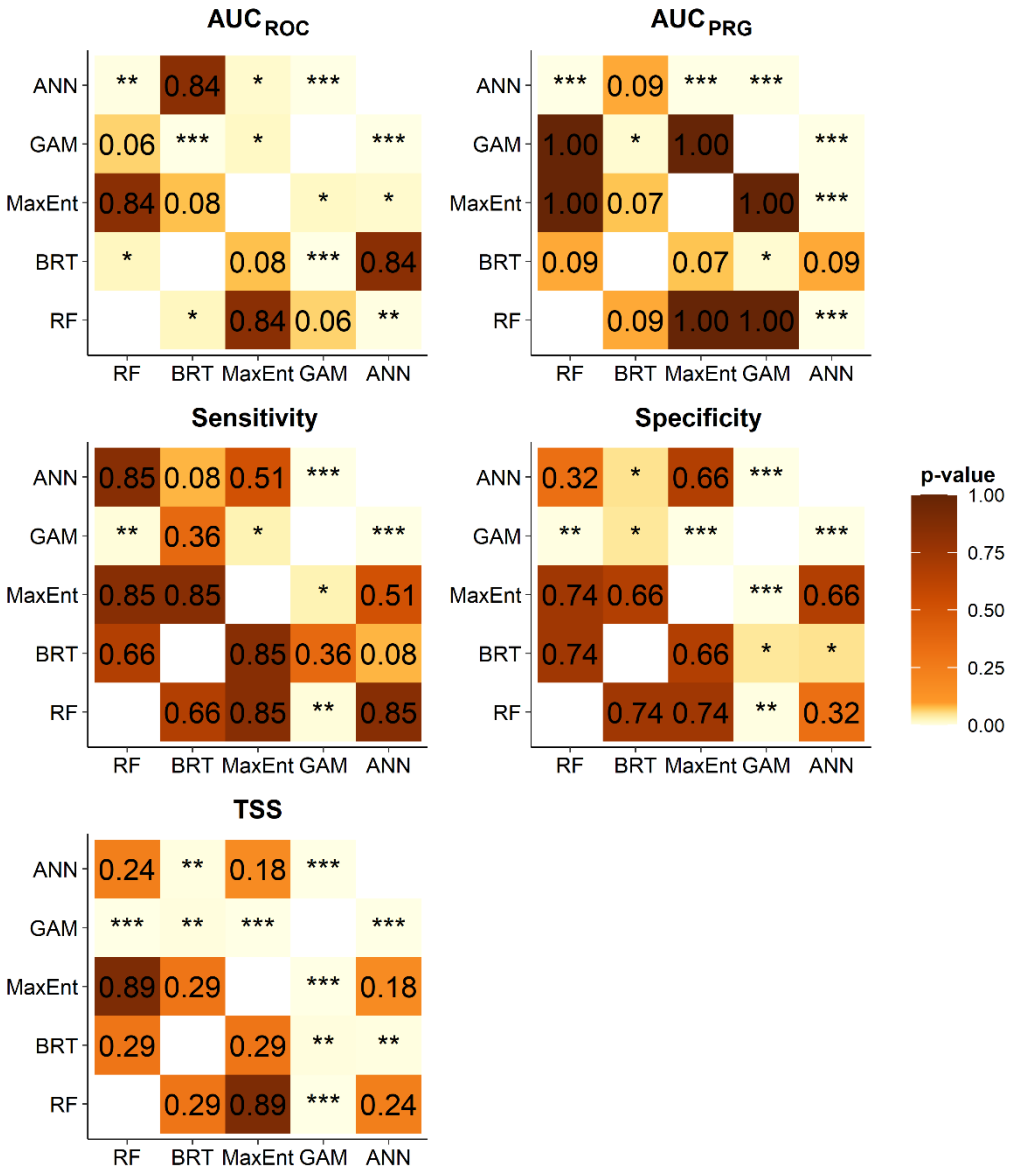

Figure S6. The *p* values of the post-hoc of Friedman Aligned Rank test with the Shaffer correction.